Exploring the Roles of Chromatin Remodelers in Regulating Chromatin Organisation and Transcription in *Dictyostelium discoideum*

Mark Robinson

THESIS SUBMITTED FOR THE DEGREE OF DOCTOR OF PHILOSOPHY

SEPTEMBER 2016

Declaration

This work has not been submitted in substance for any other degree or award at this or any other university or place of learning, nor is being submitted concurrently in candidature for any degree or other award.

Signed …… (candidate) Date……

STATEMENT 1
This thesis is being submitted in partial fulfilment of the requirements for the degree of PhD.

Signed …… (candidate) Date……

STATEMENT 2
This thesis is the result of my own independent work/investigation, except where otherwise stated. Other sources are acknowledged by explicit references. The views expressed are my own.

Signed …… (candidate) Date ……

STATEMENT 3
I hereby give consent for my thesis, if accepted, to be available online in the University's Open Access repository and for inter-library loan, and for the title and summary to be made available to outside organisations.

Signed …… (candidate) Date ……

Acknowledgements

My thanks to Adrian Harwood and Nicholas Kent for their supervision, and to Dr's Alan Kimmel, Annette Müller-Taubenberger, Jonathan Chubb and Amy Baldwin for providing samples and helpful discussions. Particular thanks to Dr James Platt for cell lines, techniques and data used throughout the current study and for advice and training provided. Finally, thanks to my friends, family, TNMT and imgur.

Abstract

Nucleosomes comprise the most basic repeating unit of chromatin and provide hubs for the regulation of DNA transcription, replication and repair. ATPase chromatin remodelling complexes establish nucleosome occupancy, positioning and structure in a dynamic fashion to allow fine-tuning of protein-DNA interactions. The ISWI and CHD families of remodelers possess the ability to sample DNA linker length between nucleosomes and space nucleosomes evenly. How these spacing remodelers combine their functions to maintain phasing of nucleosomal arrays, and re-organise these arrays during development remains poorly understood. Furthermore the relationship between nucleosomal array structure and transcriptional regulation is unclear.

Dictyostelium discoideum provides a complex chromatin environment and remodeler repertoire, while retaining a compact genome and ease of genetic manipulation. Thus we have utilized this model to generate remodeler null mutants, and double mutants to observe phenotypic effects and interactions. We further compiled comprehensive nucleosome mapping and RNA sequencing data sets for all spacing remodelers in *Dictyostelium*. Bioinformatic analysis of these data provide novel insights into remodeler functions, and help to establish a paradigm to explain the relationship between remodeler-mediated chromatin organisation and transcriptional regulation.

Contents

Table of Contents

Declaration ..... **I**
Acknowledgements ..... **II**
Abstract ..... **III**
Contents ..... **IV**
Introduction **6**
1.1 Nucleosome and Chromatin Structure 7
1.2 Chromatin and Transcription Regulation 10
1.2.1 Histone Post-Translation Modifications 12
1.2.2 Linker and Variant Histones 12
1.2.3 Looping and Architectural Chromatin Proteins 13
1.2.4 Nucleosome Positioning 15
1.3 Chromatin Remodeling Complexes 18
1.3.1 SNF2 Proteins 18
1.3.2 SWI/SNF 20
1.3.3 ISWI 21
1.3.4 CHD 22
1.3.5 INO80 and SWR 24
1.3.6 Spacing Remodelers 24
1.4 *Dictyostelium discoideum* 27
1.4.1 *Dictyostelium* as a Model Organism 27
1.4.2 *Dictyostelium* Development 28
1.4.3 The *Dictyostelium* Genome and Chromatin Architecture 29
1.4.4 Chromatin Remodelers in *Dictyostelium* 30
1.5 Project Aims 31
Materials and Methods **32**
2.1 Dictyostelium Strains and Cell Culture 33
2.2 Cloning 33
2.2.1 Genomic DNA Extraction 33
2.3.2 Knockout Construct Design 34
2.3.3 Dictyostelium Transformation 35
2.4 Knockout Screening 35
2.5 Western Blotting 36
2.6 Multinucleate Assay 36
2.7 Time Lapse Development Assay 37
2.8 Chemotaxis Assay 37
2.9 RNA Sequencing 37
2.9.1 mRNA Sequencing 37
2.9.2 RNAseq Bioinformatics 38
2.10 Nucleosome Mapping 38
2.10.1 Chromatin Digestion 38
2.10.2 MNase-seq Bioinformatics 38
2.11 Analysis Scripts 39
Characterising the Roles of *Dictyostelium* ATP-Dependent Chromatin Remodelling Complexes in Growth, Development and Chemotaxis **40**
3.1 Introduction 41

3.2 The SNF2 Family in *Dictyostelium*....42
3.3 Generating Remodeler Null Cell Lines....44
3.4 Differential Growth Defects of Remodeler Mutants....46
3.5 Detecting Developmental Roles of Chromatin Remodelers....48
3.6 Chemotaxis Defects Displayed by Remodeler Mutants....50
3.7 Summary....52
***Dictyostelium* Spacing Remodelers Play Distinct Roles in the Maintenance of Chromatin Structure....53**
4.1 Introduction....54
4.2 MNase-Sequencing of Isw Null Mutants....55
4.3 Generation and Comparison of WT Nucleosome Maps....58
4.3 Optimising Nucleosome Scoring....61
4.4 Remodeler Loss Leads to Distinct Global Chromatin Changes....64
4.5 Improving Nucleosome Peak Calling....66
4.6 Quantifying WT Nucleosome Parameters....69
4.7 Nucleosome Parameter Changes in Remodeler Mutants....72
4.8 Visualising the Localisation of Chromatin Defects....74
4.9 Summary....77
Exploring the Relationship between Chromatin Structure and Transcriptional Regulation....78
5.1 Introduction....79
5.2 The Gene Expression Profile of Isw Null Mutants....80
5.3 Comparing the Transcriptional Effects of Remodelers....83
5.4 Impact of Remodeler Loss is Dependent on Transcription Level....85
5.5 Comparison of Gene Sets Mis-Regulated in Remodeler Mutants....87
5.6 Identifying Severely Mis-Modeled Genes....89
5.7 Association between Transcriptional and Structural Defects....91
5.8 Antagonistic Occupancy Effects of ChdA and ChdB....93
5.9 *ChdA*$^{-}$*/ChdB*$^{-}$ Double Knockout Mutant....95
5.9.1 Phenotypic Effects of Double Knockout on Growth and Development....95
5.9.2 Chromatin Profiling of *ChdA*$^{-}$*/ChdB*$^{-}$ Double Knockout Cells....97
5.9.3 Transcriptional Disruption in *ChdA*$^{-}$*/ChdB*$^{-}$ Double Knockout Cells....97
5.9.4 Combined Occupancy Defects of *ChdA*$^{-}$*/ChdB*$^{-}$....100
5.10 Summary....101
Discussion....102
6.1 Project Aims....103
6.2 Generation of *Dictyostelium* SNF2 Protein Mutants....103
6.3 *Dictyostelium* SNF2 Proteins in Growth, Development and Chemotaxis....104
6.4 CHD and ISWI Complexes Regulate Distinct Remodeling Events....108
4.5 ChdA and ChdB Control Genic Nucleosome Occupancy....109
6.6 ChdC Influences Nucleosome Positioning, Spacing, Size and Organisation....111
6.7 Isw Organises Nucleosomal Arrays to Repress TE....112
6.8 Spacing Remodelers are Required for Optimal Transcriptional Regulation....114
6.9 Summary....114
Bibliography....116

Chapter 1:

Introduction

1.1 Nucleosome and Chromatin Structure

To meet the topological and regulatory challenges posed by the abundance of DNA contained within the nucleus of eukaryotic cells, DNA is packaged with histones, and other proteins, into a nucleoprotein complex, termed chromatin. The basic repeating unit of chromatin is the nucleosome, consisting of approximately 147bp of DNA wrapped ~1.7 times around an octomeric disc of histone proteins (Fig1.1A; Kornberg 1974; Luger et al. 1997). Canonical nucleosomes contain two of each major-type histone protein: H2A, H2B, H3 and H4, whose structured regions form regular hydrogen and electrostatic bonds with the DNA phosphate backbone (Luger et al. 1997). The flexible histone N-terminal tails make minimal contact with the DNA but provide hubs for chemical modification and interaction with neighbouring nucleosomes and nuclear factors. Nucleosomes are connected by variable lengths of DNA between ~20-90 bp, depending on both the organism and cell type, termed linker DNA. This "beads on a string" arrangement is termed the 10 nm fibre (Olins & Olins 1974), and comprises the primary structure of eukaryotic chromatin.

Beyond the 10 nm fibre, chromatin is further compacted into secondary structures, representing local interaction between nucleosomes and fibres, and tertiary structures including long range interactions such as enhancer-promoter loops, chromosome territories, and condensed chromosomes (Fig1.1B). Despite extensive efforts, understanding of the secondary structure remains primitive, largely due to a lack of techniques to validate structural predictions. Classical models of secondary structure were based on observations that *in vitro* purified 10nm fibres together with linker histone H1 in low cation concentrations will form a 30nm fibre (Finch & Klug 1976). The exact structure of this 30nm fibre remains unclear, with two main models proposed: the one-start helix or solenoid, and the two-start helix (Song et al. 2014; Widom & Klug, 1985; Woodcock et al. 1984). However, cryo-EM, X-ray scattering and electron spectroscopic imaging analyses examining the *in vivo* structure of chromatin in mammalian nuclei have provided almost no evidence of 30nm fibres (McDowall et al. 1986; Eltsov et al. 2008; Nishino et al. 2012; Fussner et al. 2011). These studies in stead converge on a less structured, dynamic model of irregularly folded 10nm fibres, described as a liquid-like state, even in mitotic chromosomes and chromocenters (Maeshima et al. 2016).

As opposed to the relative dearth of data on *in vivo* secondary chromatin structure, recent sequencing based methodologies have allowed high-throughput, high-resolution examination of primary and tertiary structures genome wide. At the primary level these include techniques mapping DNA modifications such as whole-genome bisulphite sequencing (WGBS; Krueger et al. 2012) and those mapping the accessibility of the genome to restrictive enzymes and transposable elements: DNase-seq (Crawford et al. 2006), MNase-seq (Lee et al. 2007) and assay for transposase-accessible chromatin sequencing (ATAC-seq; Buenrostro et al. 2013). Histone modifications, chromatin architectural proteins, DNA-binding factors and non-coding RNA binding at specific loci can be analysed using standard chromatin immunoprecipitation sequencing (ChIP-seq; Landt et al. 2012), ChIP-exo (Rhee & Pugh 2012) and chromatin isolation by RNA purification (CHIRP-seq; Chu et al. 2011) approaches. At the tertiary level, long-range interaction between genomic loci can be observed with the chromatin conformation capture (3C) family of techniques (e.g. 3C, 4C, 5C, Hi-C, scHi-C; Dekker et al. 2002; Dostie et al. 2006; Nagano et al. 2013; Lieberman-Aiden et al. 2009) which rely on proximity ligation. These techniques have provided a wealth of information on the complexities of chromatin states, and the regulatory roles of chromatin structure on DNA transcription, replication and repair.

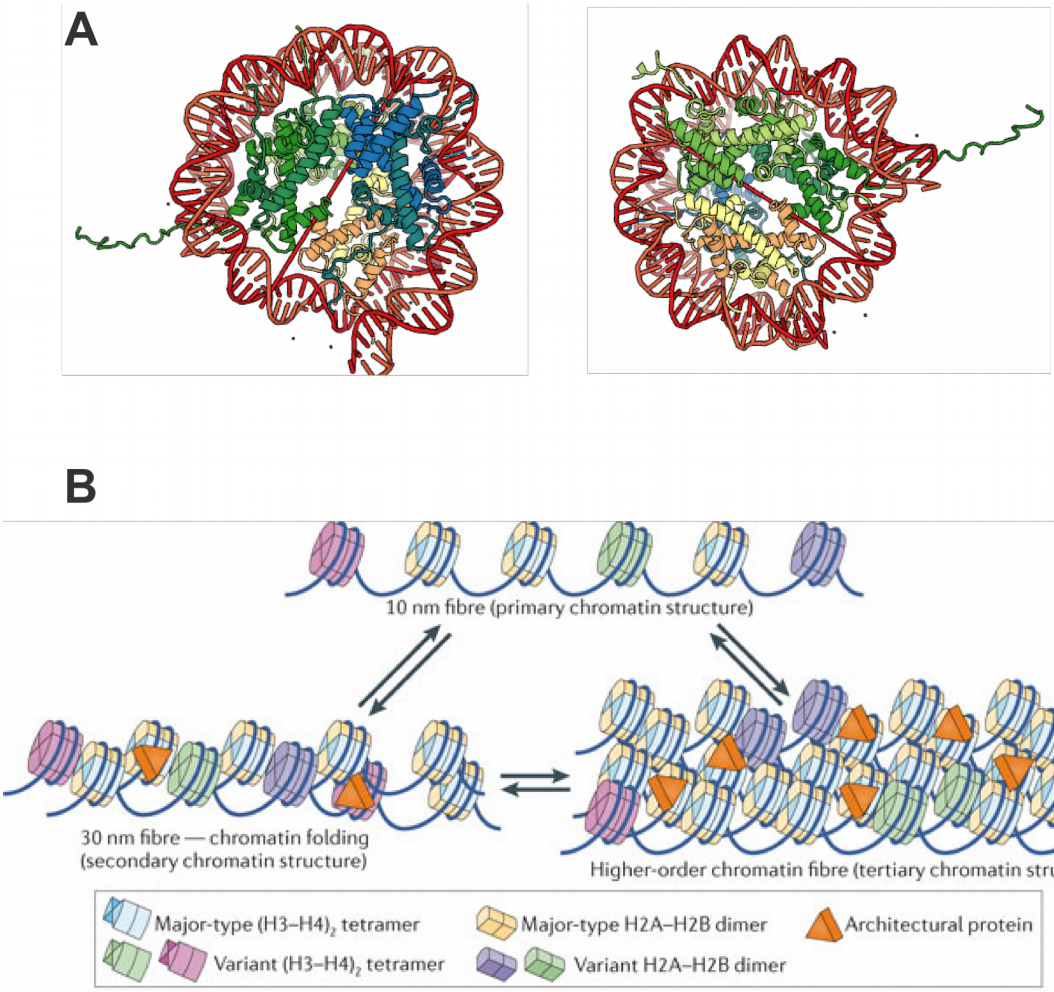

Fig1.1: Nucleosome and Chromatin Structure.

A. Ribbon trace structure of the *Xenopus laevis* nucleosome core particle, depicting 146 bp of DNA (red) wrapped around the histone octomer (H2A: light greens, H2B: blues, H3: dark green & orange, H4: yellow & turquise-green). The superhelical axis is indicated by red bar. Protein Data Bank code: 1AOI, Luger et al. 1998.

B. Diagram of possible chromatin structures at primary, secondary and tertiary compaction levels. In addition to canonical (blue/yellow) nucleosomes, nucleosomes can be modified with histone marks and variant histone proteins (purple and green) to modify the local and higher-order chromatin properties. Architectural proteins such as linker histones and CTCF facilitate the formation of higher-order structures. Figure reproduced with permission from Luger et al. 2012.

1.2 Chromatin and Transcription Regulation

The complex and dynamic structure of chromatin provides a host of regulatory opportunities to control access to the underlying DNA, essential for control of transcription, replication and repair of the genome. In the current study we focus on the interplay between chromatin and transcriptional regulation. Transcription is primarily driven by the binding of transcription factors (TF) and formation of the pre-initiation complex (PIC) at core promoters (Zhang & Reese 2007; Zawadzki et al. 2009); however chromatin accessibility in turn influences the binding of TF and PIC components (Wu 1980; Carr & Biggin 2000). Promoters are, in general, more inherently accessible than other regions of the genome, possessing poly(dA-dT) tracts in yeast and CpG islands in mammals, both of which are refractory to nucleosome occupancy (Kaplan et al. 2009; Valouev et al. 2011). However the DNA-encoded accessibility bias of a given locus can be modified by a multitude of factors in order to optimise cell-type specific gene expression programs; these factors including histone modifications, linker histones, histone variants, nuclear factors, architectural chromatin proteins and ATP-dependent chromatin remodelers (Luger et al. 2012).

Chromosomes occupy distinct territories within the nucleus (Cremer et al. 1982), but the positioning of genes within these territories has a significant impact on their transcriptional regulation. The classical observation of more repressive/compact and active/open chromatin – termed heterochromatin and euchromatin respectively, represent the most fundamental compartmentalisation of chromatin (Heitz 1928). Hi-C studies have reconfirmed this gross binary division of the genome (Lieberman-Aiden et al. 2009). More recent insights include the observed localisation of active regions to nuclear pores (Casolari et al. 2004) and the association of repressed regions with the nuclear lamina (Pickersgill et al. 2006). At higher resolution it is possible to further divide chromatin into topologically associated domains (TADs) of ~0.1 to 1 megabase in size (Dixon et al. 2012; Hou et al. 2012; Nora et al. 2012; Sexton et al. 2012). While these territories and TADs appear recurrently across cell types and even species (Dixon et al. 2012), the specific intra-domain, inter-domain and inter-chromosome interactions of individual loci are highly dynamic and cell-type specific (Nagano et al. 2013; Phillips-Cremins et al. 2013).

These observations at the tertiary and primary scales of chromatin structure suggest a general principle governing the relationship between chromatin and transcriptional control; that the chromatin state of a given gene represents a balance between constitutive genome ordering and dynamic locus-specific remodeling events to optimise cell-type specific transcriptional programs. The key determinants of these locus-specific effects are briefly summarised below.

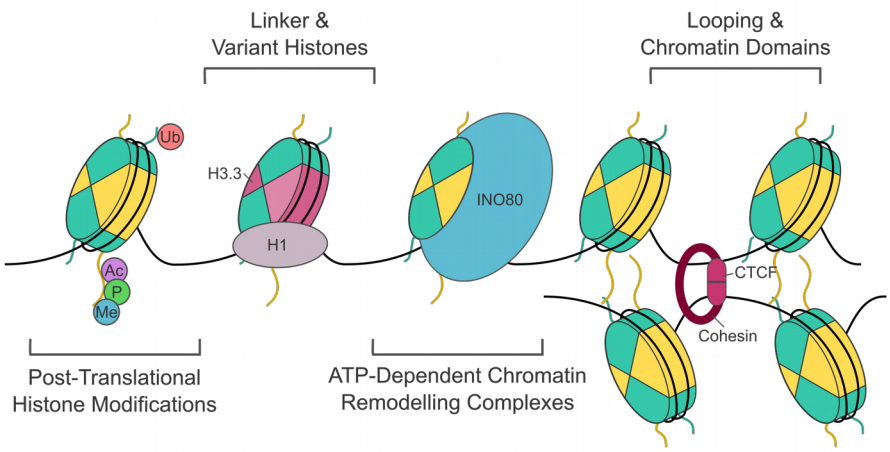

Fig1.2: Mechanisms of Chromatin Modification.

Diagram of four broad categories of chromatin modification mechanisms utilised to regulate transcription of genes to establish and maintain cell-type specific transcriptional programs. Histone post-translational modification of histone tails such as H2B ubiquitination (Ub), H3 acetylation (Ac), phosphorylation (P) and methylation (Me) influence the properties and interactions of histones. Incorportation of variant histones such as H3.3, and binding of linker histones including H1, alters the interaction surface of nucleosomes. Chromatin remodelling complexes such as INO80 are able to incorporate, evict, shift and remodel nucleosomes affecting both primary and tertiary chromatin structure. Finally looping between distal chromatin sections and formation of chromatin domains help to functionally demarcate chromatin regions.

1.2.1 Histone Post-Translation Modifications

Histones can host a surprising number of distinct post-translational modifications, including methylation, acetylation, phosphorylation, SUMOylation and ubiquitination, targeted to specific residues within the histone tail (Strahl & Allis 2000; Tan et al. 2011). A number of these are well known markers of active transcription – such as tri-methylation of histone 3 lysine 4 (H3K4me3), H2B ubiquitination (H2Bub) and H3K26me3. Others are associated with repressive states – including H3K9me3 and H3K27me3. The presence of both H3K27me3 and H3K4me3 is thought to mark genes in a "bivalent" state – poised for induction (Bernstein et al. 2006). While the majority of modifications are thought to influence the recruitment and retention of protein factors to genomic regions in a combinatorial fashion, others can also influence the physical properties of chromatin (Strahl & Allis 2000; Jenuwein & Allis 2001). For example, acetylation of histone tails interferes with nucleosome interactions and inhibits chromatin compaction (Shahbazian & Grunstein 2007).

1.2.2 Linker and Variant Histones

In addition to the canonical histone proteins, eukaryotes possess a repertoire of functionally specialised variant histones. Canonical histones are expressed in a replication-dependent fashion and ubiquitously incorporated throughout the genome. Variant histone expression is replication-independent, and they are targeted to specific loci by chromatin remodelers and histone chaperones.

The H2A variant H2A.Z is among the most highly studied, and is highly evolutionarily conserved across eukaryotes (Eirín-lópez et al. 2009). H2A.Z tends to be incorporated at nucleosomes flanking the TSS by SWR chromatin remodeling complexes (Albert et al. 2007). H2A.Z is generally thought to destabilise nucleosomes, facilitating transcription (Meneghini et al. 2003; Zhang et al. 2005; Guillemette et al. 2005), but has additional roles in transcriptional repression, repair and chromosome segregation (Svotelis et al. 2009). MacroH2A variants consist of a H2A-like domain linked to a large macro-domain which binds metabolic NAD+ derivatives (Kustatscher et al. 2005). The role of macroH2A is poorly understood but seems to play both repressive and activating transcriptional roles, and provides an interesting link to the metabolic state of the cell (Creppe et al. 2012; Costanzi & Pehrson 1998).

H3.3 is one of the most pervasive histone variants, replacing the canonical H3.1/H3.2 at regions of high nucleosome turnover such as the body of transcribed genes (Kraushaar et al. 2013; Elsasser et al. 2015). However it is also found at repressed genes and regions such as telomeres, and is deposited through multiple distinct mechanisms (Goldberg et al. 2010). CENP-A is another H3 variant that is both necessary and sufficient for centromere formation in metazoans (Mendiburo et al. 2011). Interestingly all of the histone variants discussed are frequently mutated or mis-regulated in human cancers (Zink & Hake 2016). H2A.Z, H3.3 and CENP-A are also essential to mammalian development – with mouse knockouts displaying embryonic lethality (Faast et al. 2001; Howman et al. 2000; Jang et al. 2015).

Binding of linker histones (H1 or H5) to the DNA entry/exit sites of the nucleosome (van Holde 1989) to form a chromatosome is largely considered repressive, limiting nucleosome mobility (Pennings et al. 1994) and potentially promoting higher order folding (Thoma et al. 1979; Bednar et al. 1998). In higher eukaryotes linker histones are essential and highly abundant – approximately equimolar with nucleosomes (van Holde 1989; Fan et al. 2003); however in lower eukaryotes H1 mutants are viable (Patterton 1998). In addition to the chromatosome, the potential for nucleosomes to form alternative structures to the canonical octomeric disc has been appreciated for some time (Luger et al. 2012). However evidence of these alternative structures are only now beginning to emerge. The Henikoff lab has suggested the presence of hemisomes – half nucleosomes containing only one copy of each histone protein, and right-handed DNA wrapping nucleosomes at yeast centromeres (Furuyama & Henikoff, 2009; Henikoff et al. 2014). ChIP-exo and H4S47C cleavage maps, which use a cysteine substitution in the H4 tail to introduce precise break locations into the genome, have proposed the presence of asymmetric nucleosomes at yeast promoters (Ramachandran et al. 2015; Rhee et al. 2014). These asymmetric structures potentially represent intermediates of RSC-mediated nucleosome remodeling. Alternate nucleosome structures remain somewhat controversial but may prove important for future understanding of chromatin structure.

1.2.3 Looping and Architectural Chromatin Proteins

Long range functional interactions of specific genomic loci via chromatin looping are abundant and highly cell-type specific (Nagano et al. 2013). Interaction can have both

repressive and activating effects on gene expression, however the best studied category is the activating effect of enhancer-promoter looping. Enhancers tend to lie in *cis* to their respective genes, but can be located inter- or intra-genically, up- or down-stream and positioned long distances from their targets. As an example, an enhancer important for regulating sonic hedgehog (*SHH*) expression in limb development is located ~1Mb upstream in an intron of *LMBR1* (Lettice et al. 2003). The enhancer-promoter interaction is essential for transcriptional regulation of SHH, with enhancer deletion eliminating expression (Sagai et al. 2005). Furthermore, gene inversion in human disease leads to alternative enhancer association, mis-expression and limb malformations (Lettice et al. 2011). While enhancer interaction appears to be important, it is not sufficient; interaction is observed in cell-types not expressing SHH, possibly representing poised populations; further re-location of the gene away from its chromosome territory towards the interior of the nucleus appears to be necessary for active expression (Amano et al. 2009). This single interaction provides a demonstrative case for the importance and intricacies of long range interactions in optimising cell-type specific gene expression.

The mechanisms of loop formation are not clear, but interaction sites are frequently associated with chromatin architectural proteins – chief among them cohesin and CCCTC-binding factor (CTCF) (Hadjur et al. 2009; Phillips-Cremins et al. 2013). A relatively recent model of loop formation posits that an extrusion complex, predicted to comprise either a single cohesin ring or a cohesin dimer and two CTCF subunits bind at a specific locus. Translocation leads to the extrusion of DNA into a central loop, while the CTCF proteins scan opposing strands for CTCF motifs. Extrusion continues until convergent motifs are bound by CTCF (Nasmyth 2001; Sanborn et al. 2015). This model explains the lack of overlap between loops, the observation of convergent CTCF sites at looped loci, and is supported by computational modelling and Hi-C data (Sanborn et al. 2015). Exactly how the extrusion model fits together with the larger scale compartmentalisation of the genome into TADs is unclear. Nonetheless compartmentalisation appears important for regulating looping; most known promoter-enhancer loops identified to date are found within individual TADs (Dixon et al. 2012; Smallwood & Ren 2013). And deletion of TAD boundaries leads to ectopic locus interactions and mis-regulated transcription within the domain (Nora et al. 2012).

1.2.4 Nucleosome Positioning

Nucleosome positioning has immediate effects to restrict access of DNA binding proteins to nucleosomal DNA, plus a wider influence on higher order structure (Iyer 2012; Struhl & Segal 2013). *In vitro* nucleosomes act as a barrier to RNA polymerase II (RNAPII) transcription initiation and elongation (Workman & Buchman 1993); and single locus studies, particularly of PHO5 and GAL1-10 genes in yeast, have provided *in vivo* evidence that nucleosome remodeling regulates transcription (Rando & Winston 2012; Korber & Barbaric 2014). In high phosphate conditions the PHO5 promoter is occupied by five well positioned nucleosomes, occluding the promoter and one of two Pho4 transcription factor binding sites (Almer & Hörz 1986). In low phosphate conditions Pho4 binding to the exposed binding site leads to nucleosome eviction, forming a nucleosome depleted region that is a prerequisite for subsequent transcription (Almer et al. 1986; Fascher et al. 1990; Boeger et al. 2003; Reinke and Horz 2003; Boeger et al. 2004; Korber et al. 2004). This remodeling process involves a host of chromatin remodelers, modifiers and histone-chaperones including SWI/SNF, RSC, INO80, Isw1 and Chd1 (Neef & Kladde 2003; Gaudreau et al 1997; Ehrensberger & Kornberg 2011; Reinke & Hörz 2003; Barbaric et al. 2007; Steger et al. 2003; Huang & O'Shea 2005; Dhasarathy & Kladde 2005; Musladin et al. 2014; Brown et al. 2011). These studies and many others demonstrate the complex role of nucleosome positioning in transcriptional regulation.

The positions of nucleosomes can be mapped by digesting chromatin within permeabilised nuclei with micrococcal nuclease (MNase), which digests accessible linker DNA, and sequencing resulting protected DNA fragments – termed MNase-seq. Numerous genome wide nucleosome mapping studies have now been undertaken in a range of organisms (Yuan et al. 2005; Albert et al. 2007; Mavrich et al. 2008; Schones et al. 2008; Shivaswamy & Iyer 2008; Valouev et al. 2008; Johnson et al. 2006). A common, average nucleosome profile is observed around transcription start sites (TSS) for all eukaryotes studied to date (Fig1.3). The first nucleosome downstream of the TSS - termed the +1, is the most prominent and well positioned, falling directly over the TSS in yeast, but positioned slightly downstream in most higher eukaryotes (Yuan et al. 2005; Albert et al. 2007; Mavrich et al. 2008). Following the +1 an array of nucleosomes occupy the gene body (termed +2, +3, etc.) with decreasing uniformity of positioning, due in part to differential gene lengths and intron locations across

averaged genes. The linker length between nucleosomes varies significantly between organisms and cell types between ~20-90 bp (Yuan et al. 2005; Albert et al. 2007; Mavrich et al. 2008; Schones et al. 2008; Shivaswamy & Iyer 2008; Valouev et al. 2008; Johnson et al. 2006). Upstream of the +1 lies a nucleosome depleted region (NDR or NFR: nucleosome free region) extending ~120 bp in *S. cerevisiae*. The prominence of upstream nucleosomes (termed -1, -2, etc.) is also variable between organisms, likely explained by organism-specific intergenic distances. The transcription termination site (TTS) of genes typically display an inverse pattern to that at the TSS, though less pronounced.

Nucleosome positions are determined by a combination of factors including the underlying DNA sequence, active remodelling by ATP-dependent chromatin remodeling complexes and interaction/competition with other DNA binding factors. The relative contribution of each, particularly of DNA sequence, has been a contentious issue within the field. Mapping of *in vitro* assembled nucleosomes using chicken histone proteins, purified yeast DNA and salt dialysis recapitulates many aspects of *in vivo* yeast maps (Kaplan et al. 2009). And *in vivo* nucleosome maps themselves indicate depletion of nucleosomes over rigid poly(dA-dT) tracts and a pattern of 10bp AA/AT/TA dinucleotide periodicities at nucleosome enriched positions (Kaplan et al. 2009; Segal et al. 2006; Yuan & Liu 2008; Ioshikhes et al. 1996; Drew & Travers 1985). This would suggest that DNA sequence plays a strong role in nucleosome positioning, yet *in vitro* assembled chromatin fails to recapitulate the ordered arrays of phased nucleosomes observed *in vivo*, indicating that precise control of positioning is dependent on nuclear factors. Null mutants of the spacing remodelers Chd1 and Isw1 in *S. cerevisiae* phenocopies this loss of phasing past the +2 nucleosome, indicating the essential role of remodelers in establishing and maintaining precise nucleosome positioning (Gkikopoulos et al. 2011). An elegant experiment from the Struhl lab found that inserting yeast artificial chromosomes (YACs) from one yeast species into the cellular environment of another largely maintains the NFRs of the donor, but adopts host nucleosome spacing and positioning (Hughes et al. 2012). Thus while gross occupancy may rely heavily on DNA sequence, precise positioning requires nuclear factors – particularly chromatin remodelling complexes.

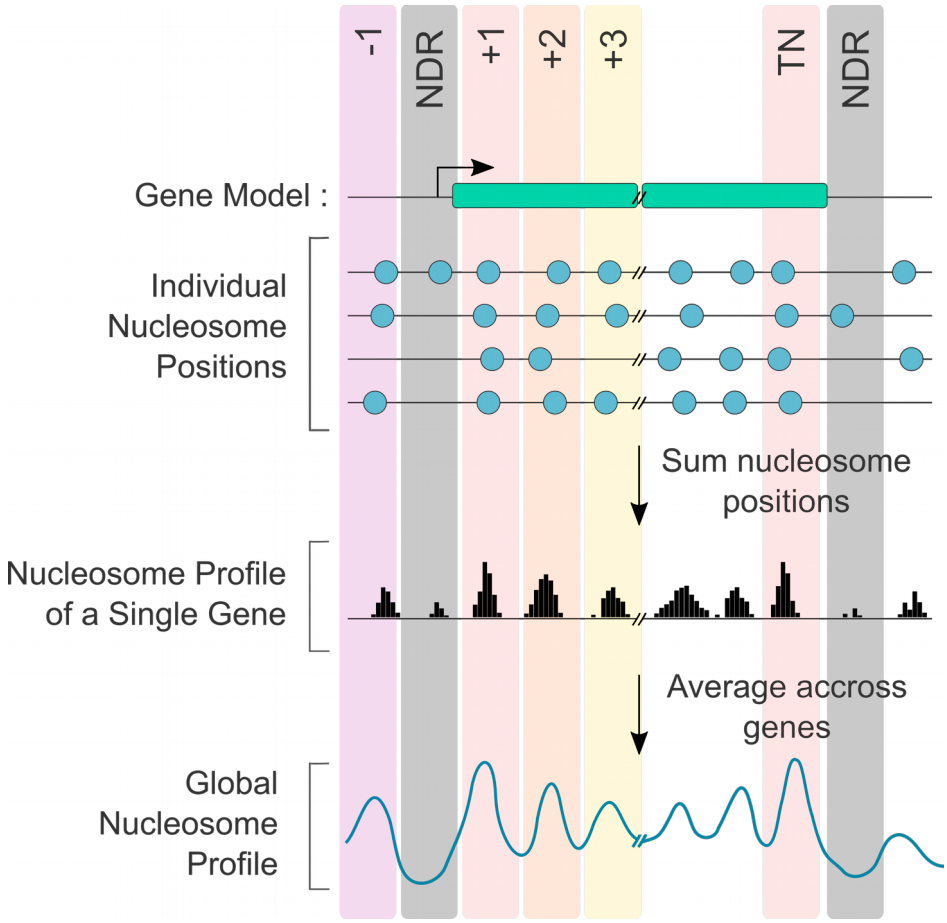

Fig1.3: Global Genic Nucleosome Profile.

MNase-sequencing on a range of organisms has revealed a common average genic nucleosome structure. The diagram illustrates how this global profile is a product of determining individual nucleosome positions at all genomic loci, scoring these to produce a genic nucleosome profile, then averaging across all genes. This profile therefore represents both the population-average, and the genome-wide average likelihood of nucleosome occupancy relative to genic features. Nucleosome positions, as highlighted on the diagram, are customarily numbered relative to the TSS: +1, +2, etc. downstream, and -1, -2, etc. upstream. This pattern is mirrored around the gene end, here we term these positions relative to the terminal nucleosome (TN) to distinguish from the TSS. Regions immediately usptream of the TSS and downstream of the TTS are typically depleted of nucleosomes, and termed nucleosome depleted regions (NDRs).

1.3 Chromatin Remodeling Complexes

1.3.1 SNF2 Proteins

The first chromatin remodelling complex (CRC) discovered was SWI2/SNF2 in *Saccharomyces cerevisiae* in screens for both defective mating type switching (SWI) and sucrose non-fermenting (SNF) mutants (Neigeborn & Carlson 1984; Peterson & Herskowitz 1992; Stern et al. 1984). The Snf2 ATPase was subsequently found to be the core catalytic subunit of the complex, and screens for suppressor mutants revealed a link with various chromatin components including histones (Kruger et al. 1995; Clark-Adams et al. 1988; Hirschhorn et al. 1992; Winston & Carlson 1992). *In vitro* studies were able to confirm the nucleosome remodeling activities of the purified complex (Côte et al. 1994; Hirschhorn et al. 1992; Laurent et al. 1993). A conserved array of remodelling complexes has since been discovered across all eukaryotes studied, with SNF2 family helicase-like ATPase proteins constituting the central catalytic subunit of each (Hargreaves & Crabtree 2011; Flaus et al. 2006). CRCs are essential for the establishment, maintenance and restructuring of chromatin during DNA transcription, replication and repair. The present study is mainly focused on the transcriptional roles of remodelers.

CRCs are able to perform various biochemical activities *in vitro*, including nucleosomes sliding, nucleosome disruption, nucleosome assembly and the exchange of core histones for histone variants (Tsukiyama et al 1994; Côte et al. 1994; Varga-weisz et al. 1997; Clapier & Cairns 2009). All CRCs share five basic properties: a core SNF2 ATPase translocase, affinity for nucleosomes over naked DNA, domains for recognition of histone modifications, domains for the regulation of the ATPase, and additional chromatin/TF recognition modules (Clapier & Cairns 2009). The ATPase binds nucleosomes at the SHL-2 region and translocates DNA to enact its remodeling activities; exactly how ATP hydrolysis is coupled to translocation remains unclear (Mueller-Planitz et al. 2013). The central Snf2 ATPase is necessary and sufficient for all basic remodelling activities *in vitro*, with the accessory proteins providing target specificity and regulation (Mueller-Planitz et al. 2013b; Clapier & Cairns 2009).

SNF2 proteins are of the helicase superfamily 2 (SF2), although only Ino80 actually possesses helicase activity (Gorbalenya 1988; Lusser & Kadonaga 2003). While the presence of SNF2 proteins is a defining feature of CRCs, the SNF2 family is large and

varied - containing TFs, repair factors, replication factors, and proteins of unknown function (Flaus et al. 2006). The chromatin remodelling SNF2 proteins are usually classified into four main groups based on homology of the core SNF2_n/DEAD/H ATPase domain and the presence of additional motifs (Fig1.4). These are the the SWI/SNF, ISWI, CHD and INO80 subfamilies (Clapier & Cairns 2009; Hargreaves & Crabtree 2011). It is important to note that while many SNF2 proteins are highly conserved across all eukaryotes, extrapolation between species can be challenging due to the gain/loss of subunits, expansion of gene families and increased specificity observed in higher eukaryotes.

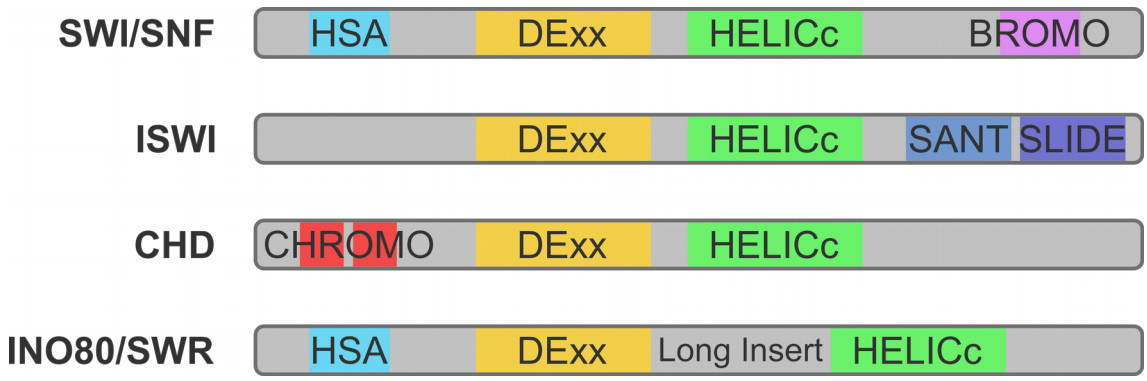

Fig1.4: Four Major SNF2 Family Chromatin Remodelers.

All chromatin remodeling complexes contain a core catalytic SNF2 protein. The chromatin remodelling SNF2 proteins are divided into four main families based on protein motifs. All four contain DExx and HELICc domains which provide the ATPase-dependent translocase activity. Additionally the four families contain additional, characteristic motifs. The SWI/SNF family have an N-terminal helicase-SANT-associated HSA domain which binds actin-related proteins and C-terminal bromo domains with affinity for acetylated histone tails. ISWI family SNF2 possess C-terminal SANT and SLIDE, or HAND-SAND-SLIDE motifs, involved in histone binding. The CHDs contain tandem chromodomains – associated with chromatin remodeling and possibly involved in methylated histone binding. Finally the INO80/SWR family also contain HSA domains, and a longer insert length between DExx and HELICc domains.

1.3.2 SWI/SNF

SWI/SNF subfamily Snf2 proteins are characterised by an N-terminal HSA (helicase-SANT) domain that binds actin related proteins, a C-terminal bromodomain involved in acetylated histone binding, and in higher eukaryotes, BRK and QLQ domains (Kim et al. 2003; Haynes et al. 1992; Tang et al. 2010). In *S. cerevisiae* the family consists of the archetypal Snf2, and Sth1 – the catalytic subunits of the SWI/SNF and RSC complexes respectively. Both complexes possess nucleosome sliding, evicting and remodelling functions *in vitro* (Kassabov et al. 2003; Dechassa et al. 2010). Sth1 is approximately ten fold more highly expressed than Snf2 and its knockout is lethal, while Snf2 mutants are viable. RSC is thought to play genome-wide roles in depleting nucleosome occupancy at constitutively expressed genes, and in positioning of +1 nucleosomes (Hartley & Madhani 2009; Narlikar et al. 2013). SWI/SNF on the other-hand appears to be primarily involved in context-dependent activation of inducible genes via promoter nucleosome eviction (Qiu et al., 2015; Shivaswamy & Iyer 2008; Schwabish & Struhl 2007; Peterson & Herskowitz 1992; Hirschhorn et al. 1992).

BRG1 associated factors (BAF) complex, the mammalian SWI/SNF complex homologue can incorporate either BRG1 (SMARCA4) or hBRM (SMARCA2) as the catalytic SNF2 core (Wang, Xue et al. 1996). In addition to the SNF2 and core components (BAF47, BAF155, BAF170) complex composition is biochemically diverse (Wang, Côte et al. 1996; Phelan et al. 1999). BRG1 but not BRM can also be incorporated into the PBAF complex, with subunit homology to yeast RSC. The BAF complex is a key tumour suppressor, exhibiting subunit mutation in ~20% of all human tumours in addition to epigenetic repression mechanisms (Kadoch et al. 2013; Shain & Pollack 2013; Versteege et al. 1998; Modena et al. 2005; Wilson & Roberts 2011). Loss of Brg1 or the essential subunit Snf5/Ini1 is embryonic lethal in mice and heterozygotes are tumour prone (Bultman et al. 2000; Klochendler-Yeivin et al. 2000). BRM knockout contrastingly has minimal phenotypic impact (Reyes et al. 1998). The BAF and PBAF complexes exhibit highly heterogeneous, cell-type specific composition and functions. Such roles including: neurogenesis (Wu et al. 2007), myogenesis (de la Serna et al. 2006), hepatocyte differentiation (Gresh et al. 2005), HIV infection (Rafati et al. 2011), cell-cycle control (Nagl et al. 2007), and many more. In summary, the mammalian SWI/SNF complexes represent context dependent transcriptional regulators with pleiotropic effects.

1.3.3 ISWI

The imitation switch (ISWI) subfamily of remodelers was initially identified in *Drosophila*, based on homology to the Brahma gene (Elfring et al. 1994; Tsukiyama & Wu 1995). ISWI is the sole family member in *Drosophila*, but there are two in *S. cerevisiae:* Isw1 and Isw2 (Tsukiyama et al. 1999), and two in mammals: SNF2H and SNF2L (Aihara et al. 1998). The characteristic feature of ISWI family Snf2 proteins is the C-terminal histone binding SANT (y**S**WI3, y**A**DA2, h**N**CoR, h**T**FIIIB) and DNA binding SLIDE (**S**ANT-**l**ike **I**SWI) domains which recognise intrinsically curved DNA sequences (Grüne et al. 2003; Dang & Bartholemew 2007; Yamada et al. 2011; Rippe et al. 2007). *In vitro* studies have demonstrated nucleosome remodelling, rearrangement and assembly actions of the purified *Drosophila* protein (Corona et al. 1999; Tsukiyama et al. 1999; Varga-weisz et al. 1997). In *S. cerevisiae* ISWI proteins are incorporated into three simple complexes; Isw1a, Isw1b and Isw2. *Drosophila* and mammalian complexes are more diverse including the ACF, CHRAC, NURF, WICH and NoRC complexes (Deuring et al. 2000; Corona & Tamkun 2004).

ISWI in higher eukaryotes is abundantly and ubiquitously expressed, with *Drosophila* ISWI and mammalian SNF2H and SNF2L proteins being essential for cell viability and development (Deuring et al. 2000; Stopka & Skoultchi 2003; Arancio et al. 2010). Yeast Isw1 and Isw2 null cells on the other-hand are viable and largely phenotypically unaffected by remodeler loss. ISWI complexes are generally considered repressive, facilitating chromatin formation and compaction, and regulating nucleosome phasing to restrict RNAPII access (Corona & Tamkun 2004; Lusser et al. 2005). ISWI loss in *Drosophila* results in dramatic chromosome de-compaction (Deuring et al. 2000; Corona et al. 2007), de-repression of differentiation in germ and somatic stem cells (Xi & Xie 2005) and reduction of linker histone H1 incorporation (Corona et al. 2007; Siriaco et al. 2009). However complexes such as NURF are known to be more disruptive (Corona & Tamkun 2004). ISWI proteins have also been associated with active transcription, and are required for efficient transcription termination (Morillon et al. 2003; Mellor & Morillon 2003; Zentner et al. 2013). Expression studies in *Drosophila* ISWI mutants do predominantly display de-repression upon ISWI loss, however only at a small subset of genes (Corona et al. 2007). Yeast Isw mutants equally have a minimal impact on transcription (Hughes et al. 2000; Fazzio et al. 2001).

1.3.4 CHD

Chromodomain, helicase, DNA binding (CHD) family remodelers are characterised by the presence of tandem chromodomains at their N-terminus. They are present in all eukaryotes but highly variable in number and complexity, with only one monomeric protein in yeast but at least nine complexes in mammals. CHDs are further divided into three classes: class I (CHD 1-2), class II (CHD3-5), and class III (CHD 6-9) (Clapier & Cairns 2012).

Class I CHD proteins posses SANT and SLIDE domains structurally related to those of ISWI (Ryan & Owen-Hughes 2011; Sharma et al. 2011; Woodage et al. 1997). Chd1 is the most studied example, and the only CHD subfamily Snf2 protein in *S. cerevisiae*, however its knockout results in only a mild sensitivity to 6-azouracil treatment (Tsukiyama et al. 1999). Chd1 associates with RNAPII and is thought to be involved in re-establishing nucleosomes displaced during elongation (Simic et al. 2003; Marfella & Imbalzano 2007; Radman-Lavaja et al. 2012), suppressing cryptic transcription (Smolle et al. 2012; Smolle & Workman 2013) and in regulating transcription termination (Alen et al. 2002). Chd1 is the sole class I CHD in *Drosophila*, and null mutants display sterility (McDaniel et al. 2008; Murawska & Brehm 2011). *Drosophila* Chd1 associates with transcriptionally active puffs on polytene chromosomes, further supporting a role in active transcription (Stokes et al. 1996). Humans possess CHD1 and CHD2, expressed in all major tissues (Woodage et al. 1997). CHD1 is enriched at active promoters and is thought to associate with elongating RNAPII to regulate co-transcriptional events including initiation, elongation, splicing and termination (Sims & Wade 2011; Murawska & Brehm 2011). How CHD1 is targeted to promoters is unclear but it associates with Mediator (Lin et al. 2011) and has been shown to have H3K4me2/3 binding activity (Flanagan et al. 2007). However the importance of H3K4me binding is contentious, and yeast Chd1 do not possess this activity (Sims et al. 2005). Mammalian CHD1 is further involved in maintenance of pluripotency (Gaspar-Maia et al. 2009). CHD2 is required for mammalian development, with homozygous truncated CHD2 mice non-viable, while heterozygous mice display reduced survival rates (Marfella et al. 2006). Recently CHD2 mutations in humans have been linked to developmental defects (Kulkarni et al. 2008) and epileptic encephalopathies (Carvill et al. 2013; Lund et al. 2014; Courage et al. 2014; Chénier et al. 2014; Suls et al. 2013).
Class II CHDs are characterised by C-terminal PHD domains. The class II CHDs in

Drosophila and mammals CHD3/Mi-2α and CHD4/Mi-2β are essential components of the Mi-2/Nucleosome remodelling and deacetylase (NuRD) complex, which functions in gene repression during differentiation, chromatin assembly and repair (Wade et al. 1998; Zhang et al. 1998; Xue et al. 1996; Lai & Wade 2011). The combined remodeling and histone de-acetylation functions are thought to be important for the dense packing of hypoacetylated nucleosomes in heterochromatin (Denslow & Wade 2007; Wang & Zhang 2001). Importantly though NuRD, and CHD4 independently of NuRD, are not purely repressive, having complex transcriptional roles (Kim et al. 2014; Miccio et al. 2010; Reynolds et al. 2012; Shimbo et al. 2013). Expression of the type II CHDs is developmentally regulated with Mi-2α detected early in development and Mi-2β later (Khattak et al. 2002). Null mutants in *C. elegans* and *Drosophila* are lethal (Khattak et al. 2002; von Zelewsky et al. 2002), and disruption of NuRD function in mammals is associated with cancers and aging (Lai & Wade 2011; Pegoraro et al. 2009).

The most studied type III CHD is *Drosophila* Kismet, a trithorax group protein important for HOX gene expression (Daubresse et al. 1999; Srinivasan et al. 2005). This role in development is conserved in human homologues; CHD7 mutations are the most common cause of CHARGE syndrome which manifests a plethora of developmental defects (Zentner et al. 2010; Lalani et al. 2006), and Chd8 is linked to Autism spectrum disorders (Bernier et al. 2014; Cotney et al. 2015). Mammals possess five members of class III CHDs (CHD5-9) with highly varied expression and roles. Mammalian CHD5 is mainly restricted to neural tissues and testes (Thompson et al. 2003) and plays roles in neurogenesis and spermatogenesis (Egan et al. 2013; Li & Mills 2014). CHD6 mutant mice are viable (Lathrop et al. 2010), whereas CHD7 and CHD8 homozygous knockouts are lethal (Hurd et al. 2007; Bosman et al. 2005; Nishiyama et al. 2004). CHD7 is widely expressed but particularly important for neural development, including neural crest formation (Bosman et al. 2005; Bajpai et al. 2010), and maintaining the quiescence of neural stem cells (Jones et al. 2014). CHD8 is involved with canonical Wnt/β-catenin signalling and interacts with CTCF, possibly linking CHD8 to insulator activity (Ishihara et al. 2006; Thompson et al. 2008; Yates et al. 2010). Finally CHD9 is poorly understood but appears to be involved in skeletal tissue development (Shur et al. 2005; Marom et al. 2006). In general, the type III CHD proteins play highly specialised and distinct developmental roles.

1.3.5 INO80 and SWR

Inositol requiring 80 (INO80) was identified as a mutant for defective induction of gene expression in low inositol and homology with ISWI (Ebbert et al. 1999; Shen et al. 2000). Both Ino80 and Swr SNF2 proteins possess a distinguishing split ATPase domain, with Rvb1/2 and Arp protein binding sites inserted between the DExx and HELICc domains of the ATPase (Morrison & Shen 2009). Ino80 has roles in repair and transcriptional activation; Swr and Ino80 also play reciprocal roles in the deposition and removal, respectively, of H2A.Z (Htz1p), commonly flanking NDRs in yeast (Krogan et al. 2003; Kobor et al. 2004; Mizuguchi et al. 2004; Papamichos-chronakis et al. 2010; Albert et al. 2007). The Swr1 homologues are SRCAP and p400 in mammals (Gévry et al. 2007; Ruhl et al. 2006); Domino in *Drosophila* and Ino80 is present in yeasts, flies and mammals (Flaus et al. 2006; Clapier & Cairns 2009).

In addition to its roles in H2A.Z deposition, Swr is able to act as a H2A.Z histone chaperone (Hong et al. 2014). Histone acetylation influences the efficiency of H2A.Z deposition via interaction with the SWR-C Bdf1 subunit (Zhang et al. 2005; Watanabe et al. 2013). The dominant targeting mechanism however is thought to be the binding of both nucleosome free DNA and histones, localising activity to NFR proximal nucleosomes (Yen et al. 2013; Ranjan et al. 2013). This thus fits with a common theme of acetylation and other histone marks fine-tuning CRC occupancy/activity rather than acting as a driving mechanism. H2A.Z is essential for viability of higher eukaryotes (van Daal & Elgin 1992; Faast et al. 2001), and reduces growth in yeast (Santisteban et al. 2000).

1.3.6 Spacing Remodelers

The ability of the ISWI and CHD families to sample DNA linker lengths through their SANT and SLIDE domains (Sharma et al. 2011; Yamada et al. 2011) is thought to modify the behaviour of the ATPase module to allow even spacing of nucleosomal arrays rather than disruption (Racki et al. 2009; Bouazoune & Kingston 2012). This spacing activity has been demonstrated *in vitro* (Tsukiyama et al. 1999) and nucleosome mapping in *S. cerevisiae* Isw1, Isw2 and Chd1 double and triple mutants support *in vivo* roles in array phasing and spacing (Gkikopoulos et al. 2011). Binding of extra-nucleosomal DNA is required to stimulate remodelling activities of these proteins

in vitro (Gangaraju & Bartholomew 2007; Zofall et al. 2004; Dang et al. 2007; McKnight et al. 2011), and it has been proposed that they can only bind the NDR and act on disrupted arrays, such as in the wake of RNAPII elongation (Zentner et al. 2013). Indeed remodeler binding levels are correlated with RNAPII elongation rate and nucleosome turnover (Zentner et al. 2013). Conversely, as discussed above, these complexes regulate transcription and co-transcriptional processes. However this relationship with transcription is complex, with minimal influence of individual ISWI or CHD loss on transcription or nucleosome positioning observed in yeast (Gkikopoulos et al. 2011). CHD and ISWI family remodelling complexes are thus referred to here as 'spacing remodelers'. Exploring how spacing remodelers function both individually and in combination, to establish and maintain *in vivo* nucleosome positioning and chromatin structure is the primary focus of the present study.

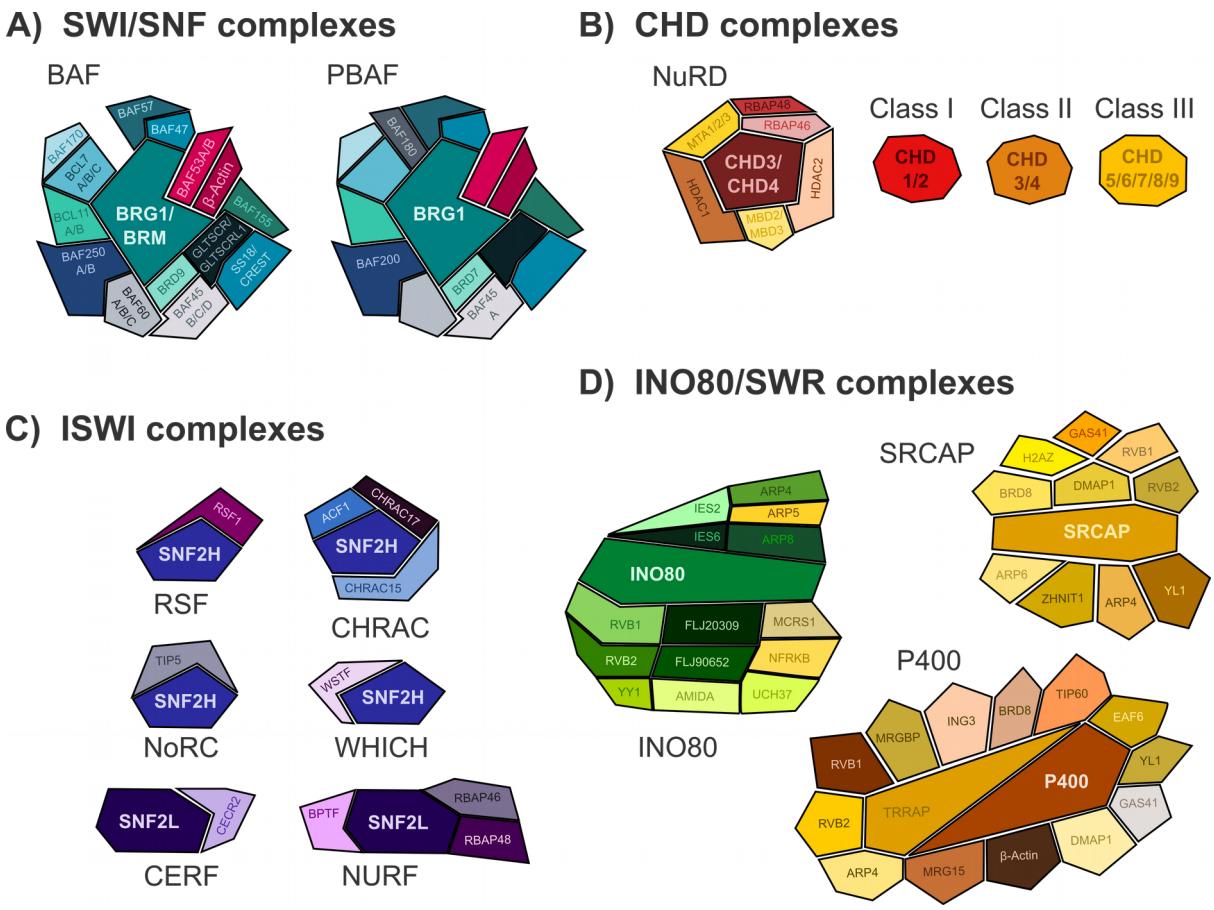

Fig1.5: Subunit compositions of major chromatin remodelling complexes.

The potential subunit compositions for some of the major mammalian chromatin remodelling complexes are diagrammed for the four main families of remodelers: SWI/SNF, CHD, ISWI and INO80/SWR. The core SNF2 ATPase is highlighted in bold for each complex, alternative subunits are separated by slashes. BAF and PBAF complexes are highly similar, and only variable subunits are labelled for PBAF.

1.4 *Dictyostelium discoideum*

1.4.1 *Dictyostelium* as a Model Organism

The amoebozoa likely branched from the evolutionary line towards animals after plants but prior to fungi (Eichinger et al. 2005); the best studied member is the Mycetozoa, *Dictyostelium discoideum*. *Dictyostelium* are soil dwelling amoeba which feed on bacteria and undergo binary fission, discovered by Kenneth Raper in 1933 (Raper 1935). *Dictyostelium* is termed a social amoeba due to its vegetative unicellular growth when provided with adequate nutrients, switching to a simple multicellular development process upon starvation (Loomis 2014). Due to the importance of cyclic adenosine monophosphate (cAMP) mediated chemotaxis in the developmental cycle and as a bacterial attractant in growth (Bonner 1947; Konijn et al. 1969), chemotaxis has been a key area of study in *Dictyostelium;* it has also proved a fruitful model system for chemotaxis in higher eukaryotes. Its simple and rapid development cycle also provides a useful model for studying developmental processes. Furthermore uncoupling of growth and development allows disruption and study of developmental factors that may be lethal in many obligate multicellular organisms. In addition to bacterially grown *Dictyostelium*, axenic mutant strains have been isolated which are capable of growth in liquid axenic media containing inorganic salts, glucose, peptone and yeast extract, facilitating standardised growth (Sussman & Sussman 1967; Watts & Ashworth 1970). These axenic strains were isolated through a process of repeated subculture with decreasing amounts of fetal calf serum and liver extract (Watts & Ashworth 1970). The causative mutations allowing axenic growth in these strains were recently found to be harboured within genes encoding a RasGAP - Neurofibromin, loss of which allows formation of enlarged macropinocytic vesicles (Bloomfield et al. 2015). Efficient methods have been established for genetic manipulation, including for the establishment of multi-knockout and knock-in strains (Faix et al. 2004). Furthermore, *Dictyostelium* has a compact, sequenced 34 Mb haploid genome and a dedicated database for genome annotation (dictybase.org; Eichinger et al. 2005; Basu et al. 2013). Thus *Dictyostelium* also provides a useful model for modern genomics.

1.4.2 *Dictyostelium* Development

Upon starvation or high cell density, ~1x10^5 *Dictyostelium* cells will aggregate into loose mound structures, and develop an extracellular matrix to form the tight mound (Gerisch et al. 1975; Chisholm & Firtel 2004). At this stage they may form a mobile slug structure that can migrate phototactically to an optimal position for development into the final fruiting body structure. The fruiting body consists of a bolus of spores on a cellulosic stalk and basal disc. The two cell types, vacuolised stalk and dormant spore cells, are preceeded by pre-stalk cells that make up the anterior quarter of the slug, and pre-spore cells that constitute the posterior (Raper 1950). This developmental cycle takes approximately 24 hours from starvation to completion (Raper 1950; Chisholm & Firtel 2004).

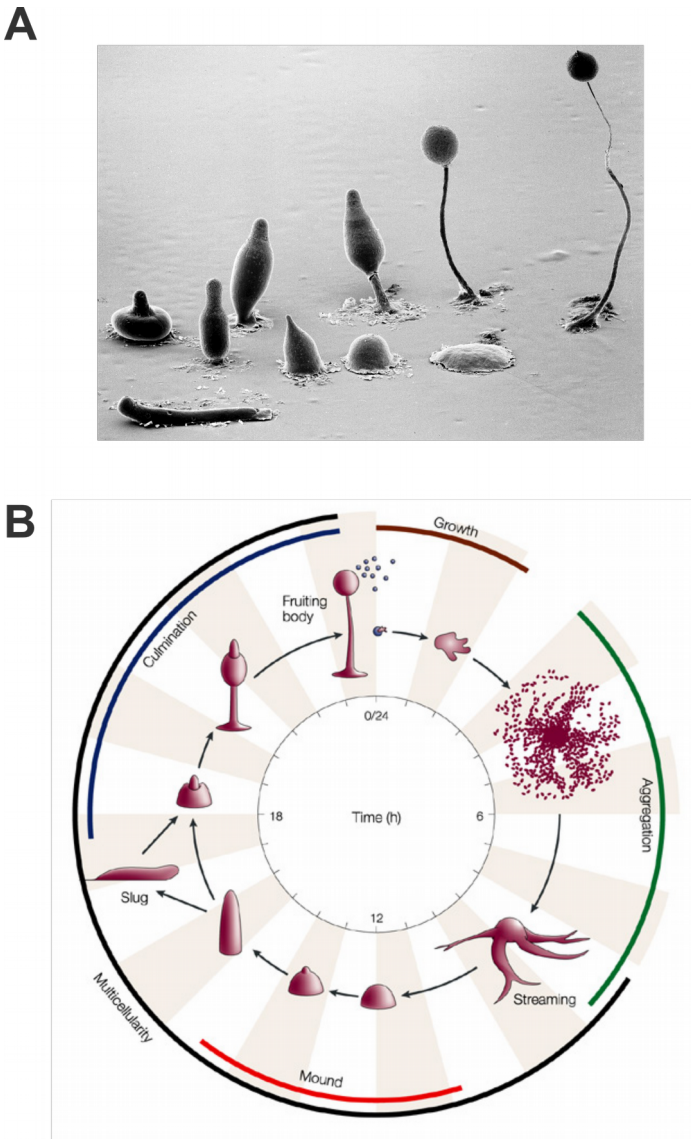

Fig1.6: *Dictyostelium discoideum* in Growth and Development.

Dictyostelium grow unicellularly in soil but upon starvation aggregate into a mutlicellular mound before progressing through a series of well defined morphological changes, ultimately forming the final fruiting body structure. A. Scanning-electron micrograph of developmental stages/morphological structures. B. Diagram of the timing of *Dictyostelium* development. Reproduced with permission from Fey et al. 2007.

1.4.3 The *Dictyostelium* Genome and Chromatin Architecture

The genome of the Ax4 strain of *Dictyostelium* consists of a 34 Mb nuclear genome across 6 chromosomes (Eichinger et al. 2005) containing ~12,700 protein coding genes (Gaudet et al. 2011), a 55 kb mitochondrial genome (Ogawa et al. 2000) and an extrachromosomal palindrome containing the ribosomal RNA genes (Sucgang 2003). Three other dictyostelids have also been sequenced: *D. purpureum* (Sucgang et al. 2011), *D. fasciculatum* and *Polysphondylium pallidum* (Heidel et al. 2011; Basu et al. 2013). The most striking feature of the *Dictyostelium* genome is it's high AT content, with a GC content of 22.4% overall, ranging from 27% in exons to 12% in introns (Eichinger et al. 2005). The majority of genes possess introns but typically of only ~150 bp in length (Gaudet et al. 2011). Although haploid, cells enter S phase immediately following mitosis, so contain a duplicated genome for the majority of the cell cycle (Muramoto & Chubb 2008). Gene density is high at ~62% of the genome, and with roughly double the genes contained in the *S. cerevisiae* genome it provides a useful intermediate on the spectrum of transcriptome complexity.

The chromatin environment of *Dictyostelium* includes a diverse number of histone variants, histone post-translational modifications and nuclear factors. The complement of histone proteins includes a canonical H1 linker histone, H2A.Z and H2AX, a predicted centromeric H3 variant (H3v1, Dubin et al. 2010), and a number of less well characterised histone variants (Stevense et al. 2011). Most common histone modifications have been detected by mass-spectroscopy including H3 K4, K36 and K79 methylation, H3 K9 and K27 acetylation and H3K9 di- and trimethylation (Stevense et al. 2011). The heterochromatin is late replicating, and CpG dinucleotides are under-represented suggesting cytosine methylation (Eichinger et al. 2005). Interestingly, the average placement of the first genic (+1) nucleosome is similar to most metazoans, at a distance ~115 bp downstream of the TSS, and homologs of the NELF pausing factor are evident (Chang et al. 2012). This has been suggested to be indicative of RNA polymerase pausing, only otherwise documented in metazoans (Chang et al. 2012; Mavrich et al. 2008; Valouev et al. 2011). Hence *Dictyostelium* chromatin possess a number of features usually associated with higher eukaryotes, possibly indicating their importance to multicellular development. On the other hand, a number similarities are also observed with yeast: the three main H3 genes appear to encode a H3.3-like histone, a variant normally incorporated into transcribed genes in a replication

independent manner in higher eukaryotes (Stevense et al. 2011; Ahmad & Henikoff 2002). *Dictyostelium* also appears to lack H3K27 methylation and polycomb group components (Stevense et al. 2011).

MNase-seq has been conducted in WT *Dictyostelium* by Chang et al. (2012) and our own group (Platt 2013). Resultant nucleosome maps are highly similar despite varying methodologies, sequencing platforms and cell strains, indicating the robustness of this technique. The +1 nucleosome is positioned ~70 bp downstream of the ATG initiation codon, the NDR is approximately 170 bp wide, and arrays have an average nucleosome repeat length of ~170 bp (Platt 2013; Chang et al. 2012). Compared to yeast profiles, intergenic and intronic sequences are more nucleosome depleted, possibly as a result of high AT content affecting both nucleosome occupancy and MNase digestion (Platt 2013). A very slight increase in spacing of ~3 bp is observed in chromatin at aggregation (Chang et al. 2012) and mound stages of development (Platt 2013). Furthermore, our lab has shown that a subset of developmentally regulated genes representing ~20% of the genome are dramatically remodelled between growth and mound stages (Platt 2013). Importantly though not all remodelled genes have expression changes and not all developmentally regulated genes undergo remodelling.

1.4.4 Chromatin Remodelers in *Dictyostelium*

Members of each of the main remodeler families are present in *Dictyostelium*, plus more unusual SNF2 proteins such as JBP2 (Clapier & Cairns 2009). *Dictyostelium* CHD family remodelers have previously been examined in our lab (Platt et al. 2013). In addition to the class I CHD protein (ChdA) homologous to yeast Chd1, *Dictyostelium* possesses two additional CHDs. ChdB lacks a PHD finger but contains a CHDCT2 domain – two class II associated motifs, however overall ChdB shows closest homology to Class III proteins (Platt et al. 2013). ChdC is more clearly categorised as class III, being closely related to the Chd6-9 (Platt et al. 2013). Null strains have been generated and phenotypically characterised for the three core-SNF2 CHD proteins (Platt et al. 2013). Additionally, an arp8-null strain is also available (unpublished), arp8 is an essential component of the INO80 complex in yeast, and its knockout phenocopies Ino80 SNF2 mutation.

1.5 Project Aims

Chromatin remodelers are essential for all of the fundamental processes of chromatin metabolism, exemplified by their conservation across all eukaryotes (Flaus et al. 2006). *In vitro* studies have provided fundamental understanding of their remodeling mechanisms; and *in vivo* studies, primarily in *S. cerevisiae*, have provided insights into their general biological functions. Nonetheless, why such a diverse array of energetically expensive complexes with common catalytic activities are required remains unclear. And a broader understanding of how remodeling activities enact cell-type specific transcriptional programs is yet lacking. This is particularly true of the spacing remodelers, loss of which individually has minimal effect on phenotype, chromatin structure or transcription in yeasts, yet are essential to higher eukaryotes. *Dictyostelium* provides a tractable model with surprisingly metazoan-like chromatin and a simple developmental program; representing a unique system to explore remodeler function while avoiding the KO lethality and inhibitory costs involved in studying remodelers in higher eukaryotes. I therefore aim to establish *Dictyostelium* as a novel model in which to conduct exploratory analysis of remodeler functions and interactions.

To this end, I aim to generate null strains for the remaining four core remodelers in *Dictyostelium*: Isw, Snf2a, Snf2b and Swr1. Phenotypic affects across growth, development and chemotaxis will then be compared for all core remodelers. MNase-sequencing will be performed on newly generated Isw null cell lines. This *Isw*$^{-}$ MNase-seq data, together with previously generated, but un-analyed *ChdA*$^{-}$ and *ChdB*$^{-}$ MNase-seq data, and published *ChdC*$^{-}$ data, will provide high-resolution, genome-wide nucleosome maps for all spacing remodeler mutants. Finally, RNA-sequencing will be conducted in the *Isw*$^{-}$ cell line, and analysed alongside the published transcriptional profiles of the CHD null cell lines. The proposed work will generate a comprehensive resource on the impact of remodeler loss. Detailed bioinformatic analysis on these data will generate novel insights into the distinct and combinatorial roles of the CHD and ISWI family remodelers in establishing and maintaining primary *in vivo* chromatin structure, and the effects of chromatin disruption on transcriptional regulation.

Chapter 2:

Materials and Methods

2.1 Dictyostelium Strains and Cell Culture

Ax2 was used as the wild-type (WT) strain in all cases otherwise stated, and was the parent strain of all mutants generated. Cells were grown axenically either in shaking culture or adhered to bacteriological plates in HL-5 medium (Formedium; 14 g/L peptone, 7 g/L yeast extract, 13.5 g/L glucose, 0.5 g/L KH_2PO_4, $NaHPO_4$) supplemented with 100 µg/ml Streptomycin-sulphate. For selection of mutants, HL-5 was also supplemented with either 40 µg/ml G418 or 10 µg/ml Blasticidin. Cells were also grown on bacterial lawns of *Klebiella aerogenes* on SM agar plates (Formedium; 17 g/L agar, 10 g/L peptone, 1 g/L yeast extract, 10g/L glucose, 1.9 g/L KH_2PO_4, 1.3 g/L $K_2HPO_4.3H_20$, 0.49 g/L $MgSO_4$). Washing and starving of cells was carried out in KK2 buffer (Formedium; 2.25 g/L KH_2PO_4, 0.51 g/L K_2HPO_4) or KK2 agar (KK2 buffer + 18 g/L agar). Cells were grown at 22˚c, and centrifugation steps carried out at 500 x g for 2 minutes.

2.2 Cloning

Plasmid digests were generally carried out with 10 U RE/µg of DNA with enzymes from New England Biolabs under manufacturer recommended conditions. DNA fragments were checked by agarose gel electrophoresis with EtBr staining, final plasmids were also sequenced. Ligation steps were carried out with T4 DNA ligase (New England Biolabs) under recommended conditions, and generally a 3:1 insert to vector ratio.

2.2.1 Genomic DNA Extraction

10^7 cells were pelleted, washed once in KK2 and lysed in 750 µl DNAzol (Invitrogen), 350 µl of 100% ethanol added and incubated at RT for 2 min to precipitate DNA. Precipitated DNA was centrifuged at 4000 x g for 5 min at RT and washed twice with 70% ethanol, air dried and resuspended in 50 µl 8 mM NaOH and 7.95 µl 0.1M HEPES buffer (pH 7.5).

Quick extraction of DNA for PCR screening was carried out as follows. Cells in a 96-well plate were resuspended in 25 µl of KK2, 10 µl transferred to PCR tubes and 10 µl lysis buffer (50 mM KCl, 10 mM TRIS pH 8.3, 2.5 mM $MgCl_2$, 0.45% NP40 and 0.45% Tween20, 0.8 µg/µl Proteinase K) added. After 2 minutes incubation at RT, Proteinase K was inactivated by 1 minute incubation at 95°c.

2.3.2 Knockout Construct Design

Regions of ~1 kb upstream of the ATG and downstream of the ATPase domain were amplified from genomic DNA using Phusion high-fidelity DNA polymerase (New England Biolabs) and the primers in table 2.1. The inner primers were designed to incorporate RE sites SalI and NdeI, outer primers were then used to combine the first two PCR products. The ~2 kb fragment was cloned into the TOPO blunt II vector (Life Technologies) and confirmed via restriction digest. The vector and plasmid containing the resistance cassette, pLPBLP (Faix et al., 2004) were cut with SalI and NdeI and ligated to create a floxed Blasticidin cassette flanked by homologous arms to the gene of interest. Four constructs were created: pCR-Blunt-II-TOPO-Isw+Bsr, pCR-Blunt-II-TOPO-Snf2a+Bsr, pCR-Blunt-II-TOPO-Snf2b+Bsr and pCR-Blunt-II-TOPO-Swr1+Bsr. Constructs were linearised, restriction enzymes heat inactivated and ethanol precipitated (1/10th volume 3M sodium acetate, 3 volumes 100% ethanol) prior to transformation.

Target	Forwards Primer (5'->3')	Reverse Primer (5'->3')	Target Coordinates
Isw Upstream	ATAACATATTGTCGTGAAGG	CATATGGCGGTCGAC AATATTGGCGGGTAAATTTG	Chr6: 2252855 - 2253920
Isw Downstream	GTCGACCGCCATATG TTGACAATAGTGGAAAGATG	TCTGGAAGTTCACCTTTATC	Chr6: 2256451 - 2257410
Snf2a Upstream	CATGTTCAGTAATGTCAACG	CATATGCGGCGCGTCGACATCT TTTATTTATTTCGCTACC	Chr4: 2919477 - 2920404
Snf2a Downstream	GTCGACGCGCCGCATATGGGT GAGTTGTGGGCATTG	GATCTCCAATTTATCGGTGG	Chr4: 2924468 - 2925333
Snf2b Upstream	GGCCCTTGAAAGATATCGATAT G	AACAGCGCGCATGTA ATGGAATAGACAGCAATAAGGG	Chr1: 4513841 - 4512498
Snf2b Downstream	ATTACATGCGCGCTGTTATCAT TCAACGTCTTCATAAGG	TCTTCAGGAGAACGAGCAATC	Chr1: 4506517 - 4505624
Swr Upstream	CGGATCCTATAGTTACAGATG	CATATGCGG AGCGTCGACC GATGAACTTTCTCTTCTCTG	Chr1: 465026 - 466183
Swr Downstream	GTCGACGCTCCGCATATG CTATCCATCTTATCAACGTATG	GAGTATTATCATCAACATCTACC	Chr1: 469062 - 469863

Table 2.1: Primer Pairs for Construct Generation. Underlined region of sequence highlights primer tail with complementary sequence and restriction sites.

2.3.3 Dictyostelium Transformation

Dictyostelium were transformed via electroporation as previously described (Gaudet et al. 2007). Briefly, 10^7 Ax2 cells were washed twice in ice cold electroporation buffer (KK2 + 50 mM sucrose), and resuspended in 800 μl before transferring to 4 mm electroporation cuvettes (Cell Projects). 15 μg of linearised plasmid DNA was added, mixed and incubated for 10 min on ice. Cells were electroporated at 1 kV, incubated on ice 10 min, 8 μl 0.1M $MgCl_2$ added and incubated at 22°c 15 min. For knockout transformations, cells were resuspended in 75 ml HL5 media with 100 μg/ml streptomycin sulphate, transferred to 96 well plates and grown overnight. Media was exchanged for selective media containing 10 μg/ml blasticidin after 24 hours, and every 2 days following until clones were confluent. Clones were then screened via PCR for the correct genotype.

2.4 Knockout Screening

DNA was extracted from confluent clones using the rapid DNA extraction method described above (section 2.3). Primers (Table2.2) were designed to amplify regions spanning the insert-to-genomic border (+ve primers) or within the genomic region targeted for deletion (-ve primers). PCR was performed using GoTaq Green Master Mix (Promega) and the following PCR program: 92°c 1min, 52°c 30s, 68°c 1min x 30 cycles, 10 min 68°c final extension. Products were run on 1% agarose gels, clones with bands from +ve primers and no band in –ve were considered knockouts.

Primer Set	Forwards (5'->3')	Reverse (5'->3')
Isw +ve	GATAAAGCTGACCCGAAAGC	CCAAAGTCTGGTTCCTCCTC
Isw -ve	GATGCAGTTGTTGTTGGAGC	AGATTGGTGTCTGCTTTGGT
Snf2a +ve	GGACCAACCGATATTGTAATTC	CTTGTTGAGAAATGTTAAATTGATCC
Snf2a -ve	CACGTGATACCGAAGGTTATAG	GTAGTTGATTGGAGTGGTGAAG
Snf2b +ve	GATAAAGCTGACCCGAAAGC	CGACCTCTTTAGTGATCCAAC
Snf2b -ve	GCACCAGGTCAATTCAATGC	TCTTCAGGAGAACGAGCAATC
Swr +ve	GATAAAGCTGACCCGAAAGC	GTTGTTTTGTAACAGTACCATATG
Swr -ve	CCACCTAAACATACTCATATC	GTTCCTCTAATAACTTTGATGG

Table2.2: Primers for Knockout Screening. Primers used for PCR screening of potential KO clones.

2.5 Western Blotting

Western blotting was performed for confirmation of Isw and double KO strains and assay of relative Isw protein levels. Cells were washed before lysis in 1x NuPAGE LDS Sample Buffer (Life Technologies) with 5% β-mecaptoethanol and 1x protease inhibitors (Roche) and incubated at 70°c for 10 min. Cell extract was loaded on either NuPAGE Novex 3-8% Tris-Acetate, or NuPAGE Novex 4-12% Bis-Tris Protein Gels (Life Technologies). Western blotting to a nitrocellulose membrane was carried out overnight at 13V and 4°c using the XCell II Blot Module (Life technologies) and NuPAGE Transfer Buffer (Life Technologies) supplemented with 10% methanol.

Membranes were blocked in 5% milk in TBST (tris-buffered saline + 0.1% Tween 20) 1 hour at RT prior to primary antibody incubation in 5% milk TBST, overnight 4°c. Membranes were washed three times in TBST and incubated with the appropriate secondary HRP-linked antibody for 2 hours at RT. Membranes were washed three times and incubated with SuperSignal West Pico Chemiluminescent Substrate (Thermo Scientific), 5min RT. Membranes were exposed to Carestream Kodak BioMax MR film (Sigma-Aldrich) and developed, or imaged with the GeneGnome imager (Syngene). Band intensities were quantified using ImageJ software (Schneider et al. 2012).

Primary antibodies used: polyclonal anti Isw antibodies raised in rabbit (70-day protocol) using synthesized Isw peptides (peptide sequence: EEPDFGDLSKEEQDLKER, amino acid positions 906-923) (Perbio/Thermo Scientific; concentration 2.5 µg/ml), ChdA, ChdB and ChdC polyclonal antibodies were produced by Drs James Platt and Benjamin Rogers (Platt 2013; Rogers 2010; all used at 2.5 µg/ml), monoclonal anti-RNA polymerase II (clone CTD4H8) antibody (Merck Millipore), and monoclonal anti-actin (plant) (clone 10-B3) antibody (Sigma-Aldrich; used at 1 µg/ml).

2.6 Multinucleate Assay

WT and Swr cells were grown either in suspension or adhered to Nunc Lab-Tek II Chamber Slides (Thermo Scientific) for 5 days. Cells were fixed in 4% formaldehyde in phosphate buffered saline (PBS) for 15min, washed and stained with Concanavalin A (ConA) FITC conjugate at 10 ng/ml in PBS for 10 min, washed and stained with 300 nM 4',6-Diamidino-2-Phenylindole, Dihydrochloride (DAPI) (Life Technologies) in PBS

for 5 min, and washed. Imaging was carried out on an Olympus 1X71 inverted microscope and processed using a custom CellProfiler pipeline (Carpenter et al. 2006).

2.7 Time Lapse Development Assay

1.5 ml of KK2 agar was added to 6 well plates, 5 x 10^6 cells/condition were washed twice in cold KK2, resuspended in 1ml KK2 and added to each well. After 15min incubation to allow adherence, excess KK2 was aspirated and plate transferred to an Olympus 1X71 inverted microscope. Images were taken in 3 by 3 grid of each well every 2 minutes for 25 hours, and image stacks for each well combined with ImageJ (Schneider et al. 2012).

2.8 Chemotaxis Assay

5 x 10^7 cells were washed twice in KK2 and placed in shaking suspension for 5 hours with 100 nM pulses of cAMP every 6 minutes. Cells were then diluted 1:4 in KK2 and added to a Zigmond chamber (Zigmond, 1988) (Neuro Probe), and a cAMP gradient established using 1 μM cAMP and KK2 in respective wells. After 20 min incubation, cells were imaged every 6 seconds in 6 fields over 15min at 20x magnification using differential interference contrast (DIC) on an Olympus 1X71 inverted microscope. DIAS 3.4.2 image analysis software (Soll Technologies Inc.) was used to track cells and calculate their speed, directionality, polarity and chemotactic index parameters (Kay et al., 2008). A minimum of 100 cells was analysed per condition over at least 2 biological replicates.

2.9 RNA Sequencing

2.9.1 mRNA Sequencing

Total RNA was extracted from WT and mutant cells following the Qiagen miRNeasy kit protocol, and polyA purified using Dynabeads mRNA DIRECT micro kit. RNA integrity was measured on a Bioanalyzer 2100 mRNA pico chip, only RNA with an RNA integrity number (RIN) greater than 8 were taken into final library preparations. RNA sequencing libraries were prepared following the TruSeq® Stranded mRNA LT kit (Illumina) protocol. Libraries were quanitified using Qubit and KK4824 Illumina KAPA Library Quantification Complete kit. Sequencing was conducted on the NextSeq500 (Illumina) with NextSeq® 500 Mid Output v2 Kit reagents to produce 75 bp paired end reads.

2.9.2 RNAseq Bioinformatics

Data was obtained from Dr James Platt (Platt et al., 13) for CHD mutants, and analysed in parallel with sequenced *Isw-* and WT data from the current study. Reads were aligned to the *Dictyostelium* genome from Dictybase (Basu et al. 2013) using Tophat2 (Trapnell et al., 2010) with standard parameters. Gene counts were quantified using HTseq-count (Anders et al. 2015) against the Dictybase reference GFF release 2.12. The DESeq2 package was used for normalization and detection of differentially expressed genes (Anders and Huber, 2010). The R statistical project (R Development Core Team 2016) was used for statistical and graphing purposes throughout.

2.10 Nucleosome Mapping

2.10.1 Chromatin Digestion

Dictyostelium chromatin digestion was carried out following the method developed in Platt 2013. Briefly, $1x10^8$ cells were washed once in ice cold KK2 and once in 100mM sorbitol, resuspended in 400µl digestion buffer (100 mM sorbitol, 50 mM NaCl, 10 mM Tris-HCl (pH 7.5), 5 mM $MgCl_2$, 1 mM $CaCl_2$, 1 mM β-mercaptoethanol, 0.5 mM spermidine, 0.1% NP-40). Permeabilised cells were transferred to tubes containing 300 U micrococcal nuclease (MNase, Affymetrix) and incubated for 2 min at 37°c before adding 40µl stop solution (5% SDS, 250mM EDTA) and vortexing to lyse cells. DNA was phenol/chloroform extracted, RNAse A treated (15µl, 10mg/ml) at 37°c 30 min. DNA was phenol/chloroform extracted again and ethanol precipitated before air drying and resuspending in TE buffer (10mM TRIS pH 8.0, 1mM EDTA). 10µl of each sample was run on 1.5% agrarose gels to check digest extent. Sequencing library preparation was performed using the Ion Plus Fragment Library Kit (Ion Torrent) and Ion Chef workflow system (Ion PI Template OT2 200 kit v3). 200 bp single end reads were sequenced on the Ion Proton system using (Ion Torrent; Ion PI Chip Kit v2 and Ion PI Sequencing 200 kit v3).

2.10.2 MNase-seq Bioinformatics

MNase-seq reads were aligned against the *Dictyostelium* reference genome (Basu et al. 2013) using Bowtie-1.0.1 (Langmead et al. 2009) with parameters: -t -n 0 --trim3 14

--maxins 5000 --fr -k 1 --best -p 2, for Illumina PE data, and parameters: -t -n 2 -k1 --best -p5, for Ion Torrent SE data. Nucleosome mapping was conducted as described in Platt 2013, or using the analysis pipeline developed in the present study. Briefly, the following analysis steps were performed: fragments were size selected to within 120-180 bp, and fragment mid-points/dyads determined. Final 'nucleosomal' fragments were defined as regions spanning one third of total fragment size centered on the fragment dyad. Nucleosome scoring was performed by summing total fragment overlaps within 5 bp genomic bins. The average size of fragments mapping to each bin was recorded as the fragment footprint size of the region. Nucleosome maps were normalised to total mapped fragment count across the genome. For peak calling: Gaussian smoothing was applied to nucleosome maps and first derivative of Gaussian (FDoG) and Laplacian of Gaussian (LoG) convolutions performed. Local minima, maxima and peak edges were identified as zero-crossing points in the FDoG and LoG products respectively, and regions fitting the expected peak profile were defined as nucleosome positions. Consensus nucleosome positions were first identified in averaged WT maps before identifying matched peaks in test samples by searching for local minima and maxima within 200 bp of the reference nucleosome region. All downstream analyses were performed on these peak sets, and only matched digest samples directly compared. All downstream visualization and statistical analyses were performed in R (R Development Core Team 2016).

2.11 Analysis Scripts

Scripts used for analysis of RNA-seq and MNase-seq, and plotting functions for downstream analysis are available at: https://github.com/MERobinson/phd_scripts.

Chapter 3:

Characterising the Roles of *Dictyostelium* ATP-Dependent Chromatin Remodelling Complexes in Growth, Development and Chemotaxis

3.1 Introduction

Mutagenic screens in *Dictyostelium discoideum* for strains displaying lithium resistance and late-stage developmental defects identified a type III CHD protein named ChdC (Keim-Reder 2006; Platt 2013). Subsequent bioinformatic analysis identified a further ten SNF2 family protein-coding genes present in the *Dictyostelium* genome. Studies conducted in both the Müler-Taubenberger lab (unpublished) and our own (Platt 2013) led to the generation and characterisation of knock-out cell lines for all three CHD proteins: ChdA, ChdB and ChdC, and Arp8 – an essential component of the Ino80 complex (Shen et al. 2003; Joseph et al. 2008). Each of these mutant cell lines exhibited distinct phenotypic effects: in *ChdA*$^{-}$ the slugging stage of development was extended and the speed and directionality of chemotaxis towards cAMP was inhibited. ChdB loss caused only a minor inhibition of proliferation in shaking culture, while *ChdC*$^{-}$ displayed severe phenotypic effects - halting development at the mound stage and exhibiting a similar level of chemotactic inhibition to *ChdA*$^{-}$. Finally, loss of Ino80 activity led to a novel chemotactic inhibition at high but not low cAMP concentrations (Rogers 2010). Genome-wide transcriptional profiling through RNA-sequencing found that respective mutant phenotypes were explained by mis-regulation of key signalling pathways, such as the de-repression of inositol signaling genes observed in Arp8 null cells.

In order to establish Dictyostelium as a model system for further functional studies of chromatin remodeling complexes, I aimed to more fully characterise the role of the core remodelers involved in transcriptional regulation. I first re-examined the structure of the *Dictyostelium* SNF2 family to identify any previously unannotated SNF2 family members, then generated knock-out mutant cell lines for the remaining, un-studied core chromatin remodelers. Phenotypic profiling of cell growth, development and chemotaxis was then performed, and compared with results from Arp8 and CHD family mutants. These studies provide insight into the molecular pathways potentially regulated by the core remodelers and the degree of redundancy between remodeling complexes.

3.2 The SNF2 Family in *Dictyostelium*

Eleven SNF2 family proteins were previously identified in *Dictyostelium* (Platt et al. 2013) including members of the four core remodeler families: three CHDs (ChdA; DDB_G0284171, ChdB; DDB_G0280705 and ChdC; DDB_G0293012), two SWI2/SNF2 (Snf2a; DDB_G0285205 and Snf2b; DDB_G0271052), one ISWI (Isw; DDB_G0292948), and two INO80/SWR (Swr1; DDB_G0267638 and Ino80; DDB_G0292358) (Platt et al. 2013). Three SNF2 proteins more distantly related to ChdC were also identified (Mot1; DDB_G0286219, Rad54a; DDB_G0282997 and Rad54b; DDB_G0285117). In order to confirm that all Dictyostelium SNF2 proteins have been identified, homology searches were conducted with HMMER3, a profile hidden Markov model (HMM) based algorithm (Eddy 1998). Profile methods use positon-specific scoring models, as opposed to the position-independent scorings of pairwise algorithms such as BLAST, making them more sensitive; Hidden Markov models have the additional benefit of probabilistically modeling the “hidden” state - i.e. the true ancestral sequence, and provide model gap and insertion scores rather than using arbitrary penalties (Eddy 1998). A HMM profile was generated from the Pfam SNF2_N domain seed sequence and used to search the *Dictyostelium* protein database (Basu et al. 2013). This produced a list of 21 putative proteins (E-value < 0.05), including the 11 previously reported (Platt et al. 2013), plus an additional nine potential SNF2 members. To visualise the phylogenetic relationships between the putative *Dictyostelium* SNF2 members and human, mouse and *Drosophila* homologs, the full SNF2 protein sequences from the four species were aligned using MUSCLE and a maximum likelihood phylogenetic tree generated to explore SNF2 family topology (Fig 3.1).

The eleven reported SNF2 proteins cluster with their previously annotated sub-family homologs, and seven putative proteins cluster into distinct sub-families: FUN30 (DDB_G0267556), ERCC6 and ERCC6-like (ercc6 and pich respectively), ATRX (DDB_G0293120), SMARCAL (DDB_G0281559), SHPRH (DDB_G0287171) and RAD5 (DDB_G0272082). The subfamily groupings for helE and DDB_G0282115 remain unclear and may require alignment with a larger range of organisms to classify. The SNF2 family proteins play a large range of roles as transcription factors, repair proteins and maintenance of structural chromatin (Flaus et al. 2006); however in the present study we focus on the roles of SNF2 members known to be primarily involved in transcriptional regulation through their ATP-dependent chromatin remodeling activity:

ChdA, ChdB, ChdC, Isw, Snf2a, Snf2b, Swr and Ino80.

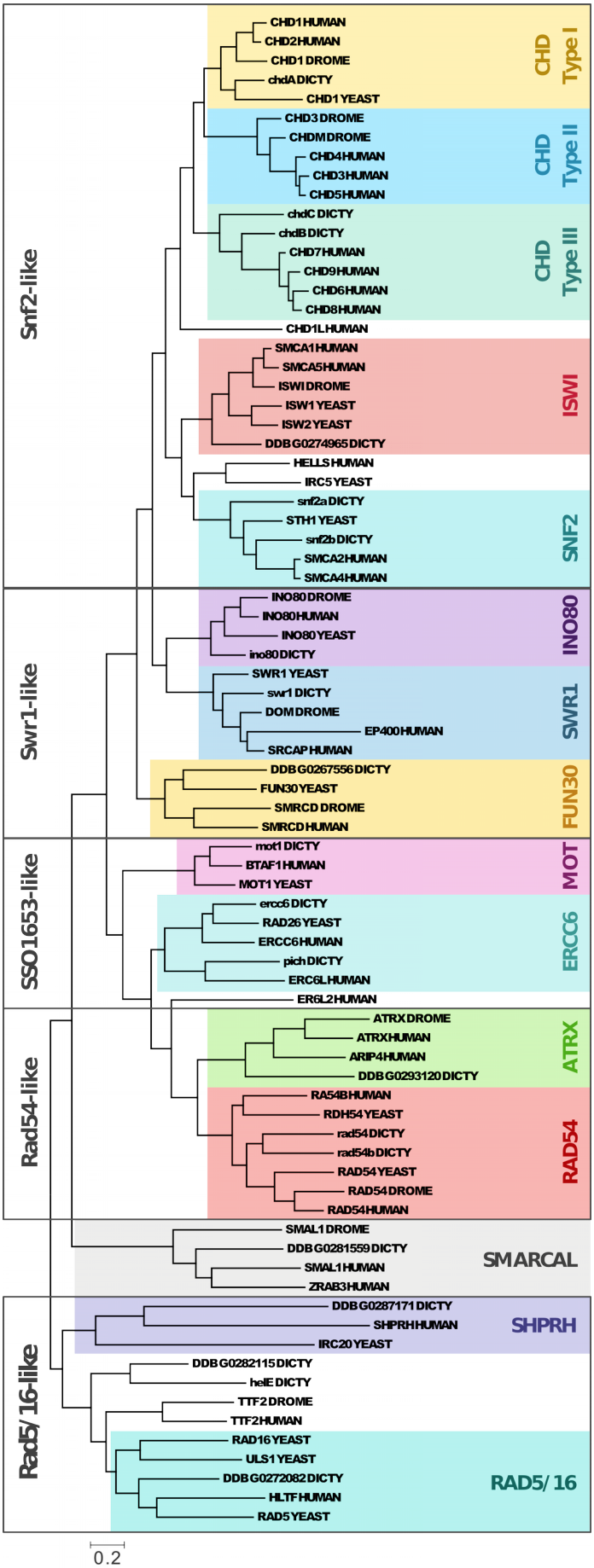

Fig3.1: Structure of the SNF2 Family in Dictyostelium. Full-length SNF2 family proteins present in the Uniprot database from *S.cerevisiae, D. melanogaster* and *H. sapiens* were aligned with identified SNF2 proteins in *D. discoideum*. An un-rooted maximum likelihood tree was constructed from alignments. Clustered subfamilies containing one or more identified Dictyostelium proteins are highlghted, and subfamily groupings (as determined by Flaus et al. 2006) are indicated as grey boxes.

DICTY = *D. discoideum*
YEAST = *S. cerevisiae*
DROME = *D. melanogaster*
HUMAN = *H. sapiens*

3.3 Generating Remodeler Null Cell Lines

To allow phenotypic characterisation and comparison with existing remodeler mutants, I aimed to generate null mutants for Isw, Snf2a, Snf2b and Swr. Constructs were designed as outlined in Figure3.2A for homologous recombination-mediated deletion of a region spanning from upstream of the ATG translational start site to downstream of the catalytic SNF2_N domain. To generate constructs, DNA sections of approximately 1kb flanking the target region were PCR amplified from genomic DNA. Primer tails contained complimentary overhangs to allow fusion of the two regions in a second round of PCR, and restriction sites for NdeI and SalI. Fused DNA segments were cloned into the TOPOII vector and a floxed blasticidin resistance cassette from pLPBLP (Faix et al. 2004) was inserted between flanking sequences via restriction digest with NdeI and SalI. Knockouts were generated in the Ax2 strain background and screened by PCR to confirm both deletion of target region and insertion of resistance cassette (Figure 3.2B). Multiple independent clones were successfully generated for *Isw*$^{-}$, *Swr1*$^{-}$ and *Snf2a*$^{-}$, however no *Snf2b*$^{-}$ clones were obtained from five separate transfection attempts, suggesting possible lethality of Snf2b KO.

A custom antibody was raised against *Dictyostelium* Isw N-terminus peptides to further validate the Isw null mutant. Western blotting performed on WT and mutant cell lysates reconfirms the loss of Isw protein (Figure 3.2C). The antibody was also used to profile the expression pattern of Isw throughout development. WT Ax2 cells were plated on nitrocellulose membranes under nutrient depleted conditions and samples taken every two hours over 24 hours for western blotting. Blots were probed with the custom anti-Isw and control anti-actin antibodies followed by quantitation of band intensities and normalisation to peak abundance (Fig 3.3D). Isw is expressed throughout most of development with peak abundance at 14 hours - approximately corresponding to the late mound stage, and decreasing to very low levels by 22 hours. To compare Isw protein levels with transcript levels, the the normalised read counts from publicly available RNA-seq data at various developmental stages was examined (Rosengarten et al. 2015; Basu et al. 2013). Protein abundance closely shadows relative expression levels throughout development, with peak transcript abundance at 12h post-starvation.

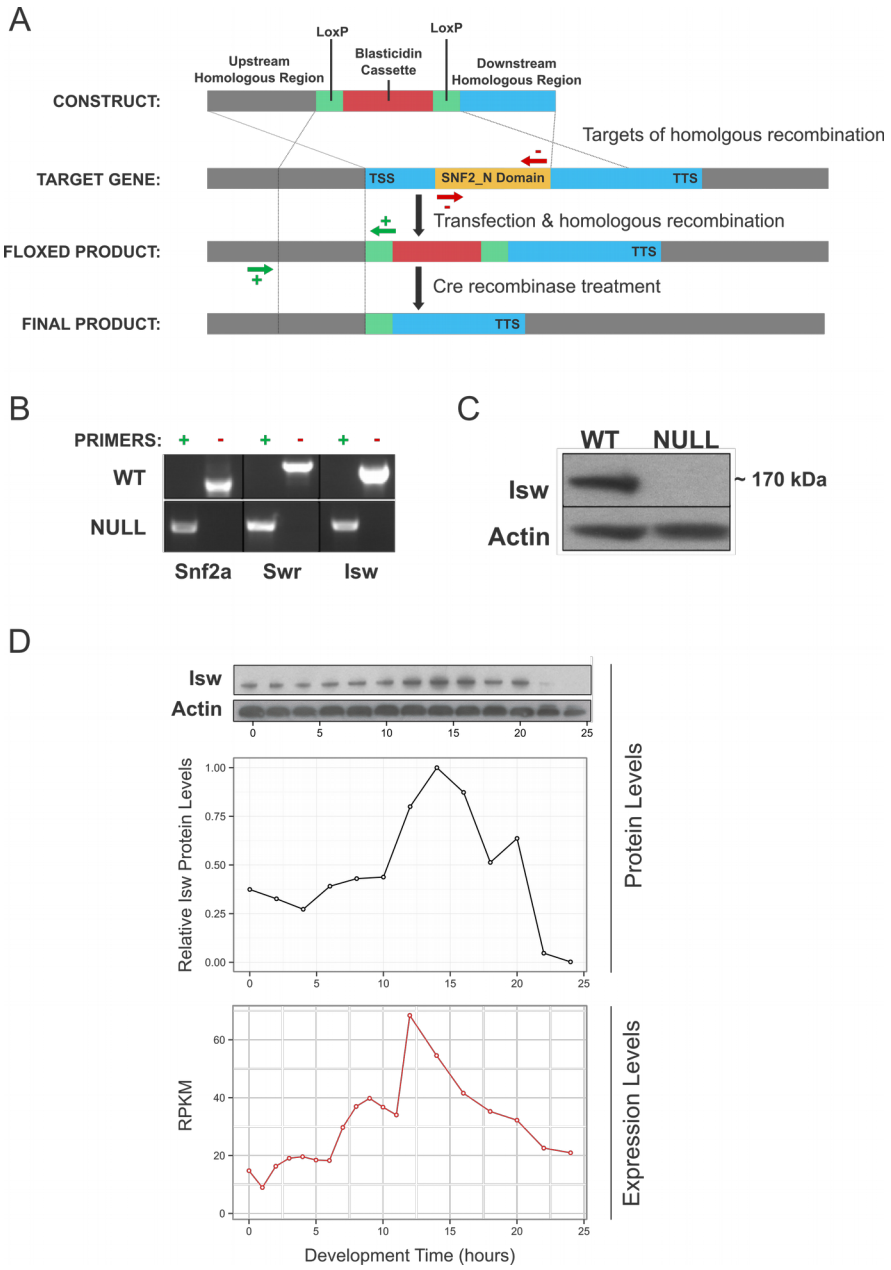

Fig3.2: Generation of Remodeler Mutants.

A) Diagram of the strategy used for homologous recombination mediated deletion of regions spanning from upstream of the ATG to downstream of the catalytic SNF2_N domain to generate remodeler mutants. Red and green arrows indicate primer targets for negatve [i.e. un-recombined] and positive [i.e. recombined] PCR primer pairs respectively. **B)** Mutant clones and WT controls screened for deletion by PCR amplification of genomic DNA with primers as indicated in A. **C)** Western blot for Isw protein in WT and isw- cells. **D)** Proteins levels of Isw throughout development (upper), band intensities were quantified and normalised to actin levels (middle) and plotted relative to peak protein abundance. Protein levels are compared to publicly available RNAseq data for Isw RNA expression in development (Rosengarten et al. 2015).

3.4 Differential Growth Defects of Remodeler Mutants

Mis-expression of metabolic genes in *ChdC*$^{-}$ causes growth inhibition in shaking culture, resulting in a replication rate approximately twice that of WT cells, *ChdA*$^{-}$ and *ChdB*$^{-}$ on the other hand have little impact (Platt et al. 2013). To identify potential involvement of the remaining remodelling proteins in metabolic signalling pathways, all remodeler null cell lines and WT controls were grown in shaking culture from an initial dilution to ~1x10^{6} cells/ml and cell numbers monitored for 72 hours (Figure3.3). While *ChdA*$^{-}$, *ChdB*$^{-}$, *Isw*$^{-}$, *Snf2a*$^{-}$ and A*rp8*$^{-}$ all exhibit no significant change in replication rate, Swr loss results in a doubling time approximately three fold higher than the WT.

In addition to reduced proliferation exhibited by *Swr*$^{-}$ cells grown in shaking culture, it was observed that adherent culture of *Swr*$^{-}$ led to the production of large, non-uniform cells not apparent during shaking culture, suggestive of a cytokinesis defect dependent upon culture conditions. *Swr*$^{-}$ and WT cells were thus diluted to ~1x10^{5} cells/ml and grown either in shaking culture or adhered to glass coverslips; after five days cells grown in shaking suspension were transferred to glass coverslips and incubated for one hour to allow adherence. Cells from both conditions were washed, fixed and stained with DAPI to mark nuclei, and concanavalin A (ConA) to mark the cell membrane. *Swr*$^{-}$ mutant cells grown in shaking culture exhibit no change in the average number of nuclei/cell, adherent culture conditions on the other hand produced large, multi-nucleated cells (Figure3.4). To our knowledge this is the first example of an adherence-dependent multi-nucleated phenotype.

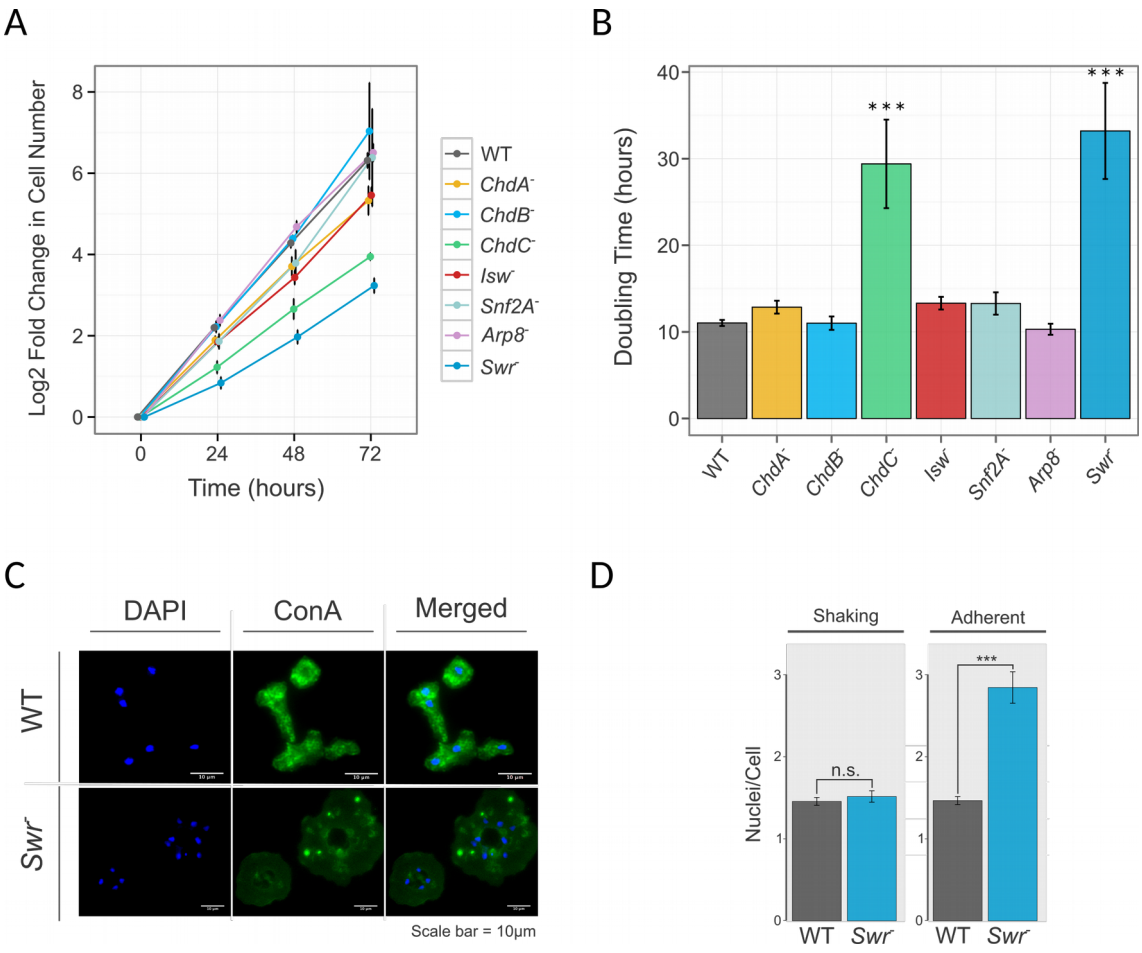

Fig3.3: Effects of Remodeler Loss on Cell Growth.

WT and remodeler mutant cell lines were grown in shaking culture from an initial dilution to 1 x10^6 and cell number measured every 24h. **A)** Cell counts normalised to starting concentration and log transformed. **B)** Doubling times calculated from log phase growth. **C)** Imaging of WT and Swr- cells grown in adherent culture stained with DAPI and concanavalin A (conA) to mark nuceli and cell membranes respectively. **D)** Quantification of the number of nuclei/cell for WT and Swr grown in either adherent or shaking culture conditions. Experiments conducted on three cones per condition with the exception of Swr, for which only two clones were isolated.

3.5 Detecting Developmental Roles of Chromatin Remodelers

Upon nutrient depletion *Dictyostelium* enters a multicellular development cycle, whereby ~10^5 cells will aggregate into a mound before differentiating to ultimately form the fruiting body (FB). Previously studied remodeler mutants display distinct developmental defects; the onset of aggregation is delayed ~1-2 hours in *ChdA*$^-$ and *ChdB*$^-$, and terminal differentiation is further delayed in *ChdA*$^-$, extending the migratory slug stage (Platt et al. 2013). ChdC null cells exhibit the strongest development defect with a delay of ~2 hours during aggregation and developmental arrest at the mound stage (Platt et al. 2013). Finally, *Arp8*$^-$ cells display an aggregation delay of ~5 hours (Rogers 2010). To establish the potential roles of Isw, Snf2a and Swr in development, cells were plated on KK2 agar under nutrient depleted conditions and imaged over 24 hours (Figure 3.5A).

Isw null cells exhibited a minor delay (~30 min) in the onset of aggregation compared to WT. Although only very slight, this delay was consistently observed for all replicates. Formation of loose mounds and slugging also appear proportionally delayed, but with no defects in terminal morphology were observable. Snf2a disruption also causes a minor (~30 min) delay at all stages. Additionally, a sub-population of cells fails to enter aggregation with a high proportion of individual, unaggregated cells still observable at 12h and 24h in both *Snf2a*$^-$ (Figure 3.5A). Arp8 null lines display a similar aggregation defect, and in both cell lines it was observed that the unicellular population sometimes enter a second aggregation stage at ~12 hours post-starvation. Distinct streams are not observed in the Swr null condition, with cells forming a greater number of small mounds. Imaging of terminal structures at 48h post-starvation reveals that *Swr*$^-$ also form stunted fruiting bodies with reduced height (Figure3.5B), likely caused by reduced cell numbers per mound.

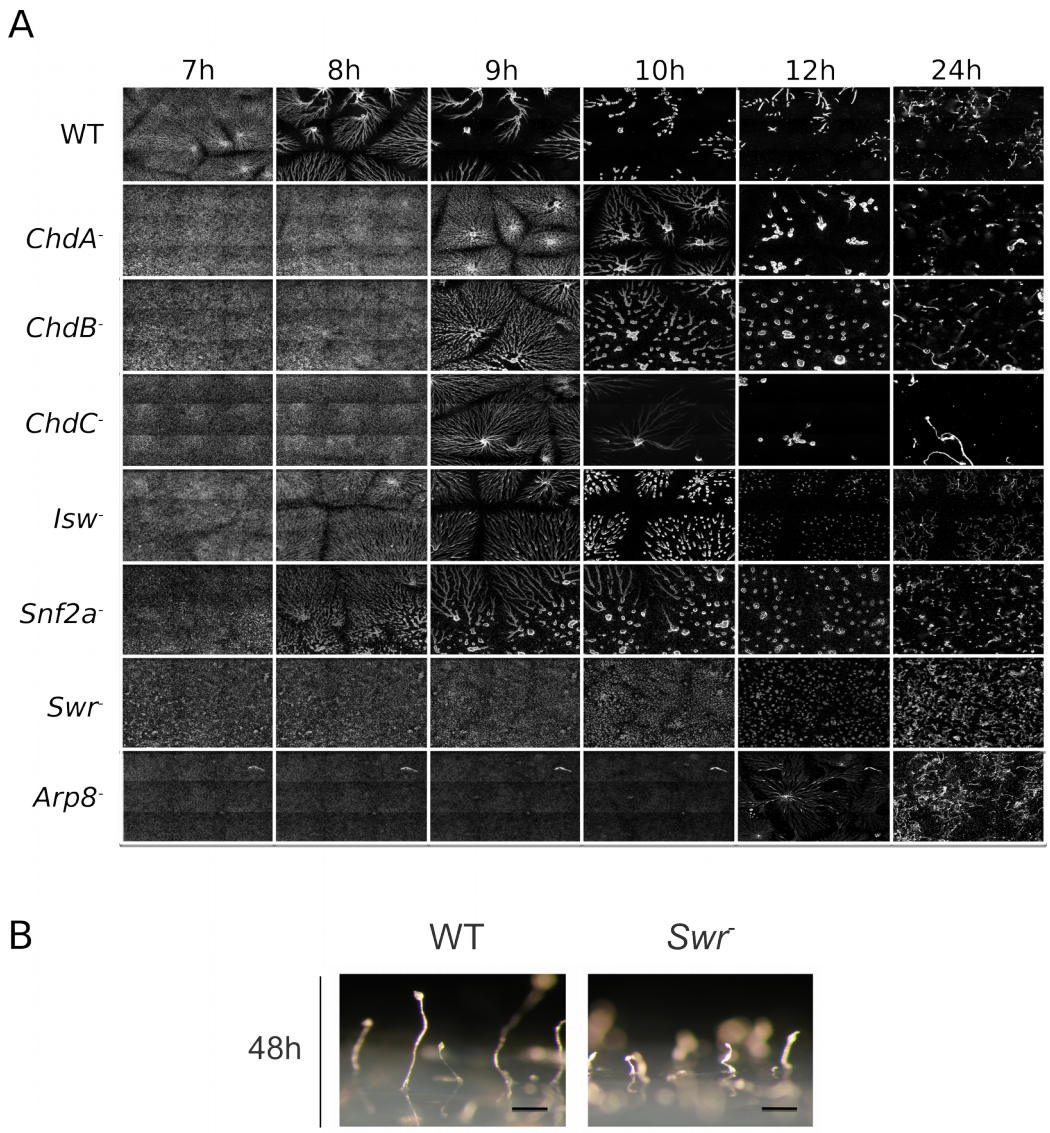

Fig3.4: Developmental Defects in Remodeler Mutants.

A) WT and remodeler null mutants were grown in nutrient depleted conditions on KK2 agar and imaged over 24h. Developmental timing and gross morphological defects are observed by aligning frames by time-point post starvation.

B) Images of terminal morphology at 48h post-starvation for cells grown on KK2 agar as in A (scale bar = ~2mm).

3.6 Chemotaxis Defects Displayed by Remodeler Mutants

Upon starvation, Dictyostelium cells chemotaxis towards cyclic adenosine monophosphate (cAMP), and propogate the cAMP signal via its secretion, leading to streaming and aggregation of individual cells into multicellular mounds. The conditions of early development can be simulated by culture in nutrient free medium with exogenous cAMP pulses for 5 hours; subsequent assay of individual cell migration in a cAMP gradient and quantification of movement speed, polarity (cell width/height), directionality (Euclidean distance/accumulated distance) and chemotactic index (the cosine of angle between the direction of the cAMP gradient and the path of migration) allows identification of defects in the migratory response to cAMP free of confounding factors related to signal propagation. *ChdA*$^{-}$, *ChdC*$^{-}$ and *Ino80*$^{-}$ have all been reported to display significant chemotactic deficiencies (Platt et al. 2013; Rogers 2010), indicative of the underlying transcriptional mis-regulation of genes in inositol and cAMP signaling pathways.

To examine whether newly generated remodeler mutants may also be involved in the regulation of chemotactic signalling, chemotaxis assays were performed in triplicate and speed, polarity, directionality and chemotactic index (CI) parameters measured for a minimum of 100 cells per condition (Fig3.6). *Snf2a*$^{-}$, *Swr1*$^{-}$ and *Isw*$^{-}$ all display significant chemotactic defects, notably however migratory ability is not lost entirely in any of the assayed cell lines. Snf2a loss causes a reduction in directionality (-0.2 ± 0.09, $p = < 1 \times 10^{-6}$) and CI (-0.26 ± 0.2, p = 0.01); Swr loss also causes cells to migrate less effeciently towards the chemoattractant source (directionality -0.32 +/- 0.1, $p < 1 \times 10^{-6}$; CI -0.4 +/- 0.19, $p < 1 \times 10^{-6}$), and a decrease in cell polarity (-0.5 +/- 0.33, $p = 2 \times 10^{-3}$). Finally, Isw cells exhibit an significantly increased migration speed (+4.8 +/- 2.5μm/min, $p = 1 \times 10^{-6}$). Remodeler loss thus causes frequent perturbation of chemotactic signaling, however whether this is caused by direct transcriptional regulation or indirect effects remains unclear. Furthermore, the developmental delays observed in remodeler mutants may contribute to chemotactic phenotypes by extending the starvation time required for cells to progress to chemotactic competence.

A

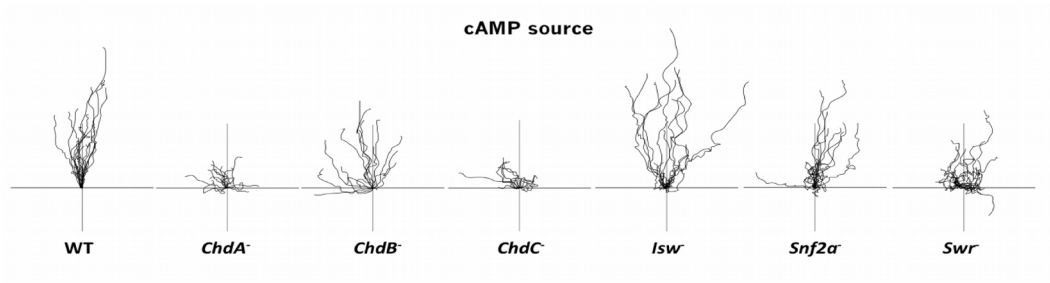

B

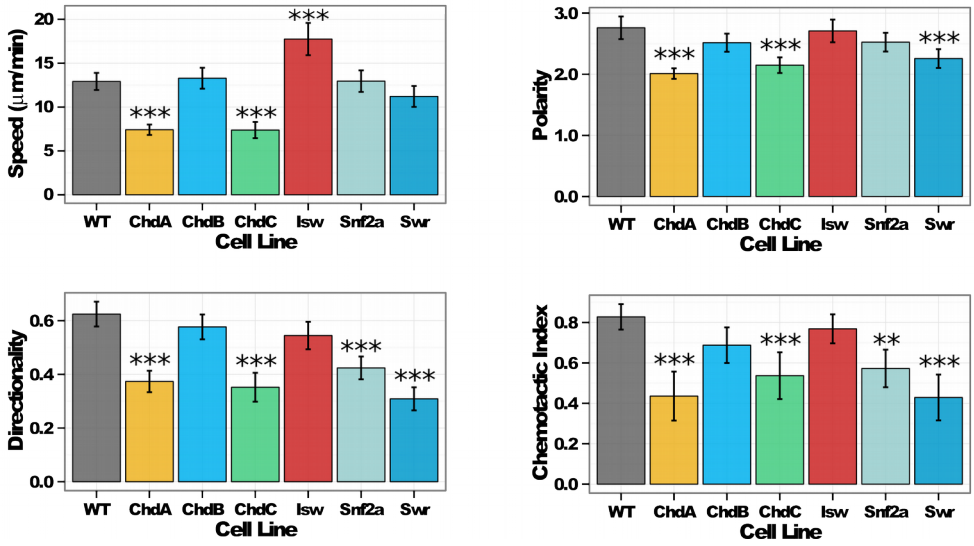

Fig3.5: Chemotactic Phenotypes in Remodeler Mutants.

WT and remodeler null mutants were pulsed with cAMP for 5h in nutrient depleted conditions before imaging their migration with a cAMP gradient over 15min.

A) Traces from twenty randomly selected cells for each condition.

B) Speed, polarity, directionality and chemotactic index (CI) were measured from a minimum of 100 cells/condition. Significance tested by one-way ANOVA with Tukey's post-test (** = $p < 0.01$, *** = $p < 0.001$), intervals indicate 95% CI.

3.7 Summary

Phylogenetic analysis of the SNF2 family has shown that Dictyostelium possess a diverse repertoire of putative remodelers. The reproduction of subfamily groupings identified previously (Flaus et al. 2006; Platt et al. 2013) indicates the robust relationships within these groupings. By identifying a number of interesting potential homologs, and generated mutant cell lines for the core CRCs involved in transcriptional regulation we have established *Dictyostelium* as a useful model for the study of remodeler function.

All remodeler mutants exhibit a unique combination of phenotypes, indicating that despite expansion of some remodeler sub-families compared to other unicellular organisms, all remodelers possess at least partially non-redundant functions. Nonetheless, phenotypic severity varies widely, and interestingly, the severity of phenotypic defects appears roughly consistent across assays, with ChdC and Swr loss causing the strongest defects to growth, chemotaxis and development; and ChdB, Isw and Snf2a causing the weakest. Whether this is indicative of the level of chromatin disruption or perhaps simply caused by transcriptional mis-regulation of key genes in individual remodeler mutants remains unclear, and will require profiling of the transcriptional and chromatin defects in a wider range of remodeler mutants to determine.

Chapter 4:

Dictyostelium Spacing Remodelers Play Distinct Roles in the Maintenance of Chromatin Structure

4.1 Introduction

Micrococcal nuclease digest sequencing (MNase-seq) followed by bioinformatic nucleosome mapping has previously been employed to study the roles of CHD and ISWI sub-family proteins in maintaining chromatin structure across the genome of yeast (Gkikopoulos et al. 2011; Hennig et al. 2012). While a loss of canonical nucleosome structure is observed upon combinatorial loss of the spacing remodelers, little global effect of individual remodeler KO was observed, and their specific *in vivo* roles remains poorly understood. However these studies examined the globally aggregated effects of remodeler loss (Gkikopoulos et al. 2011; Hennig et al. 2012), which may mask defects at gene subsets and individual nucleosomes. Furthermore, current nucleosome mapping methodologies such as iNPS and DANPOS generally do not examine nucleosome footprint size (Chen et al. 2013; Chen et al. 2014), which may provide insight into the effect of remodeler loss on nucleosome structure.

The phenotypic profiling of *Dictyostelium* remodeler mutants conducted during this study has demonstrated that ChdA, ChdC and Isw proteins are not fully redundant. Furthermore, previous analysis of nucleosome profiles from ChdC null cells in our lab revealed a specific role for this type III CHD protein in regulating nucleosome repeat length (NRL) at a subset of developmentally regulated genes (Platt 2013). We postulated that the remaining members of the CHD and ISWI families also play important, non-redundant roles in regulating chromatin structure not readily apparent from examination of the global average of structural defects, as attempted previously.

To analyse the individual roles of spacing remodelers I aim to conduct MNase-sequencing on the newly generated Isw null cell line, which together with previously generated MNase-seq data from ChdA, ChdB and ChdC cell lines will provide information on the structural defects caused by all spacing remodelers in *Dictyostelium*. Through development of novel bioinformatic methods and detailed analysis of the chromatin profiles of the previously un-studied *Isw*$^{-}$, *ChdA*$^{-}$ and *ChdB*$^{-}$ mutants, and comparison with published results from *ChdC*$^{-}$ mutants, I aim to provide insight into the specific nucleosome parameters maintained by each individual remodeler.

4.2 MNase-Sequencing of Isw Null Mutants

In order to reduce the costs and increase the efficiency of MNase-sequencing I first adapted the Dictyostelium MNase-seq protocol established previously on the Illumina HiSeq platform (Platt 2013) for compatibility with Ion Torrent sequencing. Ion Torrent sequencing uses semiconductor chips consisting of ion sensors contained within microwells to detects the pH change caused by incorporation of un-modified nucleotides, as opposed to the optical detection of flourescently labeled nucleotides on Illumina platforms (Rusk 2011). The original MNase-seq protocol consisted of *in vivo* digestion of chromatin by incubation of permeabilised cells with limiting concentrations of MNase to produce a range of protected fragments, which were then size selected to within 50-1000 bp and paired-end (PE) reads produced through Illumina sequencing to allow mapping of protected fragments back to the genome. By restricting the size range of selected digest fragments to within 75-200 bp, the nucleosomal fraction (~120-180 bp) is encompassed while allowing reduced read numbers for the same coverage depth. Furthermore this size range is within the length of Ion Torrent 200 bp reads, allowing full length single end (SE) sequencing of fragments. The adapted technique was applied to *Isw-* and WT cell lines grown in shaking culture. A summary of all MNase-seq data sets analysed in the present study is given in Table4.1.

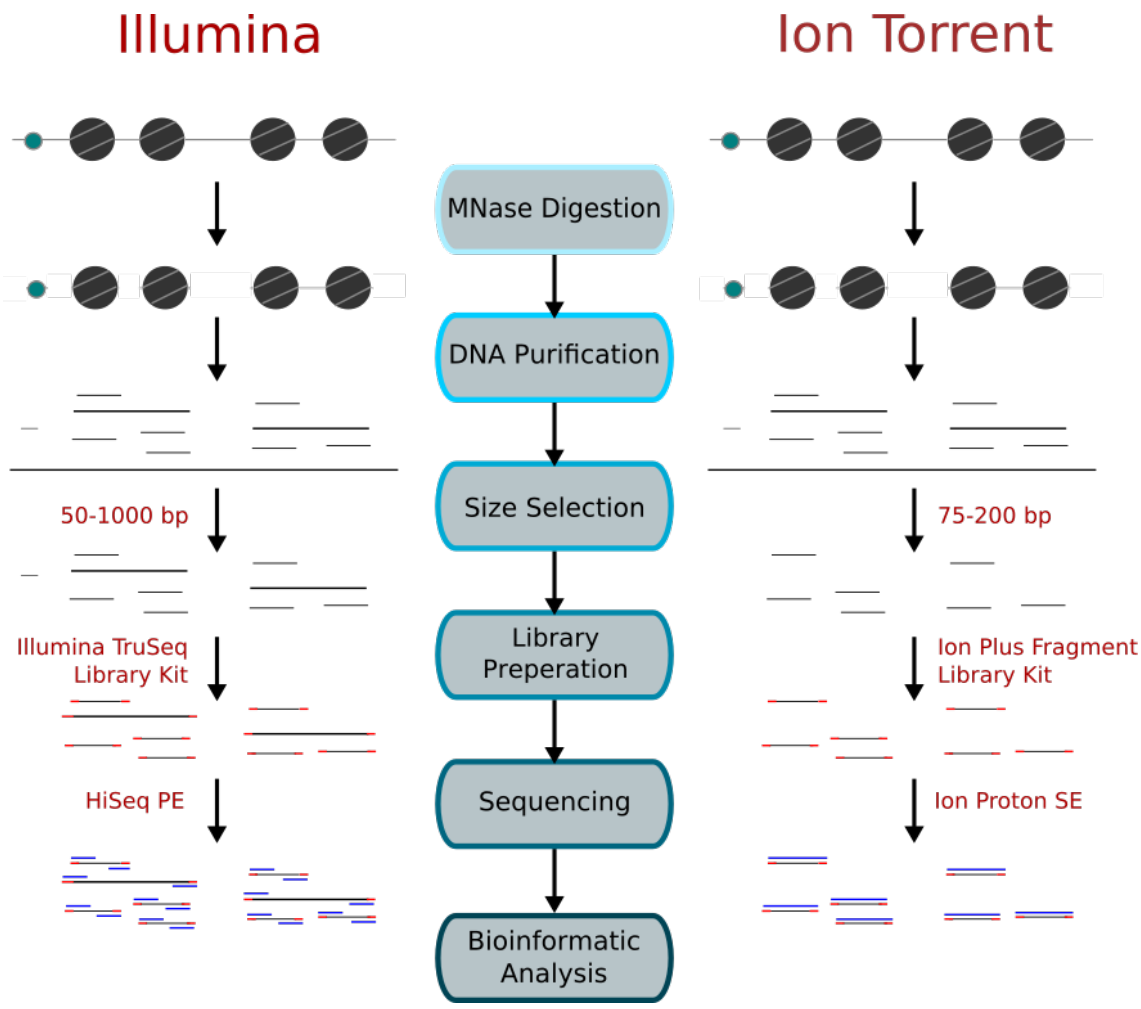

Fig4.1: MNase-Sequencing Protocol on Illumina and Ion Torrent Platforms.

Diagrammatic outline of the different protocols used for MNase-sequencing with Illumina and Ion Torrent platforms: common steps are displayed centrally while differences are highlighted in red for each platform. Key: grey lines = DNA, red lines = adapters, blue lines = sequence reads, grey circles = nucleosomes, turquoise circles = transcription factors, SE = single end, PE = paired end.

Sample	Experiment	Platform	Aligned Reads (M)	Nucleosomal Reads (M)	Previously Analysed?
WT rep1	ExpA	Illumina HiSeq	92.7	9.7	YES
WT rep2	ExpA	Illumina HiSeq	222.3	22.1	YES
ChdC rep1	ExpA	Illumina HiSeq	77.4	8.8	YES
ChdC rep2	ExpA	Illumina HiSeq	201.7	21.8	YES
WT rep3	ExpB	Illumina HiSeq	185.8	15.5	NO
WT rep4	ExpB	Illumina HiSeq	121.5	9.8	NO
ChdA rep1	ExpB	Illumina HiSeq	142.2	12.2	NO
ChdA rep2	ExpB	Illumina HiSeq	119.0	10.3	NO
ChdB rep1	ExpB	Illumina HiSeq	122.7	11.0	NO
ChdB rep2	ExpB	Illumina HiSeq	152.4	14.1	NO
WT rep5	ExpC	IonTorrent Proton	7.7	3.1	NO
WT rep6	ExpC	IonTorrent Proton	10.8	5.8	NO
WT rep7	ExpC	IonTorrent Proton	6.7	3.5	NO
Isw rep1	ExpC	IonTorrent Proton	7.9	3.3	NO
Isw rep2	ExpC	IonTorrent Proton	5.1	2.6	NO
Isw rep3	ExpC	IonTorrent Proton	8.5	4.2	NO

Table4.1: MNase-seq Samples Summary.

Information on all MNase-seq samples used in the current study. Samples are grouped into experiments with chromatin digests and sequencing conducted by the same individual under the same conditions in a common time period. Platform = sequencing platform used for each sample. Aligned reads = millions (M) of uniquely aligned reads. Nucleosomal reads = millions of uniquely aligned reads in 120-180 bp size range. Previously analysed = whether the resultant data sets have previously been analysed.

4.3 Generation and Comparison of WT Nucleosome Maps

Nucleosome maps are produced by alignment of MNase-protected fragments to the reference genome, size-selecting fragments within the nucleosomal range (120-180bp), and scoring of read mid-points, representing nucleosome dyad locations (Fig4.2A). To confirm that platform-specific errors do not introduce appreciable non-biological variation into resultant nucleosome maps, I first adapted the existing bioinformatic pipeline for compatibility with both PE and SE data, and applied it to all seven WT replicates from the three experiments (ExpA-C) conducted in our lab. Locally, nucleosome positions are faithfully re-produced between replicates, however changes in relative peak-heights are observed between experiments. Additionally, variability in the distribution of dyad locations around average nucleosome positions produces significant noise, complicating the application of peak calling algorithms for the identification of average nucleosome locations (Fig4.2B).

To globally compare reproducibility, nucleosomes were scored within 10 bp windows across the genome for all seven WT replicates and Spearman's correlation coefficients calculated between maps (Fig4.3A). Closer correlation is observed between replicates within experimental runs than between separate experiments, however this inter-experiment variation is not caused by platform-specific changes. For example, closer reproducibility is observed between ExpA and ExpC than ExpA and ExpB.

I next examined the average nucleosome structure around gene boundaries by aligning all genes (n = 12,964) by their gene start or end position and calculating average nucleosome scores within a 2,400 bp window (Fig4.3B). All replicates reproduce the canonical average nucleosome structure, with nucleosome depleted regions (NDR) flanking gene boundaries, a strongly positioned +1 and terminal nucleosome (TN), followed by common average nucleosome positions with decreasing uniformity moving into the gene body. ExpB replicates however display increased average nucleosome occupancy around the NDR, and this effect is also observed at the individual gene level (Fig4.2B). A similar phenomenon is obsevred in yeast cells under differing levels of MNase-digestion, where an MNase-sensitive particle, often termed the fragile nucleosome, is lost from the NDR under higher MNase concentraions (Xi et al. 2011; Mieczkowski et al. 2016). The inter-experiment variation observed in our data is therefore likely caused by variable digestion conditions. Further analyses are restricted to comparisons between matched sample digests to avoid this confounding issue.

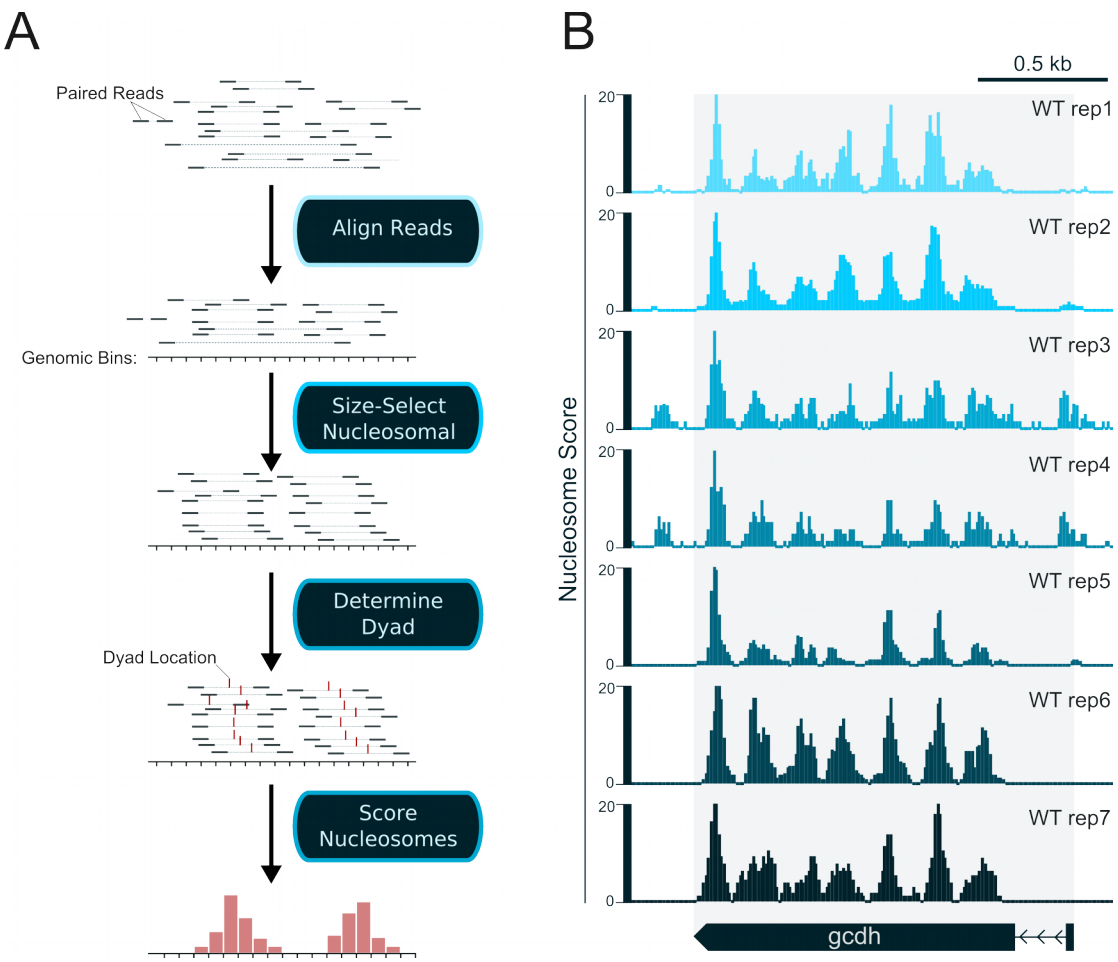

Fig4.2: Nucleosome Mapping of WT Replicates.

A) Diagram of the main steps involved in mapping MNase-seq reads to produce genome-wide nucleosome maps.

B) Nucleosome maps of all seven WT replicates focused on the gcdh gene region (DDB_G0283411).

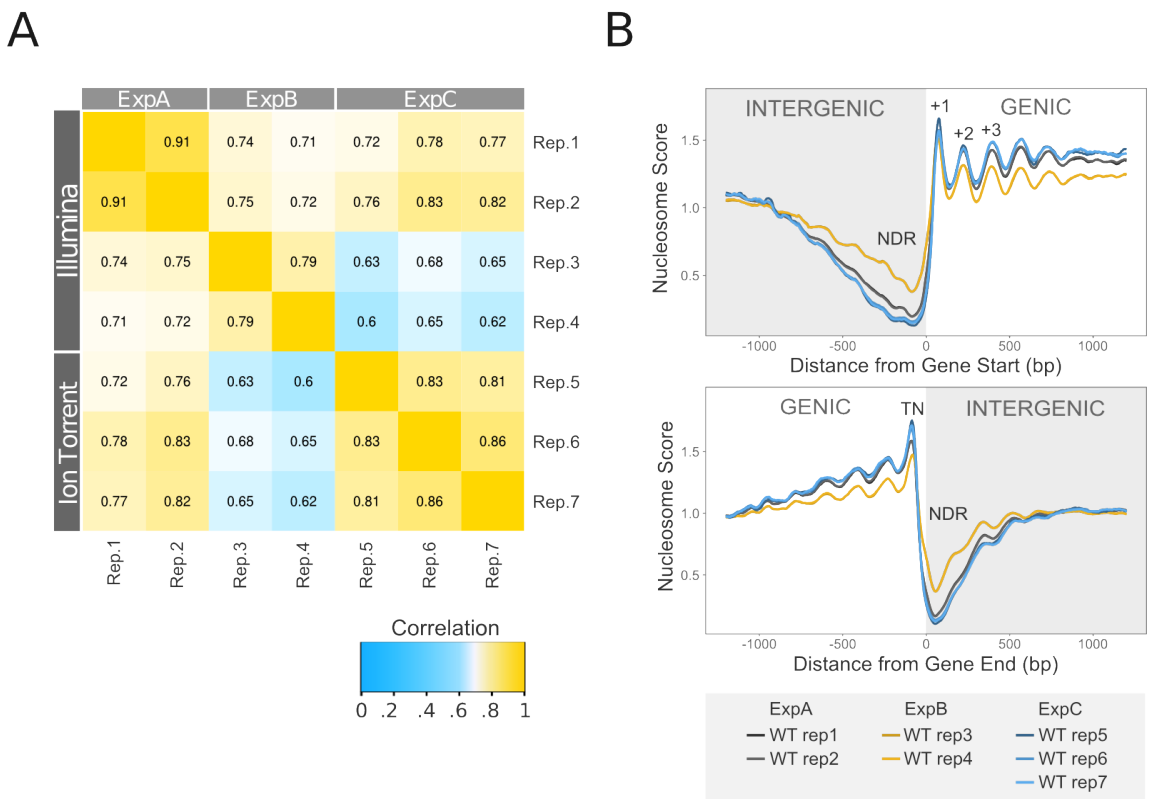

Fig4.3: Reproducibility of Nucleosome Mapping.

A) Correlation matrix of Spearman's rank correlation coefficients calculated from comparison of 10bp windows across genome between WT replicates. Sequencing platform and experiment is indicated for each replicate.

B) Average nucleosome score profiles of WT replicates around annotated gene start and end positions (± 1200 bp) for all *Dictyostelium* genes (n = 12,964). NDR = nucleosome depleted region; +1, +2, etc. = average nucleosome positions; TN = terminal nucleosome.

4.3 Optimising Nucleosome Scoring

To increase the signal to noise ratio (SNR) of nucleosome maps I aimed to develop an improved nucleosome scoring algorithm. Multiple published algorithms are available for nucleosome scoring that employ the common approach of extending reads from the nucleosome dyad by half of the canonical nucleosome footprint size (75 nt; e.g. Zhang et al. 2008, iNPS (Chen et al. 2014) and DANPOS (Chen et al. 2013)), thus increasing the SNR by reducing data loss (Zhang et al. 2008). However these algorithms suffer from three main issues:

Firstly, due to the prevalence of short SE mono-nucleosomal MNase-seq methodologies, dyad positions are commonly estimated by either shifting reads by half of the canonical nucleosome footprint size (i.e. 75 bp; Zhang et al., 2008) or by estimating nucleosome size based on the distribution of reads from the positive and negative strands (Chen et al. 2013). However inaccurate fragment size estimation can introduce false positive errors (Chen et al. 2013), and further prevents the study of nucleosome footprint size variation, which has recently been suggested to be indicative of promoter regulation (Kubik et al. 2015). As our data consist of either PE or long SE reads, the exact fragment mid-points can be determined, allowing increased accuracy of nucleosome mapping and the possibility to studying any potential effects of remodeler loss on nucleosome size or stability.

Secondly, smoothing functions are routinely applied to nucleosome maps to improve the SNR, such as the Epanechnikov kernel density estimate from the original pipeline (Kent et al. 2011; Platt 2013). Assumptions about the underlying distribution used by many of these approaches can introduce peak-shape biases and artefacts, and due to use of peak-shape parameters to study chromatin changes such manipulations may introduce errors.

Finally, common nucleosome mapping algorithms use a hard-coded read extension of 75 nt, however according to the Nyquist-Shanon sampling theorem - which states that sampling frequency must be a minimum of twice the frequency of the signal of interest to allow accurate pattern reconstruction, this limits theoretical resolution to 150 bp. While this is sufficient for individual phased nucleosomal arrays, overlapping peaks produced from positioning

variation across the cell population would not be distinguishable.

In order to improve the SNR while avoiding the issues highlighted above, I developed a nucleosome scoring algorithm that utilises precise nucleosome mid-points to accurately map dyad positions and allow dynamic read extension based on fragment lengths, while also mapping average footprint sizes globally. To determine the effect of read extension on our own data, two sub-samples of 5 million reads were randomly selected from WT rep1 chromosome 1 and nucleosome scoring conducted with read extension lengths between 0 and 70 nt. Spearman's rank correlation coefficients are plotted alongside the theoretical resolution limit for neighbouring peaks (Fig4.4A). While the robustness of resulting maps is evidently improved by increased read lengths, this benefit is reduced above ~40-50 bp. To provide optimal balance between the SNR and nucleosome resolution, the nucleosome scoring algorithm was designed to dynamically extend reads from the dyad position by one third of total fragment length, providing a nucleosome resolution of ~100 bp.

Nucleosome profiles were re-mapped with the optimised algorithm and a correlation matrix between WT samples was calculated using the same method described previously (Fig4.3A) to demonstrate the improvement in reproducibility of nucleosome scoring (Fig4.4B). Significantly increased correlations are observed between all samples (e.g. Fisher's r-to-z transformation $z = 630$, $p \approx 0$ for WT rep1 vs. WT rep2), and are also evident at the individual gene level (Fig4.4C). Importantly, the highly robust nucleosome signals generated by this algorithm negate the need to apply a smoothing function for additional de-noising, allowing more accurate measurement of individual nucleosome peak parameters.

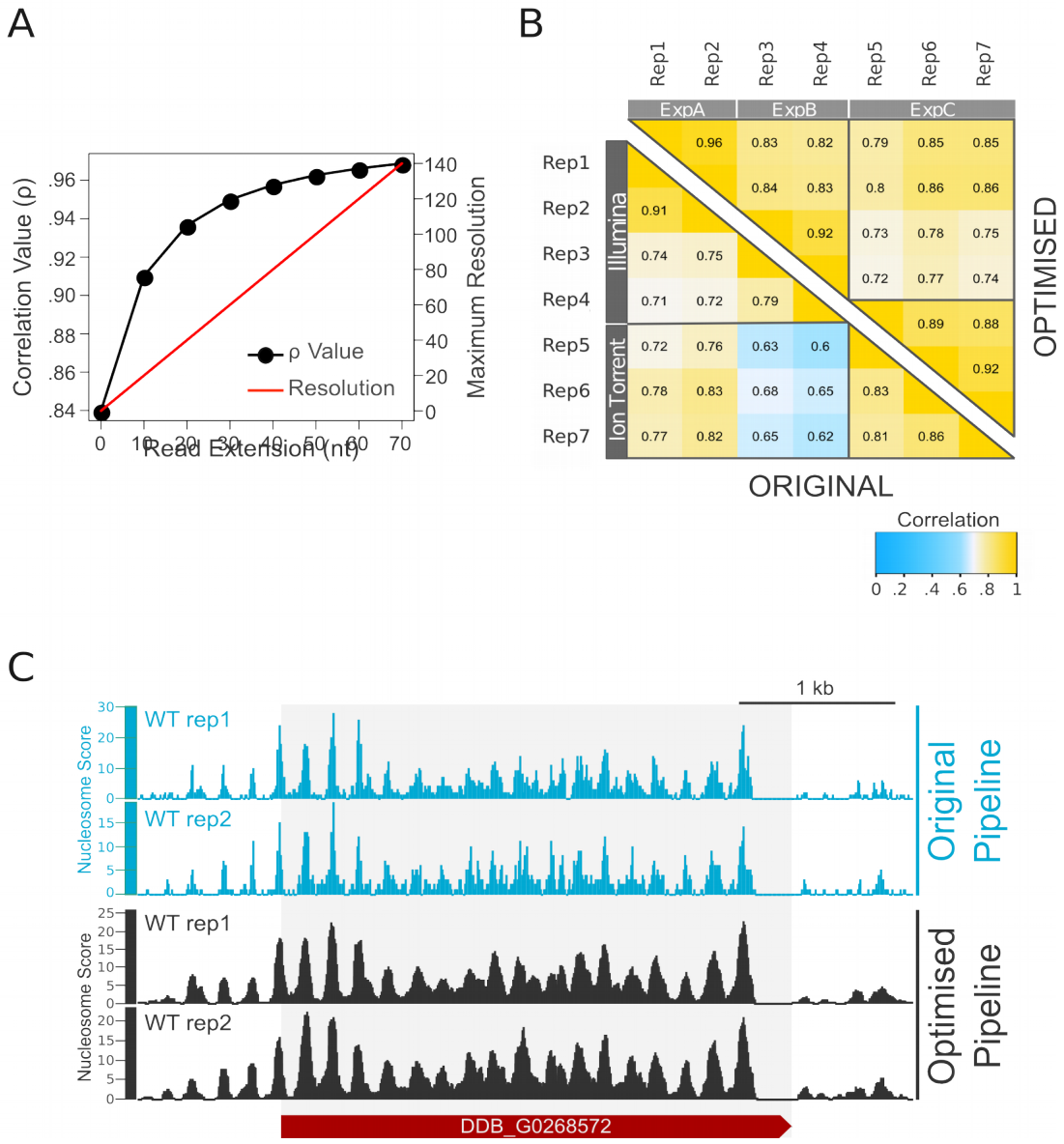

Fig4.4: Optimising Nucleosome Scoring.

A) WT rep1 chromosome 1 reads were sub-sampled and mapped with a range of extension lengths from the dyad using the optimised algorithm developed here, and Spearman's ρ scores calculated and plotted alongside the theoretical resolution limit of neighbouring peaks.

B) Nucleosome scoring was compared genome-wide between WT replicates mapped with either the original (lower panel) or optimised (upper panel) scoring algorithms. Spearman's ρ values are plotted as a heatmap with experiment and sequencing platform indicated.

C) Nucleosome mapping for an example gene, scored with either the original (blue) or optimised (black) algorithm.

4.4 Remodeler Loss Leads to Distinct Global Chromatin Changes

The optimised nucleosome mapping methodology was applied to all WT and mutants samples, including re-mapping of the previously analysed ChdC data to allow comparison. To detect any gross global changes to chromatin structure upon remodeler loss, average gene start profiles were produced for *Isw*$^{-}$, *ChdA*$^{-}$ and *ChdB*$^{-}$ cell lines, and compared with the known profile of *ChdC*$^{-}$ mutants (Fig4.5). All conditions retain the canonical structure immediately around the gene boundary, with structure of the +1 nucleosomes and NDR regions largely unaffected by remodeler loss. However distinct changes relative to matched WT samples are observable for all spacing remodeler mutants.

Compared to the characteristic shift in nucleosome repeat length upon loss of ChdC, the *ChdA*$^{-}$, *ChdB*$^{-}$ and *Isw*$^{-}$ mutants do not exhibit uniform spacing changes. ChdA and ChdB KO cause reciprocal changes in peak height between genic and intergenic regions, suggesting either opposing effects on occupancy or differing localisation of activity. *Isw*$^{-}$ *o*n the other hand exhibits a complete loss of canonical structure across the gene body following the +2 nucleosome.

While global spacing defects such as in *ChdC*$^{-}$ are easily interpreted, changes in averaged peak heights and loss of canonical nucleosome structure can be caused by multiple underlying mechanisms. Possible changes include a shift in nucleosome positioning relative to the TSS at individual genes while maintaining the nucleosome repeat length (NRL); changes in the uniformity of nucleosome positioning at a given locus across the population of cells; or genuine changes in nucleosome occupancy. To analyse the underlying chromatin changes causing the average nucleosome profile defects displayed by *ChdA*$^{-}$, *ChdB*$^{-}$ and *Isw*$^{-}$, an alternative analysis method is required to de-convolute these interwoven components.

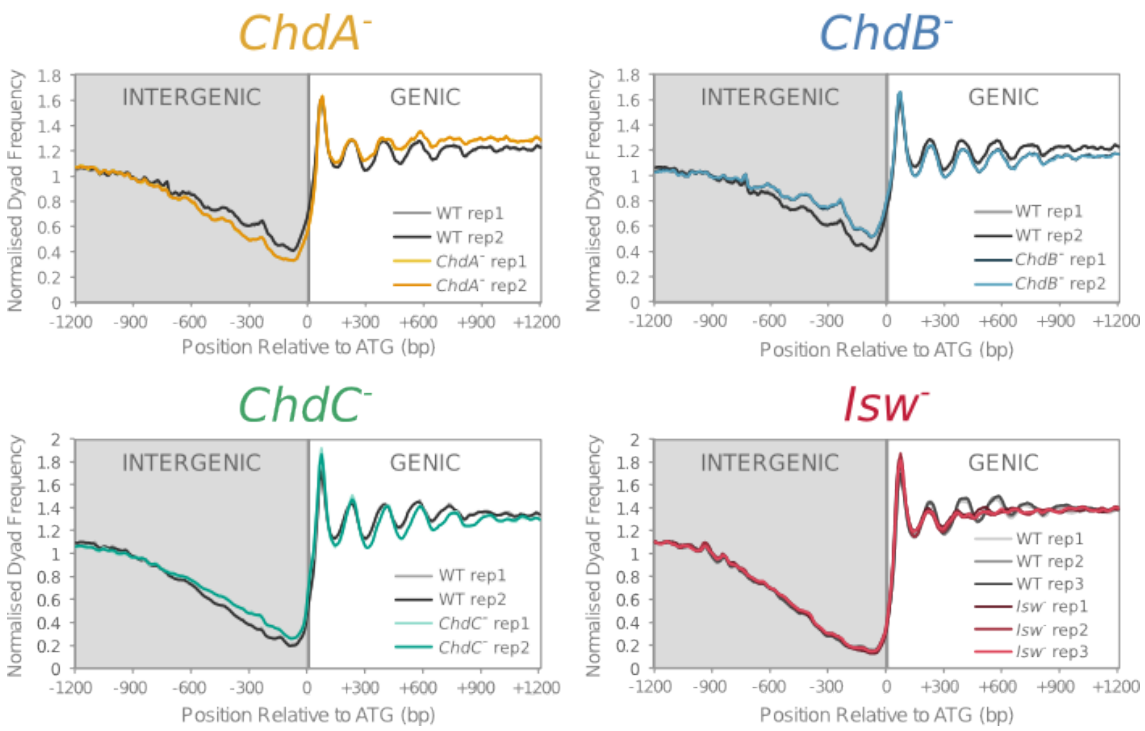

Fig4.5: Global Chromatin Defects in Remodeler Mutants.

Nucleosome scores were summed within ±1,200 bp of the ATG start site for 12,964 annotated genes in the *Dictyostelium* genome and normalised to total score within the window. Profiles are plotted separately for each remodeler mutant condition versus matched WT controls.

4.5 Improving Nucleosome Peak Calling

Peaks in nucleosome maps represent the population-level distribution of nucleosome positions; by measuring the shape properties of these nucleosome distributions it is possible to gain insight into the regulation of nucleosome structure at individual genomic loci. However accurate identification of the boundaries and summit coordinates for each peak is critical for accurate measurement of these properties. The original pipeline utilised a simple thresholding approach to call summit positions (Fig4.5A), however the performance of this method has not been previously validated, and does not allow for boundary detection. To benchmark the performance of this method relative to publicly available peak-calling algorithms I selected three common nucleosome peak callers: iNPS (Chen et al. 2014), MACS2 (Zhang et al. 2008) and DANPOS (Chen et al. 2013), and compared their performance against our original algorithm. Due to a lack of validated reference data sets it is not possible to calculate false positive or negative rates, instead, the robustness of region calling between sub-sampled SE and PE data, and the performance of border detection were tested. Following peak calling, maps were converted to a binary representation of nucleosome regions (scored 1 inside peak regions, 0 outside), and sub-sampled maps correlated as described previously. As the original pipeline does not call peak borders a window of 100 bp was set around each peak summit location. Under these criteria MACS2 is found to produce the most robust region calls, followed by iNPS, with the original pipeline performing very poorly. Conversely, when region sizes are considered MACS2 performs very poorly, with peak widths well beyond the expected nucleosome width (638.3 ± 7.3 bp). Given the ~40-60 bp read extension and ~100 bp resolution of nucleosome mapping, peak widths are expected to be within the ~50-150 bp range, which matches the distribution observed for iNPS (114.7 ± 0.4 bp).

Although iNPS out-performed other peak-callers on SE data, analysis failed on PE data, and it is not possible to incorporate replicate data sets. I therefore adapted the core peak identification approach taken by the Han group, but with significant alterations to pre- and post-processing steps, for rapid and flexible application to SE and PE MNase-seq data. To utilise replicate data I identified canonical nucleosomes positions across all WT samples before analysing individual samples for local variations. An averaged reference nucleosome map was produced from all WT replicates before applying a Gaussian kernel smoothing function to both averaged and individual nucleosome maps. The first derivitive of the Gaussian (FDoG) and Laplacian

of Gaussian (LoG) convolutions of these smoothed profiles were then calculated. Inflexions in the FDoG represent extremum points (peaks and troughs), while LoG inflexions indicate peak boundaries (Fig4.5A). Average nucleosome peaks can then be identified as regions fitting the expected peak shape profile. A simple empirical filtering threshold (< 2x or > 50x mean bin score) was then applied to remove regions at the extremes of signal strength. An example of the intermediate steps in this process and final called peak regions is shown in Fig4.5D. Canonical nucleosome positions are first identified in the averaged nucleosome map before searching within these canonical regions for shifted nucleosomes within individual maps. This use of canonical nucleosome positions improves the robustness of peak calling and allows direct comparison of matched nucleosome positions across conditions.

To validate the performance of our optimised peak calling algorithm, its performance was measured as detailed above. This approach provides a huge improvement in robustness over the original pipeline, and even out-performs iNPS from which the core concept was derived (Fig4.5B). We also observe a tighter distribution of peak widths, closely matching the expected region size (Fig4.5C). Manual inspection of resultant nucleosome regions additionally suggests congruity with visually identifiable peaks, and equally high performance on broader and overlapping peaks (Fig4.5D). This improved methodology was applied to all WT and remodeler mutants to provide a high confidence set of nucleosome positions for more quantitative analysis of chromatin properties.

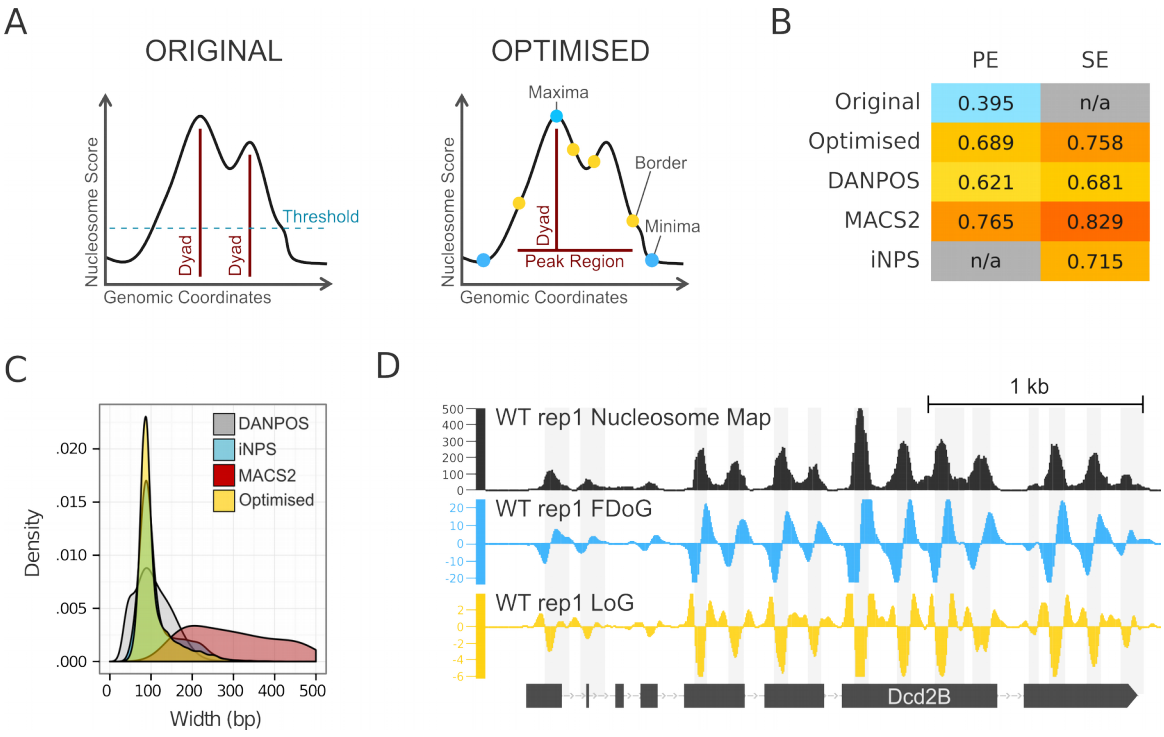

Fig4.5: Optimising Nucleosome Detection.

A) Diagrams of the peak calling strategies used in the original and optimised pipelines.

B) Spearman's correlation values for regions determined by respective peak-callers from sub-sampled WT data.

C) Density plot of region widths for regions called from sub-sampled data using respective peak-callers.

D) Example gene with WT rep1 nucleosome signals and intermediate convolution steps involved in peak calling (FDoG = First Deriviative of Gaussian; LoG = Laplacian of Gaussian). Highlighted regions in grey indicate identified nucleosome regions.

4.6 Quantifying WT Nucleosome Parameters

Given the high-confidence nucleosome dyad and boundary locations and robust nucleosome maps produced through the improved pipeline outlined above it is now possible to sensitively measure individual properties of chromatin structure at the nucleosome level. We define four main nucleosome parameters of interest for the study of chromatin remodeler functions as summarised in Fig4.6A:

- Positioning is simply the change in average dyad position (peak summit) between each nucleosome position and the canonical WT position.
- Occupancy indicates the proportion cells in the population that possess a nucleosome bound at a given locus. Occupancy is thought to be influenced by processes including nucleosome turnover, eviction and accessibility. Occupancy is measured as the sum of nucleosome scores within peak boundaries.
- Distribution relates to the uniformity of positioning of nucleosomes across the population of cells, with broader regions indicating less stringent maintenance of a nucleosome position. To measure distribution, nucleosome score values are cumulatively summed across the peak region and a cumulative probability distribution produced. The gradient of the central dyad region (dyad position ± 2 bins) is measured, with broader distributions causing a reduced gradient, and tighter distributions a sharper gradient. Notably both occupancy and distribution will affect peak heights in averaged chromatin profiles but represent very different underlying mechanisms.
- Nucleosome size is the footprint size of digest-protected fragments, measured as the average of fragment sizes for all reads contributing to the nucleosome score of a region. Nucleosome size has been previously under-studied due to the prevalence of short SE sequencing but may provide insight into nucleosome stability or alternative nucleosome structures.

After designing an algorithm to measure positioning, occupancy, distribution and size for all nucleosomes across the the genome I first applied it to the seven WT growth stage samples to characterise *Dictyostelium* nucleosome properties. While inter-experiment variations are observed, as noted previously, matched replicates are extremely closely matched - demonstrating the accuracy of the quantification pipeline. One exception to this is WT rep5 – which was subjected to fewer cycles during sequencing and shows a significantly decreased fragment size compared with other

ExpC replicates (e.g. -5.4 bp vs. WT rep6, $t = -162.65$, $p < 2.2 \times 10^{-16}$), it is therefore excluded from further analyses. Positioning of nucleosomes in *Dictyostelium* appears to be relatively dynamic, displaying a mean 8.6 bp (± 0.02 bp) shift compared to canonical nucleosome positions, however despite optimisation of peak calling we cannot rule out remaining inaccuracies. Interestingly nucleosome distribution parameters display a bi-modal distribution suggesting distinct sub-populations of tighter and broader peaks – representing more strictly and leniently regulated nucleosome positions respectively. Despite digestion-biases in nucleosome sizes between experiments, the mean footprint size of 145.5 bp closely matches the canonical nucleosome footprint of 147 bp. The average nucleosome parameters across WT replicates are summarised in Table4.2.

Sample	Position (bp)	Occupancy	Distribution	Size (bp)
WT rep1	7.68 ± 0.02	145 ± 0.25	6.70 ± 0.005	146.4 ± 0.01
WT rep2	7.45 ± 0.02	141 ± 0.25	6.70 ± 0.005	146.3 ± 0.01
WT rep3	7.61 ± 0.02	131 ± 0.18	6.35 ± 0.005	150.3 ± 0.01
WT rep4	7.85 ± 0.02	132 ± 0.18	6.37 ± 0.005	150.4 ± 0.02
WT rep5	10.08 ± 0.03	162 ± 0.33	6.95 ± 0.006	138.4 ± 0.02
WT rep6	9.91 ± 0.03	147 ± 0.30	6.77 ± 0.005	141.4 ± 0.02
WT rep7	10.14 ± 0.03	150 ± 0.30	6.83 ± 0.006	141.2 ± 0.02

Table4.2: Dictyostelium Nucleosome Parameters. Mean nucleosome parameters (± standard error) measured across WT growth stage replicates for all canonical nucleosome positions (n = 164,549).

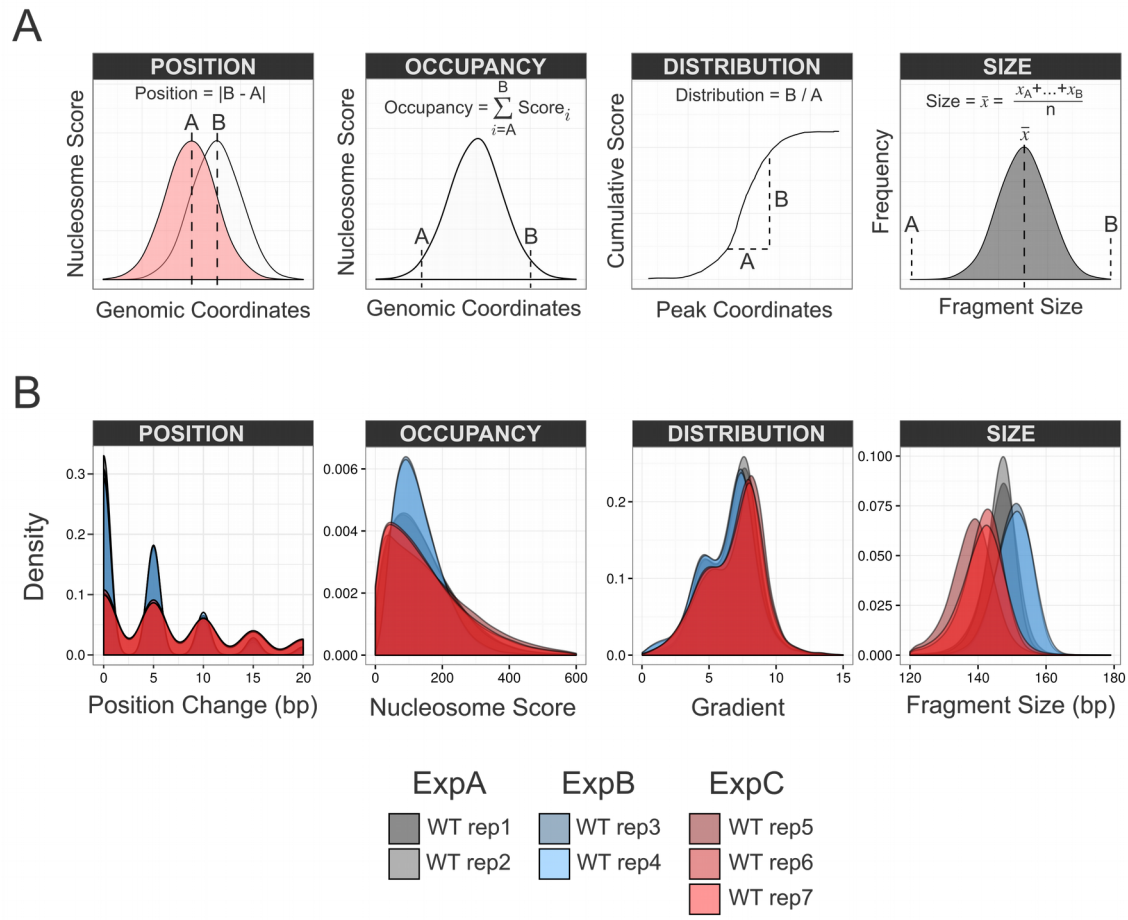

Fig4.6: *Dictyostelium* Nucleosome Parameter Characterisation.

A) Diagrammatic representation of the four nucleosome parameters measured.

B) Density plots of the four nucleosome parameters quantified for all canonical nucleosome positions (n=164,549) across all seven WT replicates.

4.7 Nucleosome Parameter Changes in Remodeler Mutants

The development of accurate quantification tools allows us to determine the global influence of remodeler loss on specific chromatin properties. Positioning shifts, occupancy, distribution and nucleosome size were measured in ChdA, ChdB, ChdC and Isw null mutants and compared globally against matched WT parameters (Fig4.7). Interestingly the majority of parameters are not globally perturbed upon remodeler loss, with all remodeler mutants displaying negligible effect sizes for distribution and occupancy changes (i.e. Cohen's d < 0.2). ChdC and Isw cause a small increase in the absolute positioning shift (d = 0.31 and d = 0.15 respectively). However the most prominent effects are surprisingly observed for nucleosome size, with ChdA causing a large decrease in average footprint size (-6.64 ± 0.2 bp, d = -1.17), and ChdC causing a moderate increase (5.67 ± 0.2 bp, d = 0.54).

The ability to capture the known spacing changes in ChdC provide a validation of the developed pipeline. The average shift of 5.5 ± 0.2 bp relative to WT nucleosome positions closely matches the spacing increase observed at TSS profiles, and measured previously (Platt 2013). Notably this positioning change also closely matches the measured change in nucleosome size, raising the possibility that ChdC in fact influences nucleosome structure, with previously reported spacing effects a result of this mechanism.

While ChdA and ChdB null mutants do not display large global shifts in occupancy, they do cause slight yet significant reciprocal changes (9.04 ± 0.2 and -9.15 ± 0.2 respectively). This is in keeping with their genic occupancy effects observed at TSS average profiles having a dominant effect on the global average due to a preponderance of canonical nucleosomes positions falling within gene bodies (genic = 131,765, intergenic = 27,023). While this is suggestive of genic occupancy maintenance being the primary role of ChdA and ChdB it is necessary to examine the localisation of changes with regards to gene bodies.
Greater overall variability is observed for samples from Ion Torrent sequencing, possibly due to reduced read depth. Nonetheless, Isw samples display a slight increase in positioning changes over matched WT samples (3.2 ± 0.1 bp). A minor reduction (d = -0.05) in distribution and increase in nucleosome size (d = 0.1) is also observed. Therefore the loss of average nucleosome structure observed within gene bodies upon Isw loss appears to represents a combination of minor changes to

nucleosome positioning, organisation across the population, and nucleosome structure or accessibility.

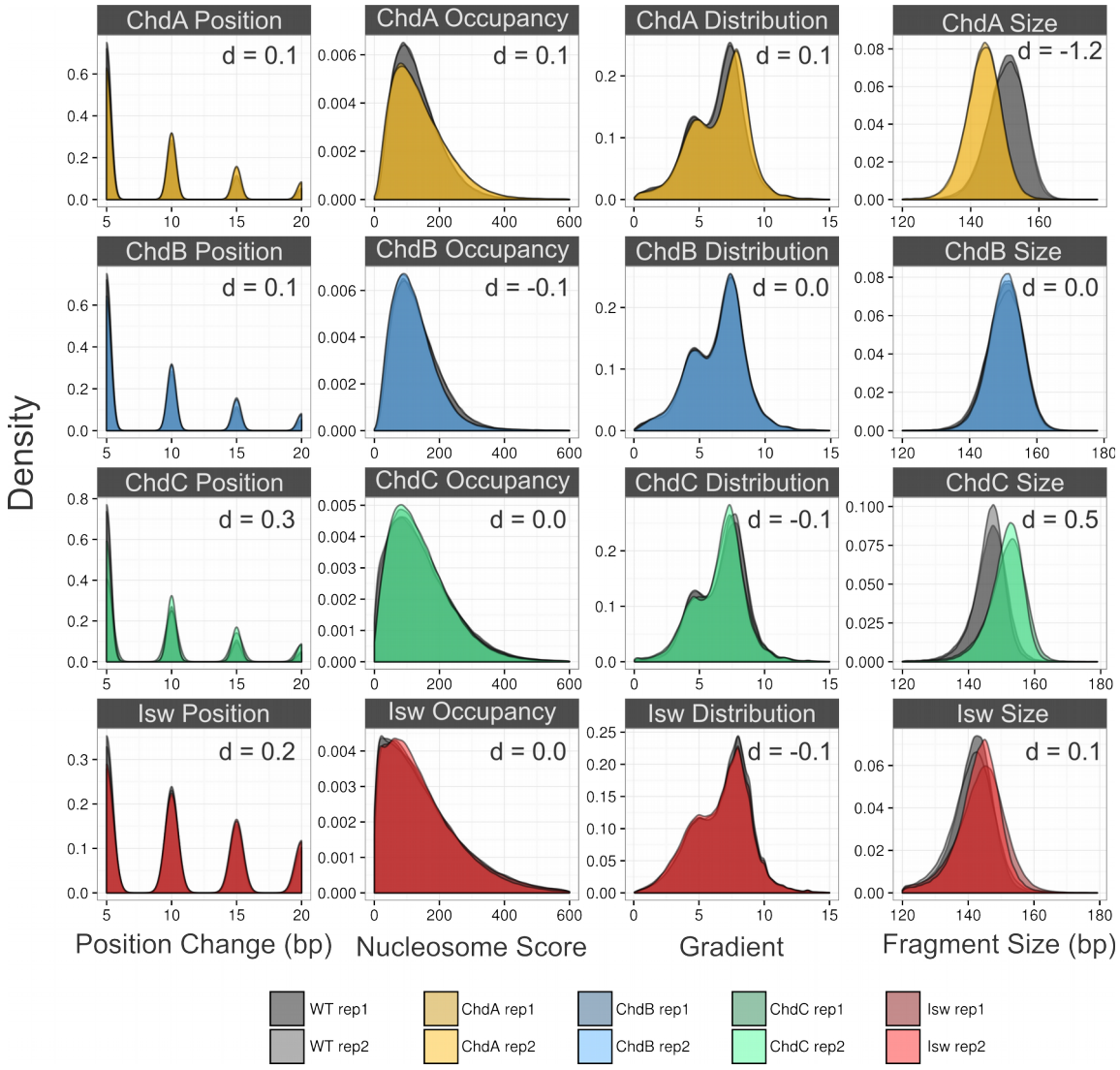

Fig4.7: Remodeler Loss Uniquely Influences Chromatin Properties.

Density plots of the distribution of global nucleosome parameters measured for all canonical nucleosomes (n = 164,549) in all chromatin remodeler null mutants and matched WT samples. Cohen's d values of effect size for the mean change in each condition are indicated.

4.8 Visualising the Localisation of Chromatin Defects

Having established the global chromatin changes induced by loss of individual spacing remodelers I next aimed to establish the localisation of these changes relative to genic features. The commonly used TSS or TTS average profiles allow a qualitative visualisation of gross chromatin changes but their interpretation is limited by the myriad factors contributing to the observed average structure. These convoluted factors include the distinct parameters at individual genes discussed above (positioning, occupancy, distribution and size), but also effects of averaging across genes. For example a change in NRL or a conservation of phasing but a shift relative to the TSS would both decrease the structure of the global profile.

I therefore established a novel visualisation method to correct for positioning differences, and visualise nucleosome structure and parameters at defined nucleosome positions. Nucleosome score distribution is averaged around individual nucleosome dyad locations rather than relative to genomic features. This allows an un-biased visualisation of occupancy and distribution changes. To provide localisation information we take the approach of using defined reference nucleosome positions relative to gene boundaries, similar to the designation around canonical TSS profiles (-1, +1, +2, etc.) to categorise individual nucleosomes. These standard categories are extended to terminal nucleosomes (TN-1, TN, TN+1, etc.), and region averages (genic, upstream and downstream) to allow simultaneous visualisation of the entire gene structure. The mean change in positioning, occupancy, distribution and size parameters within each nucleosome category is also quantified to identify significant changes at individual positions. Gene profiles were plotted for all spacing remodeler mutants relative to matched WT replicates (Fig4.8).

Examination of the positioning values observed at specific nucleosome categories in *ChdC*$^{-}$ reveals the expected ~5 bp shift away from the TSS at +2 and +3 positions and not at the +1. This recapitulates previously reported trends in ChdC mutants and provides validates the performance of the analysis pipeline. In addition to this known chromatin defect, a number of chromatin changes are observed that were not possible to detect from the original global averaging of genes. A positioning shift away from the downstream NFR and into the gene body is also seen upstream of the TN, although of reduced magnitude (~ -2bp) compared with the TSS. Occupancy is signficantly increased at -1/TN+1 positions, and decreased in the gene body. The fact that

localisation of size changes does not match that of positioning changes suggests that the altered nucleosome spacing of ChdC mutants is not a result of H1 histone incorporation or altered nucleosomes structure.

The profile of *ChdA*$^{-}$ parameters confirms that occupancy is increased throughout the gene body, excluding the +1 nucleosome, and decreased only at the -1/TN+1 positions. Additionally, a negative positioning shift specific to the TN of ~ -4 bp is observed, indicating a shift of the TN further into the gene body. Strikingly the occupancy and positioning changes observed in *ChdB*$^{-}$ are almost exactly the inverse of *ChdA*$^{-}$ - with reduced genic occupancy, increased -1/TN+1 occupancy and a positive positioning shift away from the gene body specific to the TN. This suggests that the two CHD proteins may play antagonistic roles in regulating genic occupancy and positioning of the TN, however the distribution and size changes of ChdA and ChdB are distinct, suggesting further independent roles. In *ChdA*$^{-}$ nucleosome distribution is consistently increased across all regions indicating that contrary to expectations loss of this spacing remodeler leads to stricter maintenance of nucleosome positions across the population of cells, while ChdB does not influence distribution. Finally *ChdA*$^{-}$ and *ChdB*$^{-}$ do cause reciprocal effects on nucleosome footprint size, however while in *ChdA*$^{-}$ the reduced nucleosome size appears universal, ChdB loss causes increased nucleosome size only in intergenic regions.

The high variability observed in Isw makes detailed parameter analysis more difficult, however reproducible negative positioning shifts, decreased occupancy and decreased distribution is observed at the +1 to +3 positions, consistent with moderate disruption of multiple nucleosome parameters causing the observed loss of average chromatin structure.

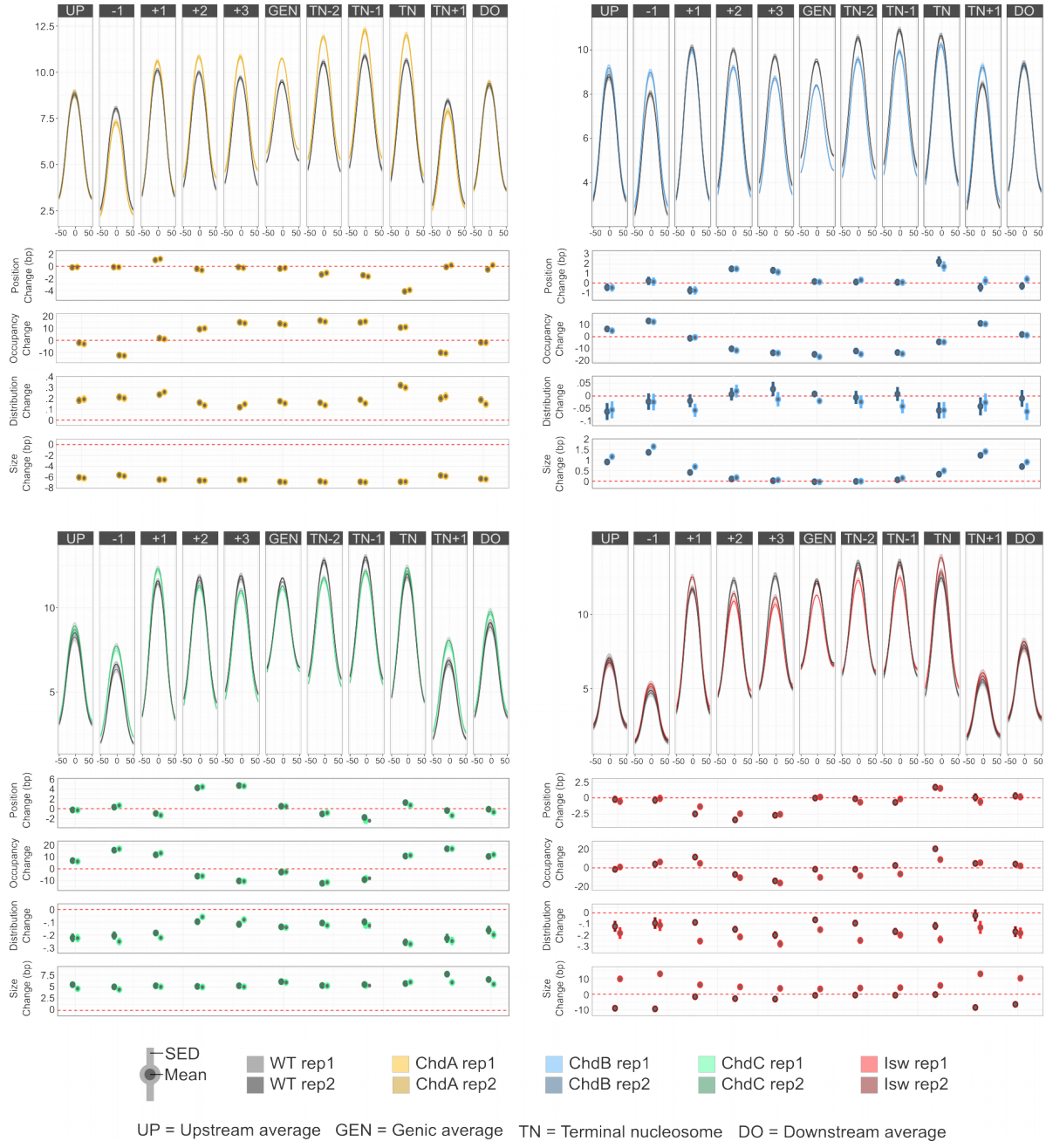

Fig4.8: Chromatin Changes are Localised to Sub-Genic Locations.

Upper panels: average nucleosome score distribution ± 50 bp of each nucleosome dyad position for all genes (n=12,964) grouped by nucleosome category (line = mean, shaded area = 95% confidence interval, UP, GEN and DO = average of upstream, genic and downstream nucleosomes repsectively, TN = terminal nucleosome).

Lower panels: average parameter change for all nucleosomes grouped by nucleosome category (circle = mean, intervals = standard error of the difference (SED)).

4.9 Summary

Current understanding of the distinct roles played by individual spacing remodelers is limited by the global genome averaging of nucleosome scores to detect chromatin defects. Here I have developed and validated novel bioinformatic methods to quantify distinct nucleosome parameters and explore the localisation of these parameter changes in remodeler mutants. MNase-sequencing of *Isw*$^{-}$ and bioinformatic analysis of *Isw*$^{-}$, *ChdA*$^{-}$, *ChdB*$^{-}$ and *ChdC*$^{-}$ has allowed detailed characterisation of the chromatin defects caused by loss of each individual spacing remodeler in *Dictyostelium*.

Notably, all remodeler mutants cause unique and complex nucleosome parameters changes across the genome, demonstrating that non-redundant roles the ISWI and CHD families. ChdA and ChdB have reciprocal effects on the relative nucleosome occupancy levels within genes. The previously reported role of ChdC in reducing linker lengths of nucleosomes downstream of the +1 position was re-confirmed and a novel effect on nucleosome footprint size detected. Isw has minor, non-uniform effects on nucleosome occupancy, positioning and distribution, and is required to maintain organised nucleosomal arrays.

Chapter 5:

Exploring the Relationship between Chromatin Structure and Transcriptional Regulation

5.1 Introduction

Having determined the individual roles of the four spacing remodelers (ChdA, ChdB, ChdC and Isw) in establishing and maintaining chromatin structure, I next aimed to examine the importance of this remodeling in the maintenance of gene expression, and how mis-regulation upon remodeler knockout leads to observed phenotypic effects. Transcriptome-sequencing (RNA-seq) was previously conducted for WT and CHD mutants in vegetative cells (Plattt et al. 2013). Enrichment of chromatin defects was observed in genes mis-expressed upon ChdC loss, however the majority of mis-expressed genes did not display significant chromatin changes (Platt et al. 2013). The detailed nucleosome profiles of *ChdA*$^{-}$, *ChdB*$^{-}$ and *Isw*$^{-}$ presented in the current study provide the opportunity to conduct a more in-depth characterisation of the relationship between nucleosome remodeling and transcriptional effects. Furthermore, cross-comparison between remodeler mutants allows examination of how remodelers interact to maintain *in vivo* chromatin structure and expression programs.

I first profiled transcriptional changes induced by loss of the remaining unstudied spacing remodeler – Isw, before conducting a detailed comparison of all CHD and ISWI mutant transcriptomes. Expression profiles were then compared with nucleosome parameter profiles, and the overlap between transcriptonally mis-regulated and structurally mis-modeled gene sets examined. Finally, I examined how spacing remodelers interact to maintain cell-type specific transcriptional programs.

5.2 The Gene Expression Profile of Isw Null Mutants

To establish the impact of Isw loss on the transcriptional landscape of vegetative *Dictyostelium*, I performed triplicate mRNA-sequencing of WT and *Isw*⁻ cell lines grown in shaking culture. Relative expression levels are highly reproducible between replicates indicating high data quality (Fig5.1A). Differential expression analysis reveals significant ($p < 0.05$) mis-expression of over 50% of analysed genes (Fig5.1B). A large number of genes are either up- or down-regulated (n = 3210 and n = 2997 respectively) upon Isw loss, with a slight bias towards de-repression. Furthermore, when only strongly altered genes are examined ($p < 0.05$ and > 2 fold change (FC)) the bias towards de-repression is amplified (n=901 up-regulated, n=728 down-regulated). Gene-ontology analysis indicates that despite this wide-spread transcriptional mis-regulation, there is little bias for specific pathways or processes (Fig5.1C). This lack of functional enrichment is also analogous to previous findings from ChdA and ChdB KO mutants, which also exhibit little ontology bias (Platt et al. 2013). Whereas ChdC-mutants displayed transcriptional disruption of metabolic pathways and a strong growth inhibition, ChdA, ChdB and Isw mutants which display little ontology bias also display no growth phenotype, possibly suggesting a more targeted regulatory role for ChdC.

Closer examination of the most strongly mis-regulated genes identifies genes involved in a range of processes including vesicle trafficking and secretion (lmcA, rabR; Bakthavatsalam & Gomer 2010), development (cotD, cotA, hbx7; Takemoto et al. 1990), and actin cytoskeleton dynamics (wipA; Myers et al. 2006) (Fig5.2A). Mis-regulation of any of these pathways could explain the enhanced migration speeds of *Isw*⁻ cells. The strong down-regulation of wipA, which regulates F-actin polymerization (Myers et al. 2006), may alone be enough to influence chemotaxis speeds. The strong down-regulation of srsA, a protein strongly induced immediately following starvation, loss of which delays aggregation (Sasaki et al., 2008), may explain the observed developmental delay. A more striking pattern however is the abundance of transposable elements (TE) and lowly transcribed genes that are strongly up-regulated in Isw null cells. Within the subset of strongly mis-regulated genes ($p < 0.05$ and > 2 FC), TE elements are highly over-enriched, and disproportionately up-regulated ($p = 3.9 \times 10^{-17}$ for both comparisons, hypergeometric distribution; Fig5.2B); revealing an important role for Isw In TE repression.

To establish whether this de-repression is specific for TE or potentially represents a

global role for Isw in transcriptional repression, I identified all genes that were up- and down-regulated upon Isw loss, and examined their expression levels under WT conditions (Fig5.2C). A strong divide is observed, with genes that are repressed in *Isw*⁻ cells exhibiting high expression in WT cells, and over-expressed genes in *Isw*⁻ exhibiting significantly lower expression in WT ($p < 1 \times 10^{-15}$). Hence Isw loss appears to have repressive effects at highly expressed genes, and an activating effect on repressed genes.

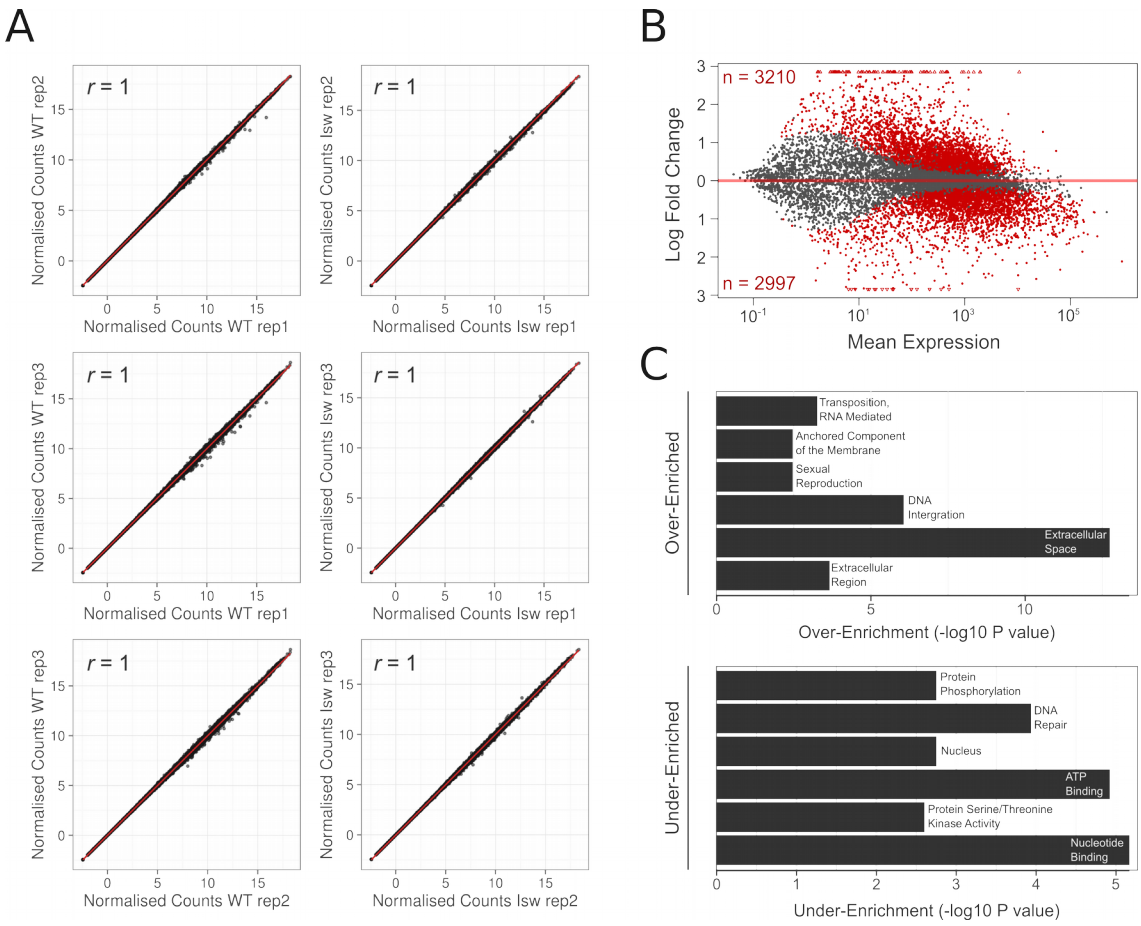

Fig5.1: Isw Loss Results in Wide-spread Transcriptional Disruption.

A) Correlation of rlog normalised read-counts between biological replicates for all analysed genes (n = 11,829, linear regression fit and Spearman's *r* are indicated). **B)** MA plot of moderated log2 fold change in expression (*Isw*⁻ vs. WT) against mean expression level for all analysed genes (n=11,829). Red points indicate significantly differentially expressed genes ($p < 0.05$), the total number of significantly up- and down-regulated genes are annotated in red. **C)** Barplots of -log10 p-values for significantly over- and under- enriched gene ontology categories within the differentially expressed gene set (*Isw*⁻ vs. WT).

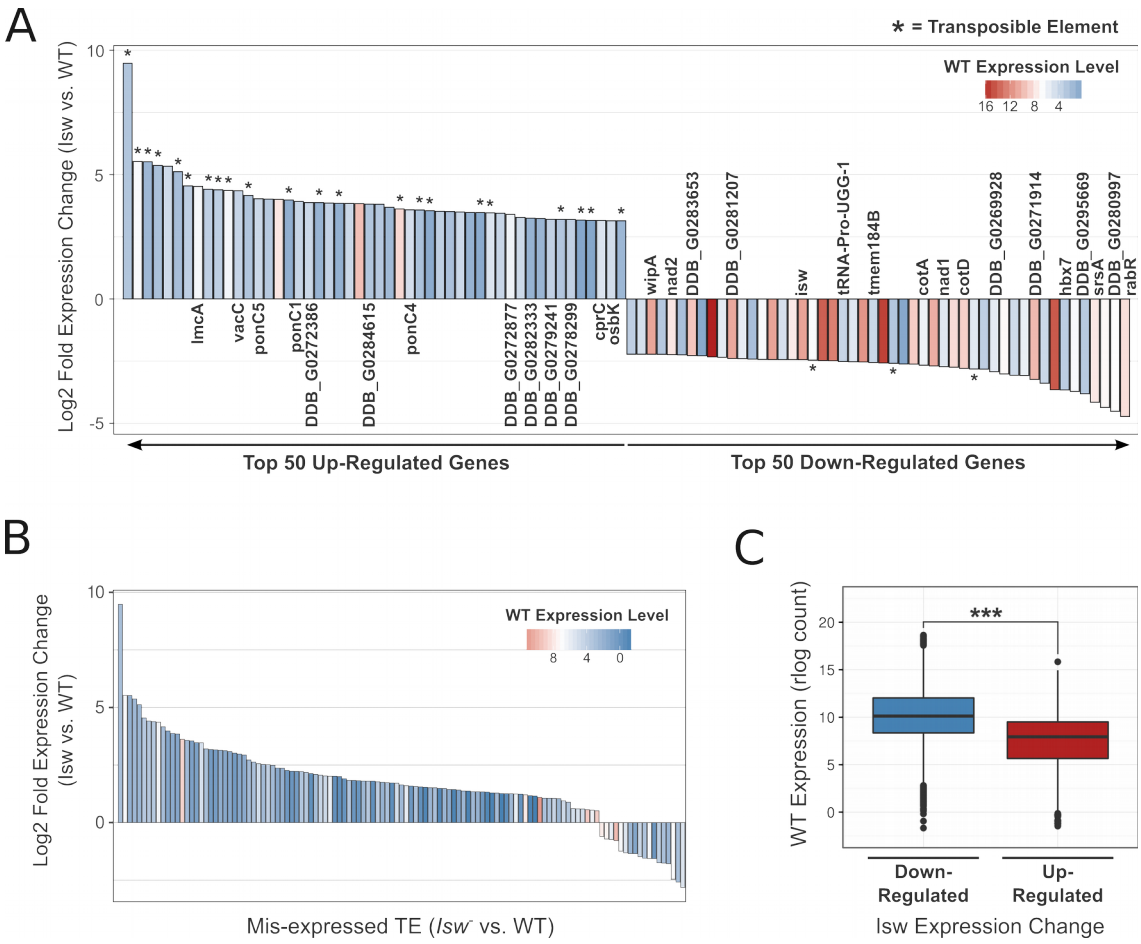

Fig5.2: Isw is Required for Maintenance of Gene Repression.

Log2 fold expression changes (isw vs WT) are plotted for: **A)** the 50 most strongly up- and down-regulated genes (genes with anotated gene products are labeled, stars indicate TE genes), and **B)** All TE genes mis-regulated in *Isw-*. Bars are coloured by WT expression level of respective genes (red=highly expressed, blue = lowly expressed, white=average expression level for all genes). **C)** Boxplot indicating the distribution of WT expression levels for all significantly up- (n=3,210) and down- (n=2,997) regulated genes (*Isw-* vs, WT; *** = $p < 0.001$).

5.3 Comparing the Transcriptional Effects of Remodelers

I next explored the relationship between the transcription profiles of each remodeler mutant; to allow direct comparison of the four spacing remodeler mutants, previously generated RNAseq data from *ChdA*$^{-}$, *ChdB*$^{-}$ and *ChdC*$^{-}$ cell lines (Platt et al. 2013) were re-analysed using the same pipeline used for *Isw*$^{-}$ analysis. The number of strongly differentially expressed ($p < 0.05$ and > 2 FC) genes identified for the CHD family mutants closely matches those observed previously (Fig5.3A), providing validation of our findings. As noted previously for Isw, the number of strongly up-regulated genes is consistently higher than those down-regulated across all remodelers. The average repression of highly-expressed genes, and de-repression of lowly-expressed genes is also apparent for all four mutants. Interestingly the overall degree of mis-regulation roughly reflects the degree of phenotypic severity (ChdC > ChdA > Isw > ChdB), which is further supported by examination of the sample-to-sample distances (Fig5.3B).

To examine the relationships between transcriptional profiles I performed principle components analysis on the most variable genes across all conditions (Fig5.3C). Two components explain over 50% of the variance and distinguish distinct transcriptional responses to remodeler loss. The strongest transcriptional effect is observed in *ChdC*$^{-}$, which is clearly separated from all other conditions. The second component identifies a lesser, divergent transcriptional phenotype separating ChdA and ChdB from Isw. To examine the genes contributing to these distinct transcriptional effects, the top 20 most heavily weighted were plotted (Fig5.3D) and gene ontology analysis conducted on the top 200 heavily weighted genes. Genes heavily mis-regulated by ChdC in this gene set are also frequently mis-regulated in all other spacing remodelers and enriched for metabolic ontologies (e.g. carbohydrate derivative metabolic process, $p < 1 \times 10^{-4}$), suggesting a common transcriptional response of metabolic pathways to remodeler loss, albeit to differing degrees. The genes divergently expressed in ChdA/ChdB and Isw on the other hand appear more varied but include ontologies related to signaling (e.g. receptor activity, $p = 0.02$ and signal transduction, $p = 0.003$) and, notably, phototaxis ($p = 0.03$) which is known to be defective in ChdA mutants (Platt et al. 2013). We conclude that *ChdC*$^{-}$ displays the strongest transcriptional disruption among remodeler mutants, affecting primarily metabolic processes in vegetative cells. ChdA, ChdB and Isw have more modest transcriptional effects, influencing a range of cellular processes.

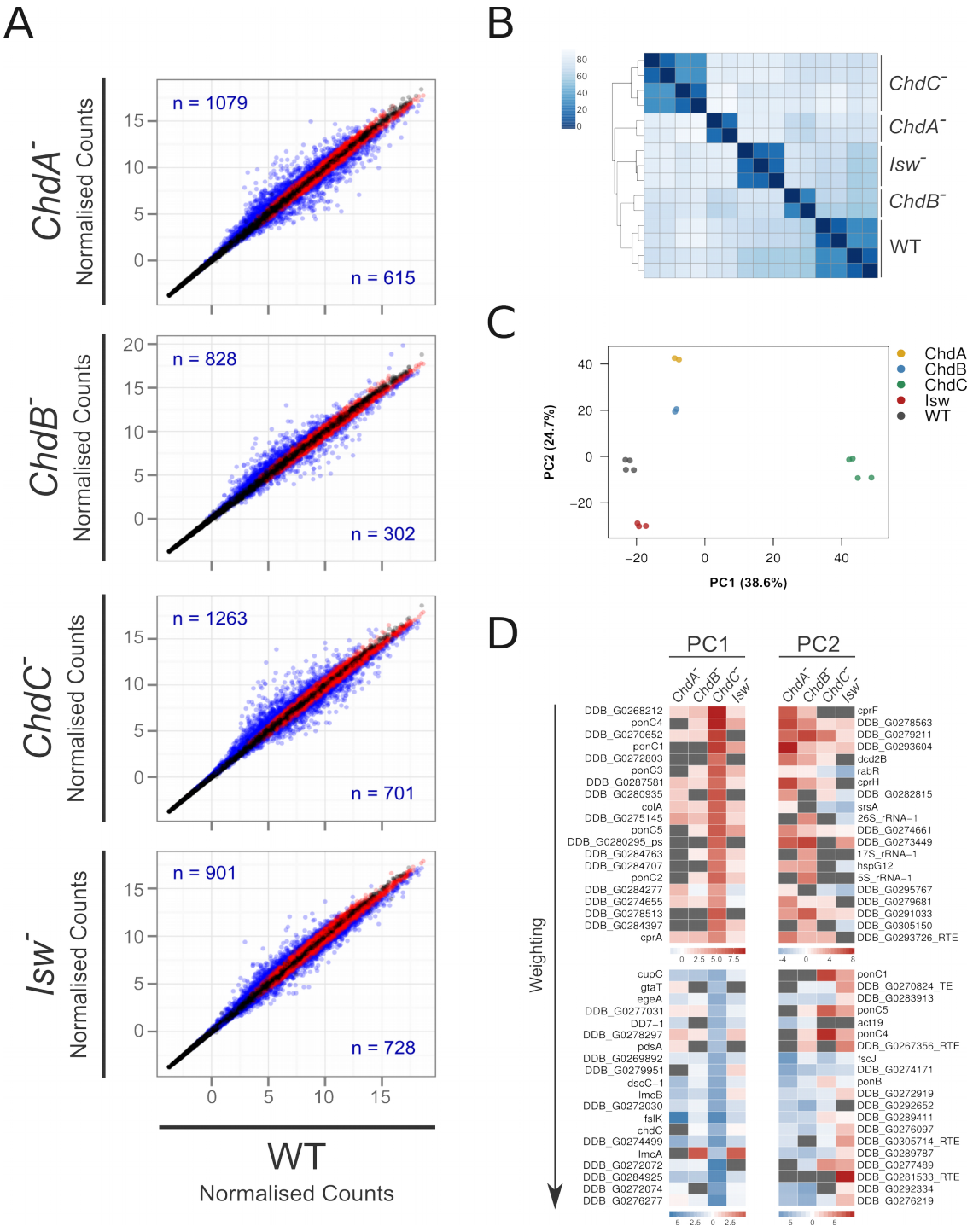

Fig5.3: Comparison of Transcriptional Disruption between Remodeler Mutants.

A) Comparisons of rlog normalised gene counts between each remodeler mutant and WT cells (n=11,829, red=differentially expressed (DE; $p < 0.05$), blue=DE by over two-fold). **B)** Euclidean distances matrix of rlog transformed counts. **C)** Principle components analysis (PCA) of RNAseq profiles, the first two PCs are plotted. **D)** Expression change of the 20 most heavily weighted genes from PC1 and PC2 (grey=non-DE).

5.4 Impact of Remodeler Loss is Dependent on Transcription Level

As noted above, examination of the global transcriptome profiles of the four remodeler mutants (Fig5.3A) suggests that highly- and lowly-expressed genes are differentially affected by remodeler loss; similar to what was observed for *Isw-* (Fig5.2C). To test this, the gene sets strongly up- and down-regulated ($p < 0.05$ and > 2 FC) in remodeler mutants were identified, and the WT expression level of each gene set plotted (Fig5.4A). As a control, publicly available RNA-seq data from an un-related ABC transporter null mutant was also analysed using the same parameters (Miranda et al. 2013). While all gene sets mis-regulated by chromatin remodeler loss display a significant difference in their WT expression levels ($p < 1x10^{-15}$ for all conditions), genes mis-regulated by loss of AbcA10 show no bias in their physiological expression levels ($p = 0.056$). This indicates that loss of any individual remodeler results in a repression of highly-expressed genes, and a de-repression of lowly-expressed genes.

This raises the question of whether repression of TE is specific to Isw, or is a more general repressive effect across remodelers. The number of strongly up-regulated TE was counted for each remodeler mutant and plotted alongside the number expected by chance based on the total number of strongly up-regulated genes in each condition (Fig5.4B). Only *Isw-* exhibits a significant enrichment of TE in the strongly up-regulated gene set ($p < 1 \times 10^{-17}$, upper-tailed hypergeometric distribution), strikingly TE are positively protected from mis-regulation in ChdA and ChdC ($p = 0.01$ and $p < 1 \times 10^{-5}$, lower-tailed hypergeometric distribution). Thus while spacing remodelers share a common, repressive effect on many lowly-transcribed genes, the role of Isw in repression of TE is unique.

I next asked whether nucleosome parameters also display a bivalent effect in lowly- and highly-transcribed genes. All genes were divided into quartiles based on their expression level in WT vegetative cells, and average nucleosome profiles plotted (Fig5.4C). In all four remodeler mutants, chromatin defects are enriched in highly expressed genes. However, the nature of parameters changes is specific to each mutant, matching the global changes observed previously.

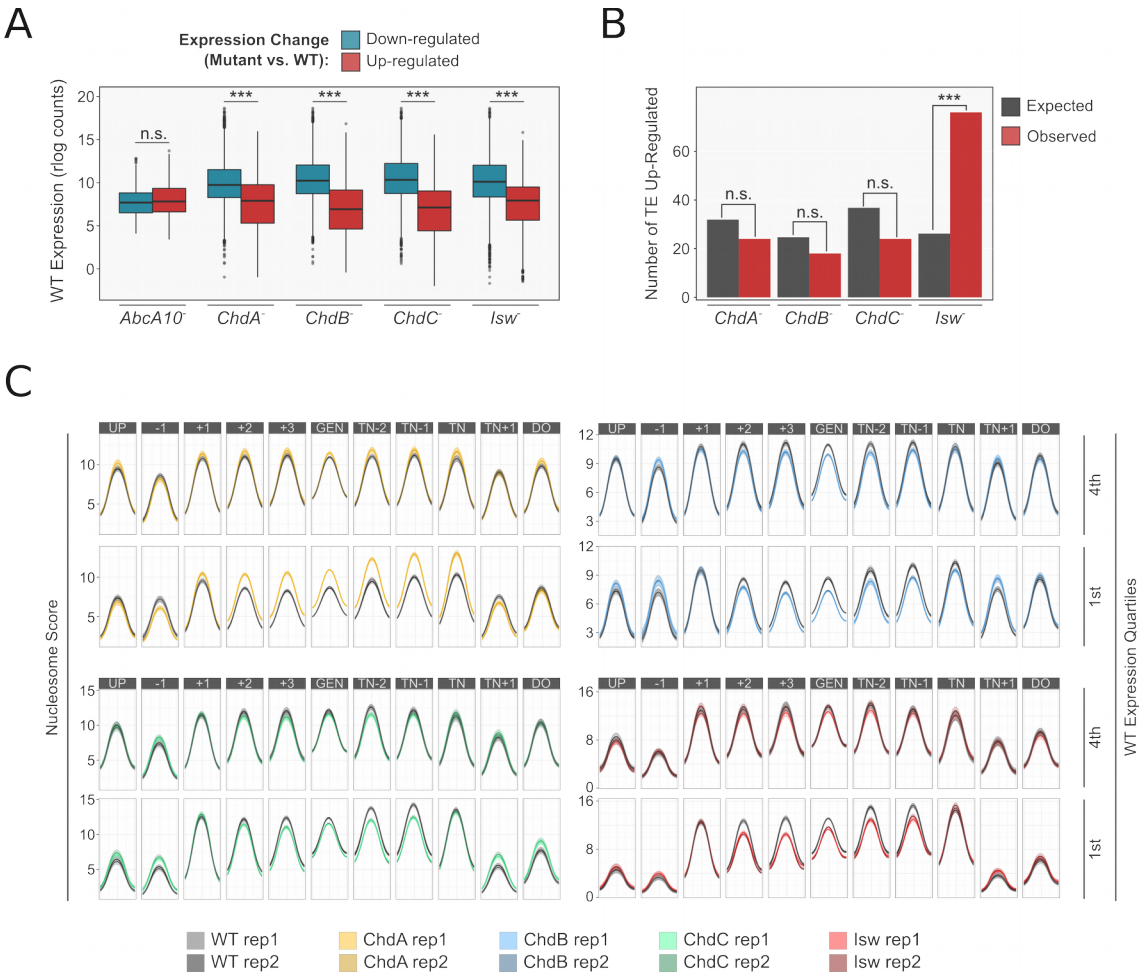

Fig5.4: The Differential Effects of Remodeler Loss on Highly- and Lowly-Expressed Genes.

A) WT expression levels of gene sets up- and down-regulated in mutant conditions (*** = $p < 0.001$, Mann-Whitney U).

B) Number of transposable elements (TE) strongly up-regulated ($p < 0.05$ and > two fold change) across each remodeler mutant, compared to the number expected by chance (*** = $p < 0.001$, upper tailed hypergeometric distribution).

C) Meta-nucleosome profiles for the 1st and 4th quartiles of genes divided by WT expression levels (UP, GEN and DO = averages of upstream, genic and downstream nucleosomes respectively).

5.5 Comparison of Gene Sets Mis-Regulated in Remodeler Mutants

The effects on highly- and lowly-expressed genes across CHD and ISWI mutants suggests a common transcriptional response to spacing remodeler loss. I therefore examined the degree of overlap for up- and down-regulated gene sets between the four mutants. Technical limitations prevent the detection of differential expression for genes with very low transcript levels, therefore to avoid overestimating the significance of the intersect between mis-regulated gene sets, the gene population used for statistical testing was restricted to genes with WT expression levels greater than or equal to that of the lowest mis-expressed gene (n = 10,909). In total, ~85% of genes (n = 9343) are mis-regulated in one or more remodeler mutants, with 35% of genes (n = 3863) displaying a greater than two-fold change in abundance. Thus spacing remodelers in combination influence the expression of the majority of the *Dictyostelium* genome. A highly significant association is observed for de-repressed gene sets between all remodeler mutants ($p < 1x10^{-20}$, hypergeomtric distribution with Benjamini-Hochberg correction); and the same is true for all repressed gene sets ($p < 1x10^{-20}$). Conversely no significant intersect is observed in any up-regulated vs. down-regulated gene set comparisons.

The genes commonly regulated by all spacing remodelers (n = 182) were more closely examined (Fig5.5B). Comparison with WT expression levels show that commonly mis-regulated genes tend to be either highly expressed or highly repressed in WT conditions. As expected, the expression change in mutants largely negatively corresponds to the WT expression level (i.e. highly expressed genes tend to be down-regulated and lowly-expressed up-regulated). Thus many genes have a common transcriptional response to chromatin disruption, which is heavily dependent upon a genes initial expression level. Furthermore, expression changes in the mutants correlate with physiological expression changes in development (0h vs. 10h development). Hence CHD and ISWI remodelers are all required to suppress developmental expression changes, and maintain the growth stage transcription program.

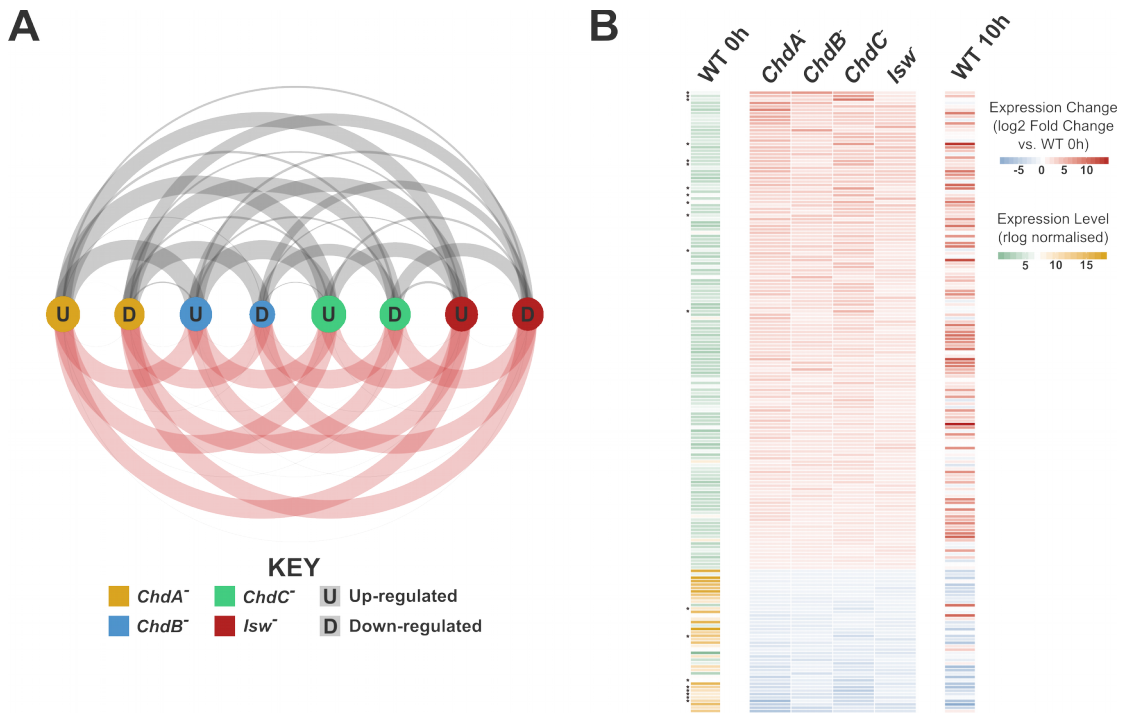

Fig5.5: Chromatin Remodelers Regulate a Common Subset of Genes.

A) Overlapping gene sets for all strongly up- and down-regulated genes between all remodeler mutant conditions, circle sizes are scaled to the number of mis-regulated genes per set, the widths of arc lines connecting pairs of gene sets represent the degree of overlap (top) and the -log10 P-value of the hypergeometric distribution test for the significance of the overlap (bottom). Arc-lines indicating significance are coloured red if significant and grey if non-significant.

B) Heatmap of the 182 genes strongly mis-regulated in all four remodeler mutant conditions. Lane 1 indicates the WT expression level, lanes 2-5 indicate the log2 fold change in expression level between remodeler mutants and WT (0h of development), and lane 6 indicates the log2 fold change in expression between WT cells developed for 10h post-nutrient depletion on filters vs. vegetative WT cells (WT 0h). The colour scale for expresion change is centered around zero, while the colour scale for WT expression level is centered around the median expression level for all genes. Stars to the left of lane1 indicate genes also identified as strongly weighted in the previously conducted PCA analysis.

5.6 Identifying Severely Mis-Modeled Genes

To determine whether transcriptional changes are associated with specific nucleosome parameter changes, genes displaying severely altered average positioning, occupancy, distribution or size properties were identified in each mutant. The average nucleosome parameters for each gene were compared to an empirical null distribution determined from Monte-Carlo resampling of all nucleosomes, and genes with an adjusted p-value less than 0.05 are defined as mis-modeled. While the numbers of significantly altered genes from each parameter category largely follow the trends expected from global chromatin profiles (Table5.1), an unexpected, bi-directional effect of ChdB loss on the occupancy of distinct gene sets is revealed, likely masking the strength of occupancy changes observed in averaged profiles.

To validate the performance of this approach in identifying mis-modeled genes, the average TSS profiles of individual mis-modeled gene sets were plotted (Fig5.6). As TSS profiles are independent of all nucleosome calling and parameter quantification steps, this also provides a validation of the parameter quantification pipeline. All mis-modeled gene sets are strongly enriched for the specified parameter changes, however the remaining population of genes do still retain the global nucleosome defects characteristic of each mutant. Notably, the number of genes with significant altered nucleosome positioning in *ChdC*$^{-}$ is approximately a third of the number of mis-modeled genes previously reported (578 vs. 1685; Platt et al. 2013). Nonetheless the isolated mis-modeled subset shown here displays a highly similar TSS profile to those previously identified (Platt et al. 2013), hence this change is likely a result of both increased specificity in nucleosome parameters and increased stringency.

	Position	Occupancy		Distribution		Size	
		Increase	Decrease	Increase	Decrease	Increase	Decrease
ChdA	221	306	186	230	179	243	5753
ChdB	291	1549	1547	150	234	769	340
ChdC	806	725	307	152	344	2069	150
Isw	381	150	957	171	227	537	471

Table5.1. Severely Mis-Modeled Gene Sets. Summary of the number of mis-modeled genes in each parameter category for all four spacing remodeler mutants.

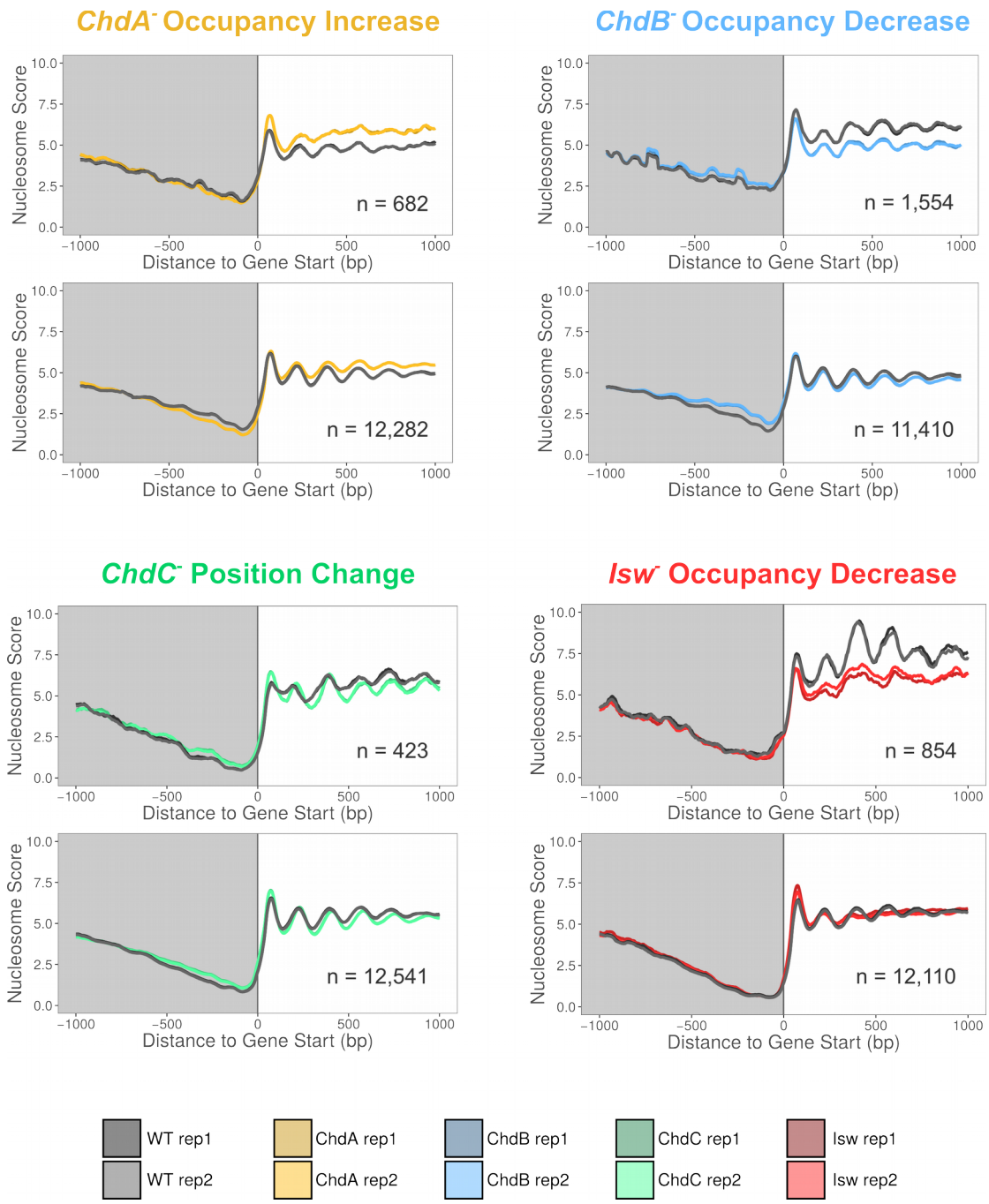

Fig5.6: Chromatin Profiles of Mis-Modeled Gene Sets.

Nucleosome scores within ±1000 bp of the gene start site were summed and normalised to total tag count for genes identified as severely mis-modeled in each condition (upper panels), and remaining, non-significantly altered genes (lower panels).

5.7 Association between Transcriptional and Structural Defects

Previous studies of chromatin remodelers, including that of ChdC from our own lab, have found that while genes displaying gross nucleosome changes are significantly associated with transcriptional disruption, the majority of mis-modeled genes are not mis-expressed. However as demonstrated by the current study, these gross nucleosome profile changes represent compound parameter changes. By examining the individual associations between parameter categories and transcriptional outcomes I aimed to discern the more causative structural changes from indirect or confounding effects. To this end, the intersects of all sets of genes identified as mis-modeled for any individual nucleosome parameter, or strongly mis-expressed were visualised (Fig5.7).

Overall, limited association is found between mis-expressed and mis-modeled gene sets, in keeping with previous observations. Indeed in the case of *Isw*$^{-}$ no significant association is observed with any individual structural defect. This potentially indicates that the transcriptional effect of Isw is an emergent property of multiple parameter changes and is not associated with any individual property of nucleosomal arrays. CHD mutants on the other hand display significant associations with specific nucleosome parameter changes. Genes up-regulated in *ChdA*$^{-}$ are associated with decreased footprint size ($p = 0.035$), and up-regulated genes in *ChdB*$^{-}$ are strongly associated with increased nucleosome occupancy ($p = 6 \times 10^{-13}$). The link between nucleosome positioning and/or occupancy changes in ChdC mutants and transcriptional changes that was previously reported (Platt et al. 2013) is re-confirmed. However, we are additionally able to de-convolute these effects – observing that re-positioning is primarily linked to de-repression, while occupancy decreases are associated with aberrant gene repression.

Surprisingly a consistent parameter-association occurs between occupancy and nucleosome footprint size across all mutants, with increased nucleosome size occurring alongside increased occupancy, and decreased size with decreased occupancy. This effect may be caused by the stability or structure of the nucleosomes, with more accessible nucleosomes more liable to over-digestion, which in the example of fragile nucleosomes, has been shown to lead to apparent occupancy losses (Xi et al. 2011).

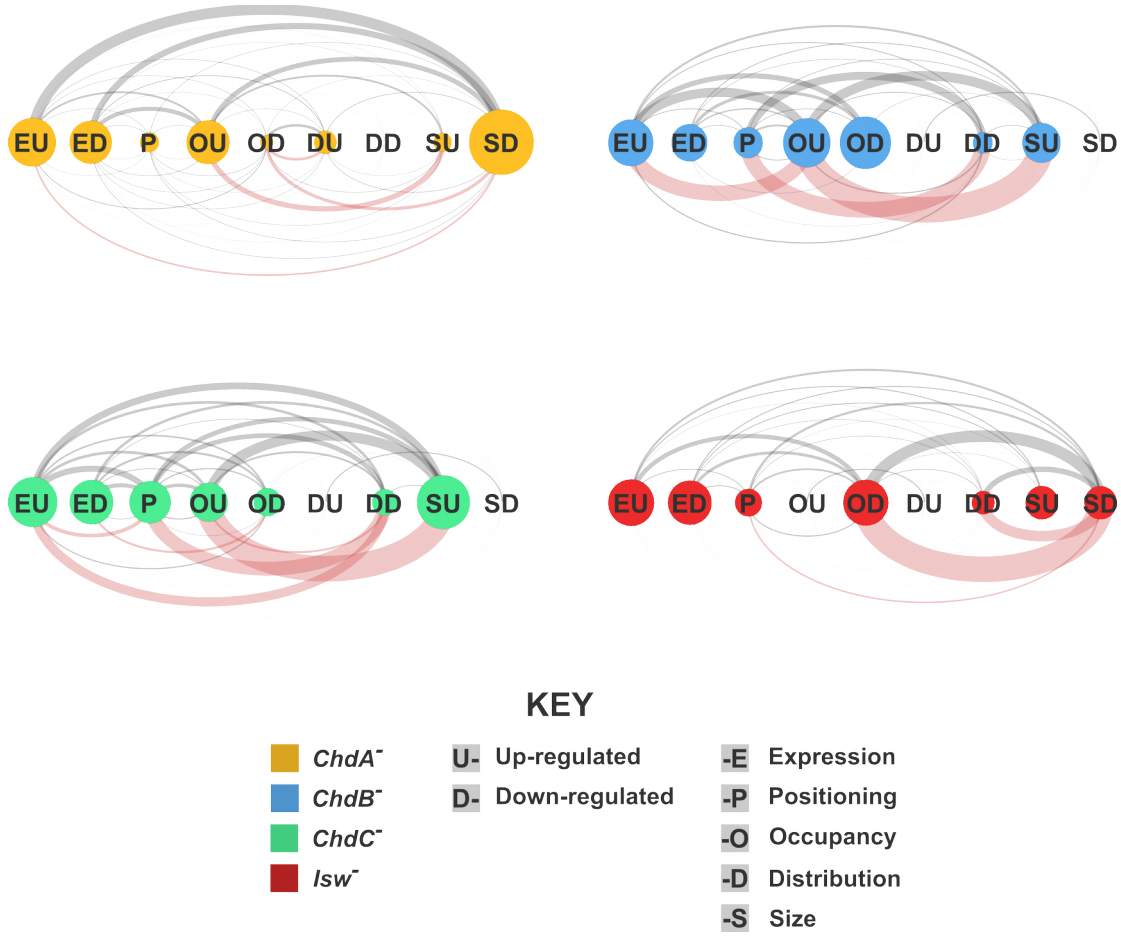

Fig5.7: Transcriptional Mis-regulation is Asscoiated with Specific Chromatin Changes. Representation of the overlap between strongly transcriptionally mis-regulated genes (>2 fold change and $p < 0.05$) and severely mis-modeled genes for each remodeler mutant. Each circle represents the gene set for one parameter change and one direction of mis-regulation as indicated by the key (with the exception of positioning changes which are absolute). Circle size indicates gene number, the width of arcs plotted above each pair of circles represent the relative degree of overlap, and the width of arcs below represent the -log10 adjusted p-value of the association; signficant associations ($p < 0.05$) are coloured red while non-significant are grey (hypergeometric distribution test).

5.8 Antagonistic Occupancy Effects of ChdA and ChdB

The finding that ChdB loss results in both increased and decreased genic nucleosome occupancy at distinct gene subsets raises the possibility that despite global average nucleosome profile differences, ChdA and ChdB could perform a common remodelling function on a subset of genes. To explore potential interaction between the two closely related CHD proteins, I first examined the nucleosome profiles of identified subsets of genes with significantly increased and decreased occupancy changes (Fig5.8A). Occupancy increased genes in ChdB- display a comparable magnitude of occupancy increase to those observed in ChdA, but additionally display an increased intergenic occupancy not seen upon ChdA loss. Intergenic occupancy changes are also not observed in the decreased occupancy subset, suggesting differences in the targeting or retention mechanisms between subsets and remodeler complexes.

To examine whether gene sets displaying differential occupancy effects in *ChdB*$^{-}$ are also mis-modeled in *ChdA*$^{-}$, the average occupancy change of genes within each subset was calculated for both mutants (Fig5.8B). Surprisingly, occupancy values display a striking inverse relationship between mutants, with genes identified as exhibiting significantly increased occupancy in *ChdB*$^{-}$ predominantly displaying reduced occupancy in *ChdA*$^{-}$. Occupancy scores of genes within this subset do display a modest negative correlated (r = -0.28, $p < 1 \times 10^{-15}$), however globally no correlation is observed (r = -0.02, p = 0.05). Thus ChdA and ChdB appear to perform antagonistic remodeling activities at a subset of genes to maintain nucleosome occupancy.

This raises the question of whether differential remodelling effects at these subsets relate to transcriptional changes. Strikingly, a significant difference in WT expression levels is observed between these two subsets ($p < 1 \times 10^{-16}$, Mann-Whitney U; Fig5.8C). In keeping with the globally averaged effects, the two subsets also display bivalent expression changes in ChdA and ChdB mutants compared to WT (Fig5.8D; $p = 4 \times 10^{-9}$ and $p < 1 \times 10^{-16}$ respectively, Mann-Whitney U). Hence highly expressed genes display increased nucleosome occupancy in the absence of ChdA and decreased nucleosome occupancy in *ChdB*$^{-}$. Furthermore these findings explain the association observed between de-repressed genes and occupancy increase in *ChdB*$^{-}$ (Fig5.7). Finally, a moderate correlation in expression change is noted between mutants within these subsets (Fig5.8E; OI: r = 0.45, $p < 1 \times 10^{-15}$; OD: r = 0.62, $p < 1 \times 10^{-15}$). This suggests that ChdA and ChdB have antagonistic activities on relative nucleosome levels, but a common effect on transcription.

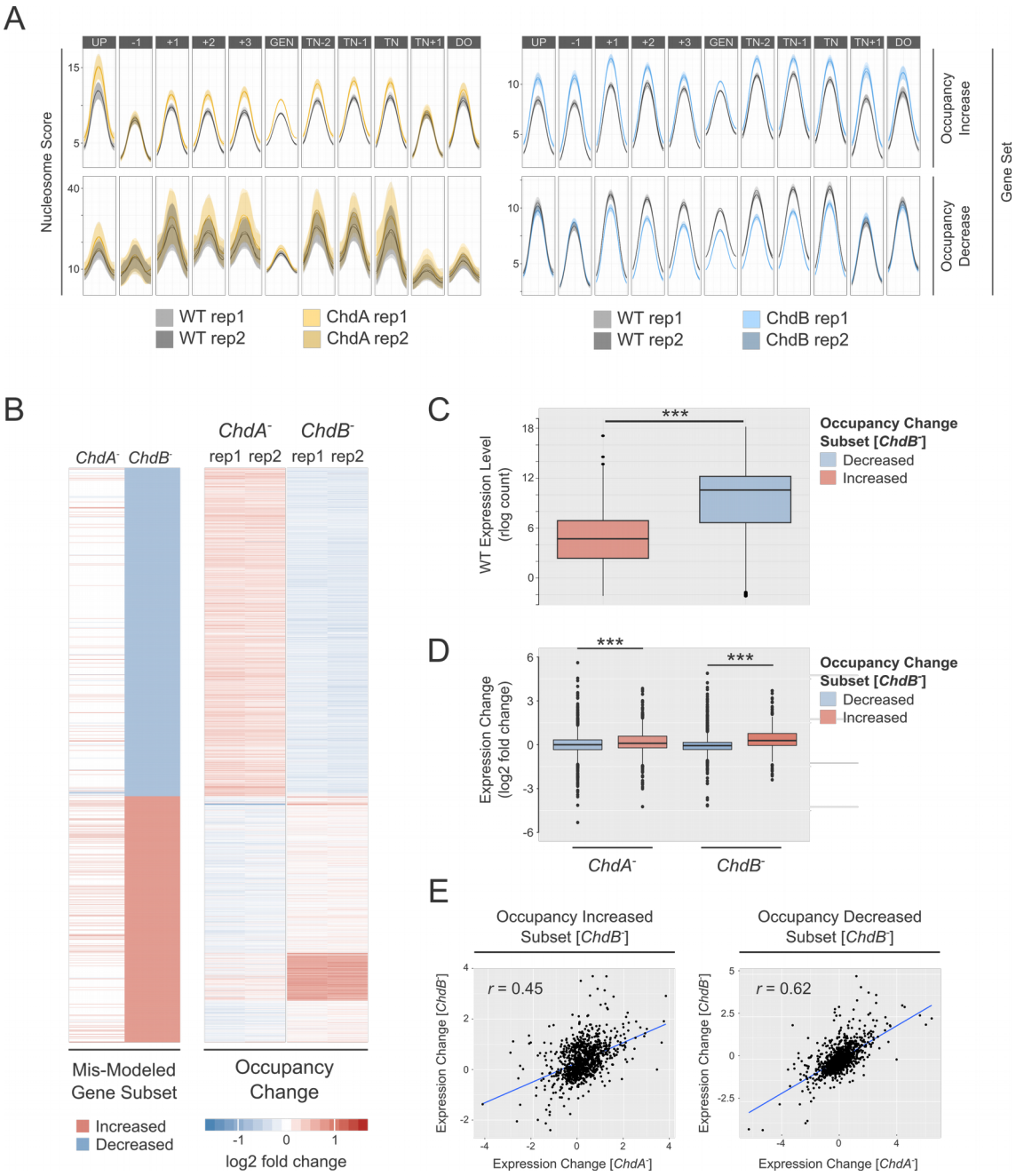

Fig5.8: Antagonistic Occupancy Effects in *ChdA*⁻ and *ChdB*⁻ mutants.

A) Nucleosome profiles of occupancy increased/decreased (OI/OD) gene sets from ChdA and ChdB mutants. **B)** Average occupancy changes for genes from the ChdB occupancy change subsets. Left panel indicates genes identified as significantly altered. **C)** WT expression levels of genes from the two subsets (*ChdB*⁻ OI and *ChdB*⁻ OD; *** = $p < 0.001$, Mann-Whitney U test). **D)** Expression change values of the two subsets in ChdA and ChdB (log2 fold change vs. WT). **E)** Scatter plot of expression change values between mutants within each gene subset, regression line and Pearson's correlation coefficient.

5.9 *ChdA*$^{-}$*/ChdB*$^{-}$ Double Knockout Mutant

The observations of antagonistic occupancy effects but correlated expression changes in ChdA and ChdB further build on the global trends of distinct nucleosome parameter effects but common transcriptional effects observed in all four remodeler mutants. This suggests that distinct and even antagonistic nucleosome restructuring is required to optimise expression in order to establish cell-type specific transcriptional programs. To test this concept I generated a *ChdA*$^{-}$*/ChdB*$^{-}$ double knockout (DKO) cell line, and examined the phenotypic effects on growth, development, chromatin structure and transcription. If ChdA and ChdB do act antagonistically at the same gene sets, we would expect loss of both ChdA and ChdB to rescue the occupancy defect phenotypes observed in the single mutant cell lines. Furthermore, if this antagonism is indeed required to optimise chromatin states in order to allow both high-expression and repression of genes, we would expect the split transcriptional effects in single mutants to be amplified in the double mutant.

5.9.1 Phenotypic Effects of Double Knockout on Growth and Development

Floxed resistance cassettes were used for the original remodeler mutants (Faix et al., 2004), hence it was possible to generate a *ChdA*$^{-}$*/ChdB*$^{-}$ DKO mutant cell line using the original ChdB KO vector detailed previously (Platt et al. 2013) in a Cre-recombinase treated *ChdA*$^{-}$ background (Fig5.9A). Neither *ChdA*$^{-}$ nor *ChdB*$^{-}$ single mutants exhibited significant inhibition of proliferation (Platt et al. 2013); to examine whether combined knockout produces epistatic effects, the growth rate of double and single mutants was measured in shaking culture. Average doubling time is significantly increased compared to both WT (+3.5 ± 2.3 hours, $p = 0.002$) and *ChdB*$^{-}$ (+3.5 ± 2.8 hours, $p = 0.01$; 95% CI, one-way ANOVA with Tukey's post-test), but not to *ChdA*$^{-}$ (Fig5.9B). I next examined the effect of combined ChdA/ChdB knockout on development. Onset of aggregation in *ChdA*$^{-}$*/ChdB*$^{-}$ cells is delayed by approximately two hours, comparable to the delay observed for *ChdB*$^{-}$ (Fig5.9C). Additionally, as observed for *ChdB*$^{-}$ previously (Platt et al. 2013) the streaming delay in *ChdA*$^{-}$*/ChdB*$^{-}$ is propagated to loose mound and tight aggregation stages also. Thus while the double mutant exhibits both reduced proliferation and delayed development, neither of these phenotypes appear significantly more severe than those displayed by single mutants.

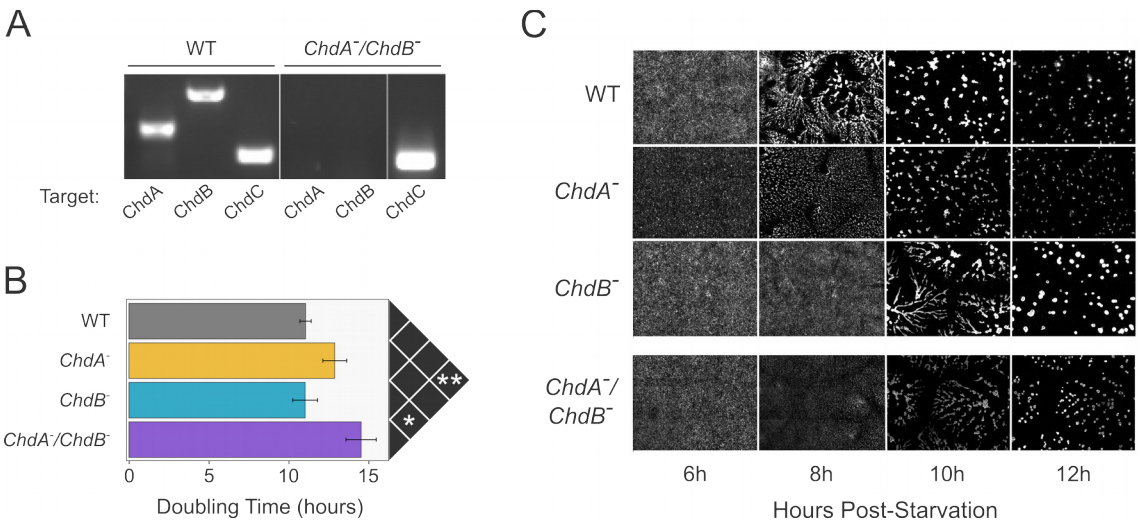

Fig5.9: Effect of *ChdA⁻/ChdB⁻* Double Knockout on Growth and Development.

A) PCR screening results for WT and double mutant: PCR primers amplifying the region targeted for excision in the mutant were used as a negative screen for mutants (see Fig3.2A negative KO primers for details). Cell line is indicated above gel lanes, primers are indicated below. **B)** Doubling times of single and double mutants measured in log phase growth in shaking culture. Significance of change in doubling time between individual conditions as measured by one-way ANOVA with Tukey's post-test is indicated in the matrix above, * = $P < 0.05$, ** = $P < 0.01$. **C)** WT, single and double mutants were grown in nutrient depleted conditions on KK2 agar and imaged over 24 hours. Developmental timing and gross morphological defects are observed by aligning frames by time-point post-starvation.

5.9.2 Chromatin Profiling of *ChdA⁻/ChdB⁻* Double Knockout Cells

MNase-sequencing and nucleosome mapping of the *ChdA⁻/ChdB⁻* mutant cell line was conducted as detailed for *Isw⁻* (see section 4.2). Strikingly, almost no change is detected in the average nucleosome score profile at the transcription start site compared to WT (Fig5.10A). Nucleosome parameter analysis confirms that average occupancy is not effected at any nucleosome position (Fig5.10B). A slight negative shift in the positioning of nucleosomes upstream of the TTS is observed (~ -1-2 bp), and a reduced distribution of genic nucleosomes suggesting less stringent regulation of genic nucleosomes across the cell population. Therefore globally, combined loss of ChdA and ChdB eliminates average occupancy changes observed in individual mutants, having only minor effects on the global chromatin landscape.

5.9.3 Transcriptional Disruption in *ChdA⁻/ChdB⁻* Double Knockout Cells

I next examined the transcriptional effect of combined ChdA/ChdB KO. Triplicate RNA-sequencing was conducted on WT and DKO mutant cell lines in growth stage cells. While a similar total number of genes are strongly mis-regulated in the combined mutant (1,175 up-regulated, 971 down-regulated) as individual mutants, the divergent effect on highly- and lowly- expressed genes is much more evident (Fig5.11A). Comparison of the gene sets strongly mis-regulated in each mutant reveals a large degree of overlap between all up-regulated and all down-regulated genes (Fig5.11B). Examining the structure of commonly mis-regulated gene sets indicates no clear enrichment of chromatin defects in mis-regulated genes (Fig5.11C). Thus despite performing antagonistic functions in regulating the primary chromatin structure, this data supports the notion that all spacing remodelers are required to maintain cell-type specific transcriptional programs.

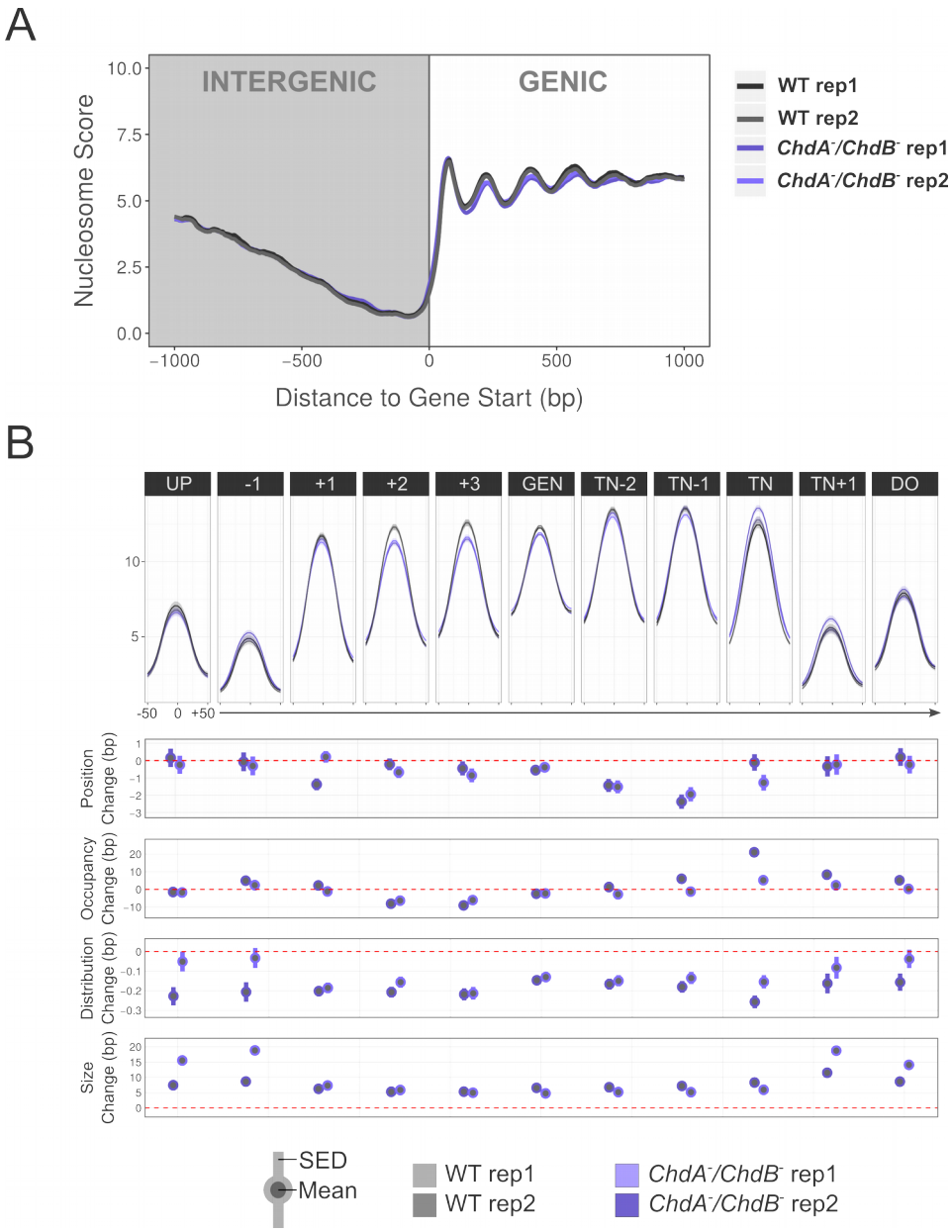

Fig5.10: *ChdA⁻/ChdB⁻* DKO Eliminates Global Occupancy Changes of Single Mutants.

A) TSS-aligned average nucleosome profile of *ChdA⁻/ChdB⁻* and WT *Dictyostelium* for all annotated genes (n=12,964).

B) Nucleosome parameter profile of *ChdA⁻/ChdB⁻* and WT *Dictyostelium*.

Upper panel: average nucleosome score distribution ± 50 bp of each nucleosome dyad position for all genes (n=12,964) grouped by nucleosome category (line = mean, shaded area = 95% confidence interval, UP, GEN and DO = average of upstream, genic and downstream nucleosomes repsectively, TN = terminal nucleosome).

Lower panels: average parameter change for all nucleosomes grouped by nucleosome category (circle = mean, intervals = standard error of the difference (SED)).

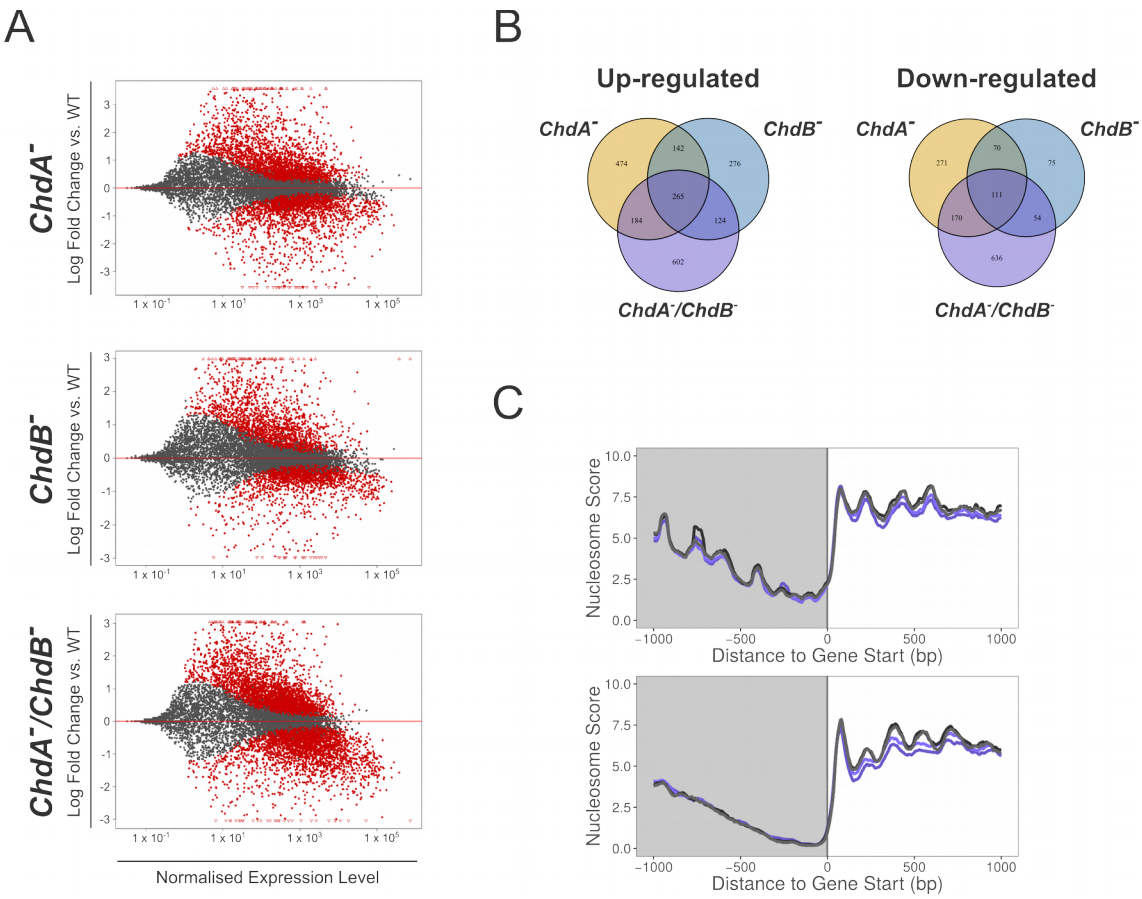

Fig5.11: Transcriptional Profiling of *ChdA*$^-$/*ChdB*$^-$ Double Knockout.

A) MA-plots of the relationship between mean gene expression and direction of mis-regulation (red = significantly mis-regulated).

B) Euler diagrams of the overlap between strongly ($p < 0.05$ & fold change > 2) up- and down-regulated genes.

C) Average nucleosome score profiles around the TSS of genes commonly up (upper panel) and down (lower panel) regulated in the three mutants.

5.9.4 Combined Occupancy Defects of *ChdA⁻/ChdB⁻*

Globally, combined *ChdA⁻/ChdB⁻* loss rescues the occupancy defects of the individual mutants. To determine whether this is also the case at the level of individual genes I re-examined previously identified subsets of divergently regulated genes in *ChdA⁻* and *ChdB⁻* (Fig5.8B). Surprisingly, combined remodeler loss does not rescue the occupancy effects at individual genes. Rather, the effect of ChdB loss appears to be dominant over that of ChdA, with both gene sets maintaining the direction of occupancy changes observed in *ChdB⁻*. The loss of a global occupancy effect therefore appears to be caused by amplification of the increased nucleosome signal within the subset of more lowly-expressed genes. Thus although ChdA and ChdB have opposing effects on nucleosome stability, they do not appear to be directly counteracting one another. The mechanism of how ChdB dominates nucleosome occupancy effects within the DKO is presently unclear.

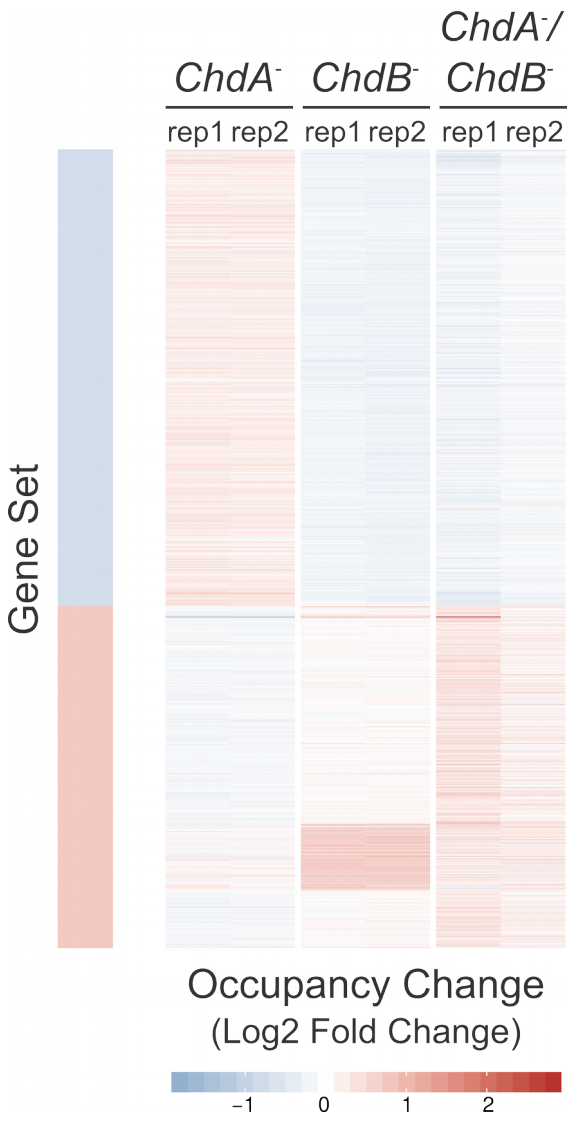

Fig5.12: Occupancy Effects of ChdB Appear Dominant over ChdA. Heatmap of average nucleosome occupancy change for genes within previously identified gene subsets. Left lane indicates gene subset (blue = reduced occupancy in *ChdB⁻*, red = increased occupancy in *ChdB⁻*). Occupancy changes are calculated over matched WT samples.

5.10 Summary

Despite unique roles in regulating chromatin structure, loss of any individual spacing remodeler has a common effect on transcriptional regulation, dampening transcription of the most highly expressed genes and de-repressing un- or lowly-expressed genes. Due to this common effect the gene sets regulated by CHD and ISWI remodelers are highly over-lapping, and in combination the spacing remodelers either directly or indirectly regulate almost the entire *Dictyostelium* transcriptome. I also find that remodeling effects are linked to the expression level of genes, with chromatin defects being enriched in highly-expressed genes. Nonetheless, in addition to their common relationship with expression level, remodelers do have distinct regulatory roles. Isw is found to uniquely repress the transcription of transposable elements, with potential importance for genomic stability. In summary CHD and ISWI remodelers exhibit chromatin-regulating roles, all of which are required to optimise cell-type specific transcriptional programs.

Chapter 6:

Discussion

6.1 Project Aims

The original aims of the current project were as follows:

- Generate knockout mutants for the previously unstudied, core SNF2 proteins present in *Dictyostelium*.
- Determine the roles of the major, transcription-related ATP-dependent chromatin remodelers in growth, development and chemotaxis through comparison of knockout mutant phenotypes.
- Perform MNase-sequencing on *Isw*$^-$ mutants, and map genome-wide nucleosome profiles in *ChdA*$^-$, *ChdB*$^-$ and *Isw*$^-$ cell lines.
- Determine the individual roles of ChdA, ChdB and Isw in the maintenance of primary *in vivo* chromatin structure
- Perform RNA-sequencing on *Isw*$^-$ cells and explore the relationship between nucleosome remodeling and transcriptional regulation for all CHD and ISWI family remoelers
- Investigate how the individual roles of spacing remodelers are combined to regulate primary chromatin structure and gene transcription

6.2 Generation of *Dictyostelium* SNF2 Protein Mutants

The presented study has highlighted the diverse repertoire of SNF2 proteins in *Dictyostelium*, reconfirming previously identified homologs (Platt et al. 2013; Flaus et al. 2006), and highlighting some previously unannotated subfamily groupings. I established knockout cell lines for three of these SNF2 family members: Isw, Snf2a and Swr. Together with previously generated *ChdA*$^-$, *ChdB*$^-$, *ChdC*$^-$ and *Arp8*$^-$ null mutants this provides a valuable resource for studying the roles and mechanisms of chromatin remodeling in this simple eukaryote.

While multiple independent clones of *Isw*$^-$, *Snf2a*$^-$ and *Swr*$^-$ mutants were generated with high efficiency, no *Snf2b*$^-$ mutants were isolated, possibly suggesting that Snf2b is an essential factor in *Dictyostelium*. Indeed SWI/SNF subfamily proteins in both yeast and mammals display a binary lethality effect. Sth1 knockout is lethal in *S. cerevisiae* (Laurent et al. 1992; Cairns et al. 1996), while Snf2 mutants are viable, although display slow growth on glucose caused by a defective transcriptional response and are

sporulation deficient (Abrams et al. 1986; Neigeborn & Carlson 1984; Hirschborn et al. 1992). BRG1 (SMARCA4) KO is embryonic lethal in mice, yet BRM (SMARCA2) loss causes only a slight increase in body weight (Reyes et al. 1998; Bultman et al. 2000; Klochendler-Yeivin et al. 2000).

This conservation of divergent effects upon SWI/SNF loss is intriguing, and suggests Snf2a homology to hBRM and Snf2b to hBRG1. However it is important to note that there are significant differences in the composition and functions of yeast and metazoan SWI/SNF family complexes, and it is presently unclear which, if either of these examples *Dictyostelium* may shadow. In *S. cerevisiae* Sth1 and Snf2 are incorporated into distinct, well defined complexes - RSC and SWI/SNF respectively. Mammalian BRG1 on the other-hand is incorporated into both the Brg1-associated factors (BAF) complex – which contains homologous subunits to ySWI/SNF, and the Polybromo-associated BAF (PBAF) complex – which contains homologous subunits to yRSC (Wang, Côté et al. 1996; Tang et al. 2010). The non-essential hBRM can also be incorporated mutually exclusively into the BAF complex. Beyond the core complex components (SNF5, BAF155, BAF170; Phelan et al. 1999), the subunit composition and functions of the BRG1- and BRM-incorporating BAFs are highly varied. BRM and BRG1 can display partially redundant, distinct or even opposing functions given the cell type and environment of the complexes (Strobeck et al. 2002; Reyes et al. 1998; Flowers et al. 2009). Understanding of the mammalian SWI/SNF complexes is confounded by this complexity, indeed it is predicted that hundreds of distinct complex compositions may exist (Wu et al. 2009). Speculatively, given the simple developmental program and limited number of cell types, the *Dictyostelium* SWI/SNF complexes may provide an useful intermediate between these two complexity extremes. Examination of the composition and function of distinct cell-type or developmental-stage specific *Dictyostelium* SWI/SNF complexes could therefore be highly informative. Given the high frequency of mutation and/or epigenetic repression of SWI/SNF complexes in human cancers (Kadoch et al. 2013; Shain & Pollack 2013; Versteege 1998; Modena et al. 2005; Wilson & Roberts 2011; Lee et al. 2012), such studies would also be highly pertinent to human disease.

6.3 *Dictyostelium* SNF2 Proteins in Growth, Development and Chemotaxis

All remodeler mutants studied display distinct phenotypic effects on cell growth, developmental timing or chemotaxis efficiency. Chromatin remodelers therefore fulfill

non-redundant biological roles in establishing and maintaining *in vivo* chromatin structure. This agrees with observations in mammalian cells, where despite expansion of of the SNF2 family from 17 in yeast to 53 in humans, examined remodelers retain unique biological functions (Flaus et al. 2006; Clapier & Cairns 2009; Ho & Crabtree 2011).

Snf2a loss has no significant effect on growth rate, but aggregation timing consistently lags slightly behind WT cells and chemotax less efficiently towards chemoattractant in a cAMP gradient. Snf2a is expressed strongly in growing cells, drops off following starvation and rises sharply again at around 8 hours, roughly corresponding to the aggregation stage (Parikh et al. 2010). Hence Snf2a may be required for the activation of genes involved in chemotactic signaling – which is important both for tracking bacteria in growing cells and streaming during aggregation. This would broadly fit with the roles of yeast Snf2. As detailed above, in contrast to the essential ySth1/hBRG1, ySnf2/hBRM knockouts display modest phenotypes. RSC complexes are thought to be required for genome-wide eviction of nucleosomes at NDRs and positioning of the +1 nucleosome, essential for regulation of constitutively expressed genes (Parnell et al. 2008; Hartley & Madhani 2009). SWI/SNF complexes on the other hand generally facilitate activation of inducible genes via promoter nucleosome eviction/remodeling, as demonstrated at numerous individual loci including heat-shock induced genes (Qiu et al. 2015; Shivaswamy & Iyer 2008; Bryant et al. 2008; Schwabish & Struhl 2007; Peterson & Herskowitz 1992; Hirschhorn et al. 1992). Although undoubtedly an over-simplification of these highly varied complexes, initial observations in *Dictyostelium* appear to fit within this general paradigm.

In contrast to the lethality exhibited by metazoan ISWI KO mutants (Deuring et al., 2000; Stopka and Skoultchi, 2003; Arancio et al., 2010), ISWI loss is relatively well tolerated in *Dictyostelium. Isw*$^{-}$ mutants display no significant growth inhibition, and only a slight developmental delay similar to that observed in *Snf2a*$^{-}$*.* The observation that Isw mRNA and protein levels peak later in development, around 12-14h, may suggest developmental roles in the late mound/slugging stages; no morphological defects were observed in the current study but further assay of slugging efficiency may be revealing. Interestingly the speed of chemotactic migration is increased in the absence of Isw. This contrasts with the reduced chemotactic speeds observed in *ChdA*$^{-}$ and *ChdC*$^{-}$ mutants, despite a shared *in vitro* nucleosome spacing role between these two

remodeler classes. Interestingly wipA, encoding a homolog of mammalian Wiskott-Aldrich syndrome protein (WASP) interacting protein (WIP), is strongly repressed in the absence of Isw. Mammalian WIP is known to stimulate F-actin polymerization at the leading edge and promote filopodia formation (Myers et al., 2006; Vetterkind et al., 2002). Knockout of wipA in *Dictyostelium* increases F-actin polymerization and reduced the speed, chemotactic index, and directionality of migration towards cAMP (Myers et al. 2006). Furthermore WIPa over-expressing cells are able to more rapidly adapt to changes in the chemoattractact gradient, whereas WIPa knock-down reduces response timing. Severe reduction of WIPa as expected in Isw mutants could therefore increase chemotactic speed by reducing the degree of directional deviation. On the other hand no significant change is observed in directionality or chemotactic index in Isw null cells, and we do observe a lesser, yet significant downregulation of other chemotaxis genes including the cAMP receptor carA-1. Hence, through its roles in transcriptional regulation, Isw may reduce the sensitivity of response to chemoattractant while simultaneously promoting the persistence of migration. Determining whether Isw directly induces wipA, and whether this regulation is conserved in human cells may be of relevance for diseases including Wiskott-Aldrich syndrome, cancer metastasis, and arthritis (Jin et al. 2008).

Swr knockout caused strong defects in all three assays – with growth rate reduced to around a third of WT *Dictysotelium*, aggregation delayed by ~3-4 hours, reduced mound sizes, stunted fruiting bodies, and reduced chemotactic speed and directionality. As opposed to ChdC remodelers, which influence growth rate through transcriptional regulation of metabolic pathways (Platt 2013), Swr appears to primarily affect cell division. *Swr*¯ mutants form large, multi-nucleated cells in adherent, but not shaking culture. This is, to our knowledge, the first example of an adherence-dependent cytokinesis defect in *Dictyostelium*, and the mechanism is presently unknown. Interestingly, myosin II heavy chain (mhcA) null and glycogen synthase kinase 3 (GskA) null *Dictyostelium* exhibit cytokinesis defects in non-adherent culture, but complete division when returned to a solid surface (Knecht and Loomis, 1987; Harwood et al., 2013). The causes of cell division failures in these mutants are distinct: myosin is essential for constriction of the cleavage furrow, whereas GSK is involved in mitotic spindle dynamics. Two alternative forms of cell division on solid substrate were proposed – a more efficient, cell cycle-dependent attachment-assisted mitotic cleavage, possibly utilising an alternative driver of cleavage furrow constriction; and a

highly inefficient, cell cycle independent traction-mediated cytofission to physically separate sections of the cell (Uyeda et al. 2000; Zang et al. 1997). Growth of *Swr⁻* cells in suspension is still highly inefficient, hence we expect that a similar physical separation of cells occurs, possibly due to shear stress within shaking culture.

Given the known roles of Swr in incorporating the H2A variant - H2A.Z (Krogan et al. 2003), an obvious explanation for exhibited defects would be mis-localisation of H2A.Z, causing gene de-repression. Interestingly however, a H2A.Z knockout mutant established by the Chubb lab displays no strong defects in growth or development (personal communication with Dr Jonathan Chubb). This would strongly suggest H2A.Z-independent roles of Swr in *Dictyostelium,* however unlike the other major chromatin remodelers, the *in vitro* nucleosome remodeling activity of Swr1 is highly dependent on the presence of H2A.Z (Luk et al. 2010). Indeed additional roles are known for SWR-C beyond transcriptional regulation including chromosome segregation, double strand break repair, checkpoint adaptation and maintenance of pericentric heterochromatin (Gerhold et al. 2015; Papamichos-Chronakis et al. 2006; Rangasamy et al. 2004). However these are all thought to be dependent on H2A.Z incorporation.

An intriguing connection exists between Swr and the localisation of the centromeric H3 variant CENP-A which is essential for centromere formation, and highly conserved despite wide variation in centromere structure across eukaryotes (De Rop et al. 2011). CENP-A is exclusively centromeric, however in yeast over-expression of CENP-A, or prevention of proteolysis by Psh1 knockout causes mis-incorporation of CENP-A at NDR-flanking nucleosomes, particularly at longer NDRs, resulting in lethality (Collins et al. 2004; Hewawasam et al. 2010; Ranjitkar et al. 2010). This pattern of mis-localisation is strikingly similar to the binding pattern of Swr1 (Ranjan et al. 2013); indeed, CENP-A co-localises with H2A.Z-variant nucleosomes, yet displays no dependence on H2A.Z itself (Hildebrand & Biggins 2016). Furthermore, CENP-A is enriched in the chromatin fraction of *swr1Δ* cells. The authors emphasise the role of INO80-C in promoting mis-incorporation; speculatively however, given observations in *Dictyostelium* we propose that SWR-C may actively oppose INO80-C to prevent mis-incorporation of CENP-A. Future work to validate this hypothesis may provide important, novel insights into the functions of the INO80/SWR family, but is also highly relevant to the mis-localisation of CENP-A in human cancers (Athwal et al. 2015).

6.4 CHD and ISWI Complexes Regulate Distinct Remodeling Events

In the present study I performed MNase-seq on the *Isw*$^{-}$ mutant cell line and developed more robust, quantitative methods to allow detailed analysis of nucleosome maps from all four spacing remodeler mutants in *Dictyostelium*. Comparison of the global chromatin profiles of each cell line revealed distinct, characteristic nucleosome defects caused by loss of individual CHD and ISWI family remodelers. Importantly these analyses re-confirmed all published characteristics of *ChdC*$^{-}$ mutant chromatin (Platt 2013). Furthermore the improved analysis pipeline was able to detect novel structural defects upon ChdC loss not identified using previous bioinformatic methods. Thus this work provides both a resource for the study of spacing remodelers in *Dictyostelium*, and contributes towards the relatively under-developed body of analysis techniques for nucleosome mapping data.

Loss of any individual CHD or ISWI chromatin remodeler disrupts the global pattern of chromatin organisation. Although the profile of nucleosome changes is unique to each remodeler, a common pattern of susceptibility to disruption is observed across the genome. Mid-genic nucleosomes generally display greater disruption than terminal (+1/TN) and intergenic nucleosomes, which are largely unaffected by remodeler loss. The CHD proteins also influence occupancy of nucleosomes flanking coding regions (-1/TN+1). This could be indicative of either remodeler targeting, or their redundancy at given genic positions. The precise binding profiles of ISWI and CHD proteins have been difficult to ascertain, likely due to a transient association with any individual nucleosome. Nonetheless studies generally observe binding at the promoter and activity at the +1 or throughout the gene body (Yen et al. 2012; Zentner et al. 2013; Tirosh et al. 2010; Siggens et al. 2015; Gkikopoulos et al. 2011; Shim et al. 2012; Pointner et al. 2012; Whitehouse et al. 2007; Simic et al. 2003). Hence the relative lack of disruption at the +1 is likely due to functional redundancy, rather than an exclusion of spacing remodelers from the gene termini. Indeed this relative insensitivity of terminal nucleosomes, and particularly the +1, to disruption under chromatin-perturbing conditions is observed in multiple systems (Yen et al. 2012; Gkikopoulos et al. 2011). On the other hand lack of distal intergenic disruption to chromatin structure likely indicates that CHD and ISWI family remodelers are primarily targeted to coding regions. Indeed the enrichment of mis-regulation in highly expressed genes across all four mutants suggests that association with transcription may be a common targeting

mechanism. Analysis of the global binding pattern of *Dictyostelium* remodelers would be informative, both to confirm predicted targeting and to advance the poorly understood mechanisms of remodeler targeting. Another general feature of chromatin profiles is the mirroring of nucleosome parameter changes at the 5' and 3' ends of genes. As has been suggested previously in yeast this likely arises from gene looping allowing simultaneous regulation of chromatin structure from both 5' and 3' NDRs (Yen et al. 2012; O'Sullivan et al. 2004; Ansari & Hampsey 2005).

4.5 ChdA and ChdB Control Genic Nucleosome Occupancy

ChdA and ChdB remodeler mutants display complementary patterns of relative occupancy changes, with ChdA increasing, and ChdB decreasing genic occupancy. In each case the reciprocal of the genic occupancy change is observed at nucleosomes flanking the coding region (-1/TN+1); however intergenic nucleosomes are not globally perturbed. ChdA and ChdB therefore have opposing influences on the steady state nucleosome binding within gene bodies. Highly expressed genes exhibit reduced average nucleosome occupancy in our own data, and have been shown to exhibit increased nucleosome turnover in *S. cerevisia*e and *Drosophila*. Given the enrichment of occupancy defects in highly expressed genes we propose roles for ChdA and ChdB in regulating nucleosome turnover. CHD proteins have also been associated with nucleosome turnover in a range of other organisms. CHD2 knockdown (KD) or CHD1+CHD2 double KD in human cells increases H3 occupancy and reduces H3.3, suggesting that both human type I CHDs promote nucleosome turnover (Siggens et al. 2015). Yeast *chd1Δ* display increased nucleosome turnover rates at the 3' end of genes (Park et al. 2014; Smolle et al. 2012). And CHD1 loss in flies decreases H3.3 levels in flies, particularly at the 3' ends of long genes (Konev et al. 2007; Radman-Livaja et al. 2012). Furthermore, as observed in the current study these effects are enriched in highly expressed genes (Siggens et al. 2015; Park et al. 2014; Smolle et al. 2012), suggesting that type I CHDs play a conserved role in regulating nucleosome turnover and stability in a transcription-linked manner.

Changes in chromatin accessibility and susceptibility to MNase-digestion provide an alternative explanation for the loss or gain of nucleosome signal. The level of MNase-digestion has been demonstrated to differentially effect nucleosome occupancy dependent on compaction of a given locus. Open regions, particularly around the NDR

and at the -1 nucleosome are more susceptible to MNase, leading to a over-digestion to sub-nucleosomal particle sizes at higher enzyme concentrations and loss of the 150 bp nucleosomal signal. Conversely more compact chromatin produces increased signal at higher MNase-concentrations (Mieczkowski et al. 2016). ChdB does not significantly influence genic fragment sizes, arguing against digestion sensitivity contributing to the decreased genic nucleosome signal. However at the -1 position ChdB mutants do display both increased size and occupancy, suggesting that ChdB may control occupancy through distinct mechanisms at distinct regions. Notably, CHD1 depletion in mammals causes decreased accessibility at a number of DNase hypersensitive loci and at the promoter (Siggens et al. 2015; Ehrensberger & Kornberg 2011; Radman-Livaja et al. 2012); and similar effects are observed at Drosophila Hsp70 promoters (Morettini et al. 2011). ChdA loss on the other hand globally decreases nucleosome size, hence chromatin de-compaction may contribute to both decreased -1 signal and increased genic occupancy. Interestingly, as opposed to decompaction, CHD1 loss in mouse embryonic stem cells allows abherent spread of H3K9me3 (Gaspar-Maia et al. 2009); and in flies CHD1 loss is associated with increased HP1 and H3K9me2 on polytene chromosomes (Bugga et al. 2013). However visually chromosomes in CHD1 KD flies appear more decondensed, and display gross higher-order structural defects including loss of chromosome banding (Bugga et al. 2013). Hence, while the precise mechanism remains unclear, Chd1 appears to play a conserved role in regulation of global chromatin structure. The roles of CHD proteins in nucleosome turnover and stability, are likely closely intertwined with higher-level effects on chromatin accessibility and structure.

Multiple targeting mechanisms of type I CHD proteins have been proposed. The chromodomains of mammalian CHD1 have been shown to bind H3K4 di- or tri-methylation which is enriched at promoters (Sims et al. 2005). However H3K4me2/3 binding is not evident in yeast or flies, and CHD proteins are not enriched at H3K4me2/3 sites in mammals (Sims et al. 2005; Morettini et al. 2011). Alternatively, type I CHD proteins in yeast, flies and mammals interact with Mediator complex and transcription elongation factors (Khorosjutina et al. 2010; Simic et al. 2003; Shema-Yaacoby et al. 2013; Smolle et al. 2012; Lin et al. 2011). The emerging model across all eukaryotes therefore suggests promoter recruitment of CHD proteins at sites of active transcription, and action within the genebody to control nucleosome turnover in association with elongating RNAPII. The localisation of nucleosome parameter

changes in *Dictyostelium* CHD mutants fit well with this model. Notably however the detailed breakdown of nucleosome parameter changes by position highlights some differences between CHD proteins – the positioning changes of ChdB and ChdC are enriched at the 5' end. We posit that H3K4me2/3 binding could focus specific remodeler actions to the 5' end of genes in a transcription-independent manner. Unlike ChdB, ChdA also affects the occupancy of terminal nucleosomes, which may be indicative of a conserved role in transcription termination (Murawska & Brehm 2011).

In summary we postulate the following model: ChdA remodelling decreases the stability of genic nucleosomes, increasing turnover and H3.3 incorporation, while also playing an important, global role to maintain higher-order chromatin structure. ChdB antagonistically acts to stabilise genic nucleosomes, and has an additional role in promoting accessibility at the promoter and intergenic regions. Both CHD proteins are recruited to expressed genes, and likely translocate with the polymerase to optimise nucleosome turnover: ChdA facilitating passage, and ChdB stabilising nucleosomes in its wake. These roles would fit with the observed bivalent occupancy effects in the ChdA/ChdB DKO mutants; It is clear from transcriptional profiles and the lack of growth inhibition in ChdA mutants that this nucleosome de-stabilising is not strictly required for transcription. Therefore in the absence of ChdA, transcription continues to evict nucleosomes as is necessary for its passage, leading to the dominant effect of ChdB loss and nucleosome destabilisation at highly transcribed genes. Globally these effects may be masked by the higher-order effect of ChdA causing a degree of reciprocal occupancy increase. While speculative this model provides a paradigm in which to design further experiments – remodeler ChIP-seq and nucleosome turnover assays would be particularly pertinent to validate the model.

6.6 ChdC Influences Nucleosome Positioning, Spacing, Size and Organisation

In addition to the previously identified nucleosome positioning shifts at the +2 and +3 positions (Platt 2013), the improved analysis pipeline has allowed detection of additional chromatin defects upon ChdC loss. Most notably, *ChdC*$^{-}$ displays increased nucleosome footprint size compared to matched WT samples. Like the size changes in *ChdA*$^{-}$ this effect does not appear to be localised to specific nucleosome positions, but globally increases fragment sizes produced by MNase-digestion by ~5bp. It is not possible with MNase-seq data to determine whether these size changes represent modification of the nucleosome structure, altered accessibility of nucleosomal DNA,

higher-order structural effects, or a change in the digestion conditions inside the nucleus influencing MNase activity. Given that H1 loss in mice has been demonstrated to cause a compensatory reduction in nucleosome repeat length (Fan et al. 2003), restriction of H1 incorporation by ChdC could potentially explain both size and spacing changes in the mutant; however we observe no enrichment of size changes in positionally altered genes. A modest decrease of genic nucleosome occupancy and stronger increase of occupancy at NDR flanking nucleosomes may alternatively indicate a role in increasing chromatin accessibility. Finally, the dyad distribution or organisation of nucleosomes across the population is decreased, in keeping with a role in maintaining nucleosomal array spacing.

6.7 Isw Organises Nucleosomal Arrays to Repress TE

Interestingly, despite displaying the strongest disruption of average nucleosome structure out of all four remodeler mutants, no dominant nucleosome parameter defect was identified in *Isw⁻*. Nucleosomes at the 5' end of genes have reduced nucleosome repeat lengths, occupancy is slightly decreased across the gene body and nucleosome positioning across the population is globally less uniform. We propose that as opposed to the more specialised roles of the CHD family remodelers, Isw plays a more general role - utilising its nucleosome spacing activity to organise nucleosomal arrays. The requirement for Isw to maintain phased nucleosomal arrays is somewhat at odds with observations in yeast – *S. cerevisiae isw1Δ* and *isw2Δ* knockouts, or *isw1Δ/isw2Δ* double knockout only modestly disrupts nucleosome array organisation at mid-genic regions (Gkikopoulos et al. 2012; Whitehosue et al. 2007; Tirosh et al. 2010; Yen et al. 2012). And additional knockout of Chd1 is required to affect nucleosome array organisation to the extent observed in Dictyostelium *Isw⁻*. Revealingly, ISWI family remodelers appear to be entirely dispensable in *S. pombe*, which possess two CHD family members, Hrp1 and Hrp3, but no ISWI. *hrp3Δ* and hrp1*Δ*/3*Δ* mutants exhibit similar nucleosomal array disruption to that observed in *isw1Δ/chd1Δ* budding yeast or *Isw⁻ Dictyostelium* (Hennig et al. 2012; Shim et al. 2012). Comparison between these three distally related species therefore suggests that, while the role of spacing remodelers to organise nucleosomal arrays is conserved, this function can be performed by either ISWI or CHD SNF2 proteins. This raises the questions of how specialised functions are therefore imposed on the CHD remodelers in *Dictyostelium;* and which spacing remodelers are responsible for nucleosome array organisation in human cells.

Global expression analysis reveals that, similar to *ChdA*$^{-}$ and *ChdB*$^{-}$, and unlike *ChdC*$^{-}$, genes mis-regulated in *Isw*$^{-}$ did not appear to be strongly enriched in specific functional categories. On the other hand we observed a significant mis-regulation of transposable elements upon Isw loss. The majority of TE are highly up-regulated in the mutant, indicating that Isw is important for repression of these potentially deleterious elements. TE are relatively abundant in Dictyostelium, making up ~9.6% of the genome in total (Glöckner et al. 2001). While transposable elements have been shown to play key roles in transcriptional regulation in mammalian genomes (Faulkner et al. 2009), most transposable elements are repressed in heterochromatin marked by H3K9me3 and DNA methylation (Groh & Schotta, 2017). Multiple targeting mechanisms are involved in TE silencing, many of which may be specific to the class of element involved. Both small interfering RNA (siRNA) and antisense transcription have been demonstrated to reduce retrotransposition of mammalian LINE-1 elements (Yang & Kazazian, 2006; Li et al. 2014); while Piwi-interacting RNA (piRNA) pathways degrade retrotransposon mRNAs and induce DNA methylation at TE (Aravin et al. 2008). Indeed CpG DNA methylation is required for epigenetically stable repression of TE in mammals (Bourc'his & Bestor, 2004). Finally, KRAB-containing zinc finger proteins (KRAB-ZFPs) directly bind TE and recruit KAP1 leading to DNA and histone methylation (Rowe & Trono, 2011; Ecco et al. 2016). Interestingly interaction of the zinc finger protein Zfp819 has previously been reported with the chromatin remodeler Chd4 (Zheng et al. 2013), raising the possibility that Isw could be directly recruited to TE via KRAB-ZFPs.

The transcriptional effect outlined would be consistent with a global role in maintaining nucleosomal arrays - loss of which would not be expected to cause mis-regulation of specific pathways, but may allow aberrant transcription of repressed regions by altering genomic accessibility. Isw loss in yeast is known to result in cryptic transcription (Whitehouse et al. 2007), potentially caused by nucleosome shifts exposing extended lengths of linker DNA which can be subsequently bound by TF and PIC components. Additionally, Isw2 is thought to have a direct repressive impact by shifting the +1 nucleosome upstream, into the NDR to physically occlude promoters and prevent PIC formation (Kent et al. 2001; Yen et al. 2012; Whitehosue et al. 2007). ISWI family remodelers form at least three separate complexes in *S. cerevisiae* (Isw1a, Isw1b and Isw2). Isw1a and Isw1b both incorporate Isw1 as their catalytic subunit but target largely separate gene regions and differentially remodel yeast chromatin (Morillon et al.

2003; Yen et al. 2012; Tirosh et al. 2010; Whitehouse et al. 2007). Hence it is likely that the chromatin defects observed in *Isw* represent the cumulative actions of multiple distinct remodeling complexes. Determining the composition of such complexes would be important for relating presented finding to human ISWI remodeling.

6.8 Spacing Remodelers are Required for Optimal Transcriptional Regulation

Unexpectedly all four CHD and ISWI mutants display a common transcriptional response to remodeler loss. Genes which are highly expressed within WT Dictyostelium at growth are frequently down-regulated, while lowly-expressed genes are up-regulated in each mutant. As a result the gene sets mis-regulated in remodeler mutants strongly overlap for all four cell lines. This is consistent with overlapping binding and transcriptional regulation of CHD and ISWI remodelers observed from yeast to mammals (Morris et al. 2014; Siggens et al. 2015; Yen et al. 2012). Furthermore the transcriptional disruption in remodeler mutants appears to correlate with the changes observed between WT cells at growth and 10h of development, roughly corresponding to the late streaming/early mound stage of development. We propose that the distinct functional roles of the CHD and ISWI family remodelers are all necessary to organise chromatin in a cell-type specific configuration. Disrupting the function of any individual remodeler impedes cell-type specific transcriptional regulation. In growth-stage *Dictyostelium* this causes aberrant de-repression of developmentally-regulated genes. Interestingly, CHD1 is essential for maintenance of pluripotency in mouse embryonic stem cells (mESC), and formation of induced pluripotent stem cells (iPSCs) (Gaspar-Maia et al. 2009). CHD1 loss in mESCs causes stochastic differentiation, primarily towards a neural lineage (Gaspar-Maia et al. 2009). Hence a requirement for spacing remodelers in stabilising or optimising cell-type specific transcriptional programs appears to be conserved from simple eukaryotes through to mammals.

6.9 Summary

Through phenotypic analysis and comparison of generated remodeler mutant cell lines I have demonstrated that *Dictyostelium* chromatin remodelers play distinct non-redundant roles in growth, development and chemotaxis. Detailed analysis of the nucleosome parameter changes in the CHD and ISWI family mutants extends this

observation, to reveal that each remodeler also has distinct non-redundant roles in regulating nucleosome positioning, occupancy, distribution and size, primarily within the gene bodies. These in-depth analyses reveal novel, testable hypotheses regarding the mechanisms of CHD and ISWI mediated remodelling. Comparison of nucleosome parameters with expression profiles suggests that all CHD and ISWI remodelers are targeted by transcriptional machinery to highly expressed genes in order to maintain chromatin structure. The distinct remodeling activities of all spacing remodelers in regulating nucleosome turnover and positioning are required to optimise cell-types specific transcriptional programs. This provides a paradigm for understanding the myriad roles of CHD and ISWI remodelers in higher eukaryotes in developmental regulation, cancer suppression and stem cell maintenance.

Bibliography

Abrams, E., Neigeborn, L. & Carlson, M., 1986. Molecular Analysis of SNF2 and SNF5 , Genes Required for Expression of Glucose-Repressible Genes in *Saccharomyces cerevisiae*. *Molecular and Cellular Biology*, 6(11):3643–3651.

Ahmad, K. & Henikoff, S., 2002. Histone H3 variants specify modes of chromatin assembly. *Proceedings of the National Academy of Sciences of the United States of America*, 99(Suppl 4):16477–16484.

Aihara, T. et al., 1998. Cloning and mapping of SMARCA5 encoding hSNF2H, a novel human homologue of *Drosophila* ISWI. *Cytogenetics and Cell Genetics*, 81(3–4):191–193.

Albert, I. et al., 2007. Translational and rotational settings of H2A.Z nucleosomes across the *Saccharomyces cerevisiae* genome. *Nature*, 446(7135):572–576.

Alen, C. et al., 2002. A role for chromatin remodeling in transcriptional termination by RNA Polymerase II. *Molecular Cell*, 10(6):1441–1452.

Almer, A. & Hörz, W., 1986. Nuclease hypersensitive regions with adjacent positioned nucleosomes mark the gene boundaries of the PHO5/PHO3 locus in yeast. *The EMBO Journal*, 5(10), pp.2681–2687.

Almer, A. et al., 1986. Removal of positioned nucleosomes from the yeast PH05 promoter upon PH05 induction releases additional upstream activating DNA elements. *The EMBO Journal*, 5(10):2689–2696.

Amano, T. et al., 2009. Chromosomal dynamics at the Shh locus: limb bud-specific differential regulation of competence and active transcription. *Developmental Cell*, 16(1):47–57.

Anders, S. & Huber, W., 2010. Differential expression analysis for sequence count data. *Genome Biology*, 11(10):R106.

Anders, S., Pyl, P.T. & Huber, W., 2015. HTSeq-A Python framework to work with high-throughput sequencing data. *Bioinformatics*, 31(2):166–169.

Ansari, A. & Hampsey, M., 2005. A role for the CPF 3' -end processing machinery in RNAP II-dependent gene looping. *Genes & Development*, 19(24):2969–2978.

Arancio, W. et al., 2010. The nucleosome remodeling factor ISWI functionally interacts with an evolutionarily conserved network of cellular factors.

Genetics, 185(1):129–140.

Aravin, A.A. et al., 2008. A piRNA pathway primed by individual transposons is linked to de novo DNA methylation in mice. *Molecular Cell*, 31(6):785-799.

Athwal, R.K. et al., 2015. CENP-A nucleosomes localize to transcription factor hotspots and subtelomeric sites in human cancer cells. *Epigenetics & Chromatin*, 8(1):2.

Bajpai, R. et al., 2010. CHD7 cooperates with PBAF to control multipotent neural crest formation. *Nature*, 463(7283):958–962.

Bakthavastsalam, D & Gomer, R.H., 2010. The secreted proteome profile of developing *Dictyostelium discoideum* cells. *Proteomics*, 10(13):2556-2559.

Barbaric, S. et al., 2007. Redundancy of chromatin remodeling pathways for the induction of the yeast PHO5 promoter *in vivo*. *The Journal of Biological Chemistry*, 282(38)27610-27621.

Basu, S. et al., 2013. DictyBase 2013: integrating multiple Dictyostelid species. *Nucleic Acids Research*, 41(Database issue):D676-83.

Bednar, J. et al., 1998. Nucleosomes, linker DNA, and linker histone form a unique structural motif that directs the higher-order folding and compaction of chromatin. *Proceedings of the National Academy of Sciences of the United States of America,* 95(24):14173-14178.

Bernier, R. et al., 2014. Disruptive CHD8 mutations define a subtype of autism early in development. *Cell*, 158(2):263–276.

Bernstein, B.E. et al., 2006. A bivalent chromatin structure marks key developmental genes in embryonic stem cells. *Cell*, 125(2):315-326.

Bloomfield, G. et al., 2015. Neurofibromin controls macropinocytosis and phagocytosis in *Dictyostelium*. *ELife*, 4:e04940.

Boeger, H. et al., 2003. Nucleosomes unfold completely at a transcriptionally active promoter. *Molecular Cell*, 11(6):1587–1598.

Boeger, H. et al., 2004. Removal of promoter nucleosomes by disassembly rather than sliding *in vivo*. *Molecular Cell*, 14(5):667-673.

Bonner, J.T., 1947. Evidence for the formation of cell aggregates by chemotaxis in the development of the slime mold *Dictyostelium discoideum*. *Journal of Experimental Zoology*, 106(1):1–26.

Bosman, E.A. et al., 2005. Multiple mutations in mouse Chd7 provide models for CHARGE syndrome. *Human Molecular Genetics*, 14(22):3463–3476.

Bouazoune, K. & Kingston, R.E., 2012. Chromatin remodeling by the CHD7 protein is impaired by mutations that cause human developmental disorders. *Proceedings of the National Academy of Sciences of the United States of America,* 109(47):19238-19243

Bourc'his, D. & Bestor, T.H., 2004. Meiotic catastrophe and retrotransposon reactivation in male germ cells lacking Dnmt3L. *Nature*, 431(7004):96-99.

Brown, C.R. et al., 2011. *In vivo* role for the chromatin-remodeling enzyme SWI/SNF in the removal of promoter nucleosomes by disassembly rather than sliding. *The Journal of Biological Chemistry*, 286(47):40556-40565.

Bryant, G.O. et al., 2008. Activator control of nucleosome occupancy in activation and repression of transcription. *PLoS Biology*, 6(12):2928–2939.

Buenrostro, J.D. et al., Transposition of native chromatin for fast and sensitive epigenomic profiling of open chromatin, DNA-binding proteins and nucleosome position. *Nature Methods*, 10(12):1213-1218.

Bugga, L. et al., 2013. The *Drosophila melanogaster* CHD1 chromatin remodeling factor modulates global chromosome structure and counteracts HP1a and H3K9me2. *PLoS ONE*, 8(3):e59496.

Bultman, S. et al., 2000. A Brg1 null mutation in the mouse reveals functional differences among mammalian SWI/SNF complexes. *Molecular Cell*, 6(6), 1287–1295.

Cairns, B.R. et al., 1996. RSC, an essential, abundant chromatin-remodeling complex. *Cell*, 87(7):1249–1260.

Carpenter, A.E. et al., 2006. CellProfiler: image analysis software for identifying and quantifying cell phenotypes. *Genome Biology*, 7(10):R100.

Carr, A. & Biggin, M.D., 2000. Accessibility of transcriptionally inactive genes is specifically reduced at homeoprotein-DNA binding sites in *Drosophila*. *Nucleic Acids Research*, 28(14), 2839-2846.

Carvill, G.L. et al., 2013. Targeted resequencing in epileptic encephalopathies identifies *de novo* mutations in CHD2 and SYNGAP1. *Nature Genetics*, 45(7):825–830.

Casolari, J.M., 2004. Genome-wide localization of the nuclear transport machinery couples transcriptional status and nuclear organization. Cell, 117(4):427-439.

Chang, G.S. et al., 2012. Unusual combinatorial involvement of poly-A/T tracts in organizing genes and chromatin in *Dictyostelium*. *Genome Research*,

22(6):1098–1106.

Chen, K. et al., 2013. DANPOS: Dynamic analysis of nucleosome position and occupancy by sequencing. *Genome Research*, 23(2):341–351.

Chen, W. et al., 2014. Improved nucleosome-positioning algorithm iNPS for accurate nucleosome positioning from sequencing data. *Nature Communications*, 5:4909.

Chénier, S. et al., 2014. CHD2 haploinsufficiency is associated with developmental delay, intellectual disability, epilepsy and neurobehavioural problems. *Journal of Neurodevelopmental Disorders*, 6(1):9.

Chisholm, R.L. & Firtel, R.A., 2004. Insights into morphogenesis from a simple developmental system. *Nature Reviews. Molecular Cell Biology*, 5(7):531–541.

Chu, C. et al., 2011. Genomic maps of long noncoding RNA occupancy reveal principles of RNA-chromatin interactions. *Molecular Cell*, 44(4):667-678.

Clapier, C.R. & Cairns, B.R., 2012. Regulation of ISWI involves inhibitory modules antagonized by nucleosomal epitopes. *Nature*, 492(7428):280-284.

Clapier, C.R. & Cairns, B.R., 2009. The biology of chromatin remodeling complexes. *Annual Review of Biochemistry*, 78:273–304.

Clark-Adams, C.D. et al., 1988. Changes in histone gene dosage alter transcription in yeast. *Genes & Development*, 2(2):150–159.

Collins, K.A., Furuyama, S. & Biggins, S., 2004. Proteolysis contributes to the exclusive centromere localization of the yeast Cse4/CENP-A histone H3 variant. *Current Biology*, 14(21):1968–1972.

Corona, D.F. et al., 1999. ISWI is an ATP-dependent nucleosome remodeling factor. *Molecular Cell*, 3(2):239–245.

Corona, D.F. V et al., 2007. ISWI regulates higher-order chromatin structure and histone H1 assembly *in vivo*. *PLoS Biology*, 5(9):e232.

Corona, D.F. V & Tamkun, J.W., 2004. Multiple roles for ISWI in transcription, chromosome organization and DNA replication. *Biochimica et Biophysica Acta*, 1677(1–3):113–119.

Costanzi, C. & Pehrson, J.R., 1998. Histone macroH2A1 is concentrated in the inactive X chromosome of female mammals. Nature, 393(6685):599-601.

Côté, J. et al., 1994. Stimulation of GAL4 derivative binding to nucleosomal

DNA by the yeast SWI/SNF complex. *Science*, 265(5168):53–60.

Cotney, J. et al., 2015. The autism-associated chromatin modifier CHD8 regulates other autism risk genes during human neurodevelopment. *Nature Communications*, 6:6404.

Courage, C. et al., 2014. 15q26.1 microdeletion encompassing only CHD2 and RGMA in two adults with moderate intellectual disability, epilepsy and truncal obesity. *European Journal of Medical Genetics*, 57(9):520–523.

Crawford, G.E. et al., 2006. Genome-wide maping of Dnase hypersensitive sites using massively parallel signature sequencing (MPSS). *Genome Research*, 16(1):123-131.

Cremer, T. et al., 1982. Rabl's model of the interphase chromosome arrangement tested in Chinese hamster cells by premature chromosome condensation and laser-UV-microbeam experiments. *Human Genetics*, 60(1):46-56.

Creppe, C. et al., 2012. MacroH2A1 regulates the balance between self-renewal and differentiation commitment in embryonic and adult stem cells. *Molecular Cell Biology*, 32(8):1442-1452.

van Daal, A. & Elgin, S.C., 1992. A histone variant, H2AvD, is essential in *Drosophila melanogaster*. *Molecular Biology of the Cell*, 3(6):593–602.

Dang, W. & Bartholomew, B., 2007. Domain architecture of the catalytic subunit in the ISW2-nucleosome complex. *Molecular and Cellular Biology*, 27(23):8306–8317.

Dang, W., Kagalwala, M.N. & Bartholomew, B., 2007. The Dpb4 subunit of ISW2 is anchored to extranucleosomal DNA. *The Journal of Biological Chemistry*, 282(27):19418-19425.

Daubresse, G. et al., 1999. The *Drosophila* kismet gene is related to chromatin-remodeling factors and is required for both segmentation and segment identity. *Development*, 126(6):1175–1187.

Dechassa, M.L. et al., 2010. SWI/SNF has intrinsic nucleosome disassembly activity that is dependent on adjacent nucleosomes. *Molecular Cell*, 38(4):590–602.

Dekker, J. et al., 2002. Capturing chromosome conformation. *Science*, 295(5558):1306-1311.

Denslow, S.A. & Wade, P.A., 2007. The human Mi-2/NuRD complex and gene regulation. *Oncogene*, 26(37):5433–5438.

Deuring, R. et al., 2000. The ISWI chromatin-remodeling protein is required for gene expression and the maintenance of higher order chromatin structure *in vivo*. *Molecular Cell*, 5(2):355–365.

Dhasarathy, A. & Kladde, M.P., 2005. Promoter occupancy is a major determinant of chromatin remodeling enzyme requirements. *Molecular and Cellular Biology*, 25(7):2698-2707.

Dixon, J.R. et al., 2012. Topological domains in mammalian genomes identified by analysis of chromatin interactions. *Nature*, 485(7398):376–380.

Dostie, J. et al., 2006. Chromosome Conformation Capture Carbon Copy (5C): a massively parallel solution for mapping interactions between genomic elements. *Genome Research,* 16(10):1299-1309.

Drew, H.R. & Travers, A.A., 1985. DNA bending and its relation to nucleosome positioning. *Journal of Molecular Biology*, 186(4):773–790.

Dubin, M. et al., 2010. Dynamics of a novel centromeric histone variant CenH3 reveals the evolutionary ancestral timing of centromere biogenesis. *Nucleic Acids Research*, 38(21):7526–7537.

Dubin, M.J., Kasten, S. & Nellen, W., 2011. Characterization of the *Dictyostelium* homolog of chromatin binding protein DET1 Suggests a conserved pathway regulating cell type specification and developmental plasticity. *Eukaryotic Cell*, 10(3):352–362.

Ebbert, R., Birkmann, A. & Schüller, H.J., 1999. The product of the SNF2/SWI2 paralogue INO80 of *Saccharomyces cerevisiae* required for efficient expression of various yeast structural genes is part of a high-molecular-weight protein complex. *Molecular Microbiology*, 32(4):741–51.

Ecco, G., et al., 2016. Transposable elements and their KRAB-ZFP controllers regulate gene expression in adult tissues. *Developmental Cell*, 36(6):611-623.

Eddy, S.R., 1998. Profile hidden Markov models. *Bioinformatics*, 14(9):755-763.

Egan, C.M. et al., 2013. CHD5 is required for neurogenesis and has a dual role in facilitating gene expression and polycomb gene repression. *Developmental Cell*, 26(3):223–236.

Ehrensberger, A.H. & Kornberg, R.D., 2011. Isolation of an activator-dependent, promoter-specific chromatin remodeling factor. *Proceedings of the National Academy of Sciences of the United States of America*, 108(25):10115–10120.

Eichinger, L. et al., 2005. The genome of the social amoeba *Dictyostelium discoideum*. *Nature*, 435(7038),:43–57.

Eirín-López, J.M. et al., 2009. The evolutionary differentiation of two histone H2A.Z variants in chordates (H2A.Z-1 and H2A.Z-2) is mediated by a stepwise mutation process that affects three amino acid residues. BMC Evolutionary Biology, 9:31.

Elfring, L.K. et al., 1998. Genetic Analysis of brahma : The *Drosophila* Homolog of the Yeast Chromatin Remodeling Factor SWI2/SNF2. *Genetics*, 148(1):251–265.

Elsässer S.J. et al., Histone H3.3 is required for endogenous retroviral element silencing in embryonic stem cells. *Nature*, 522(7555):240-244.

Eltsov, M. et al., 2008. Analysis of cryo-electron microscopy images does not support the existence of 30-nm chromatin fibers in mitotic chromosomes in situ. *Proceedings of the National Academy of Sciences of the United States of America*, 105(50):19732–19737.

Faast, R. et al., 2001. Histone variant H2A.Z is required for early mammalian development. *Current Biology*, 11(15):1183–1187.

Faix, J. et al., 2004. A rapid and efficient method to generate multiple gene disruptions in *Dictyostelium discoideum* using a single selectable marker and the Cre-loxP system. *Nucleic Acids Research*, 32(19):e143.

Fan, Y. et al., 2003. H1 linker histones are essential for mouse development and affect nucleosome spacing *in vivo*. *Molecular and Cellular Biology*, 23(13):4559–4572.

Fascher, K.D., Schmitz, J. & Hörz W., 1990. Role of trans-activating proteins in the generation of active chromatin at the PHO5 promoter in S. cerevisiae. *The EMBO Journal*, 9(8):2523-2528.

Faulkner, G.J. et al., 2009. The regulated reterotransposon transcriptome of mammalian cells. *Nature Genetics*, 41(5):563-571.

Fazzio, T.G. et al., 2001. Widespread collaboration of Isw2 and Sin3-Rpd3 chromatin remodeling complexes in transcriptional repression. *Molecular and Cellular Biology*, 21(19):6450–6460.

Fey, P. et al., 2007. Protocols for growth and development of Dictyostelium discoideum. *Nature Protocols*, 2(6):1307-1316.

Flanagan, J.F. et al., 2007. Molecular implications of evolutionary differences in CHD double chromodomains. *Journal of Molecular Biology*, 369(2):334–

342.

Finch, J.T. & Klug, A., 1976. Solenoidal model for superstructure in chromatin. *Proceedings of the National Academy of Sciences of the United States of America*, 73(6):1897-1901.

Flaus, A. et al., 2006. Identification of multiple distinct Snf2 subfamilies with conserved structural motifs. *Nucleic Acids Research*, 34(10):2887–2905.

Flowers, S. et al., 2009. Antagonistic roles for BRM and BRG1 SWI/SNF complexes in differentiation. *The Journal of Biological Chemistry*, 284(15):10067–10075.

Furuyama, T., Henikoff, S., 2009. Centromeric nucleosomes induce positive DNA supercoils. *Cell*, 138(1):104-113.

Fussner, E., Ching, R.W. & Bazett-Jones, D.P., 2011. Living without 30nm chromatin fibres. *Trends in Biochemical Sciences*, 36(1):1-6.

Gangaraju, V.K. & Bartholomew, B., 2007. Dependency of ISW1a chromatin remodeling on extranucleosomal DNA. *Molecular and Cellular Biology*, 27(8):3217–3225.

Gaspar-Maia, A. et al., 2009. Chd1 regulates open chromatin and pluripotency of embryonic stem cells. *Nature*, 460(7257):863–868.

Gaudet, P. et al., 2011. dictyBase update 2011: web 2.0 functionality and the initial steps towards a genome portal for the Amoebozoa. *Nucleic Acids Research*, 39(Database issue):D620-624.

Gaudet, P. et al., 2007. Transformation of *Dictyostelium discoideum* with plasmid DNA. *Nature Protocols*, 2(6):1317–1324.

Gaudreau, L., et al., 1997. RNA polymerase II holoenzyme recruitment is sufficient to remodel chromatin at the yeast PHO5 promoter. *Cell*, 89(1):55-62.

Gerhold, C.B., Hauer, M.H. & Gasser, S.M., 2015. INO80-C and SWR-C: Guardians of the Genome. *Journal of Molecular Biology*, 427(3):637–651.

Gerisch, G. et al., 1975. Cell communication by periodic cyclic-AMP pulses. *Philosophical Transactions of the Royal Society of London. Series B, Biological Sciences*, 272(915):181–192.

Gévry, N. et al., 2007. p21 transcription is regulated by differential localization of histone H2A.Z. *Genes & Development*, 21(15):1869–81.

Gkikopoulos, T. et al., 2011. A role for Snf2-related nucleosome-spacing

enzymes in genome-wide nucleosome organization. *Science*, 333(6050):1758–60.

Glöckner, G. et al. 2001. The complex repeats of *Dictyostelium discoideum*. *Genome Research*, 11(4):585-594.

Goldberg, A.D. et al., 2010. Distinct factors control histone variant H3.3 localization at specific genomic regions. *Cell*, 140(5):678-691.

Gorbalenya, AE. & Koonin, E. V, 1988. One more conserved sequence motif in helicases. *Nucleic Acids Research*, 16(15):7734.

Gresh, L. et al., 2005. The SWI/SNF chromatin-remodeling complex subunit SNF5 is essential for hepatocyte differentiation. *The EMBO Journal*, 24(18):3313–3324.

Groh, S. & Schotta, G., 2017. Silencing of endogenous retroviruses by heterochromatin. *Cell and Molecular Life Sciences*, 1-11.

Grüne, T. et al., 2003. Crystal structure and functional analysis of a nucleosome recognition module of the remodeling factor ISWI. *Molecular Cell*, 12(2):449–460.

Guillemette B. et al., 2005. Variant histone H2A.Z is globally localized to the promoters of inactive yeast genes and regulates nucleosome positioning. *PloS Biology*, 3(12):e384.

Hadjur, S. et al., 2009. Cohesins form chromosomal cis-interactions at the developmentally regulated IFNG locus. *Nature*, 460(7253):410–413.

Hargreaves, D.C. & Crabtree, G.R., 2011. ATP-dependent chromatin remodeling: genetics, genomics and mechanisms. *Cell Research*, 21(3):396–420.

Hartley, P.D. & Madhani, H.D., 2009. Mechanisms that specify promoter nucleosome location and identity. *Cell*, 137(3):445–458.

Harwood, A.J. et al., 2013. Aberrant spindle dynamics and cytokinesis in *Dictyostelium discoideum* cells that lack glycogen synthase kinase 3. *European Journal of Cell Biology*, 92(6–7):222–228.

Haynes, S.R. et al., 1992. The bromodomain: A conserved sequence found in human, *Drosophila* and yeast proteins. *Nucleic Acids Research*, 20(10):2603.

Heidel, A.J. et al., 2011. Phylogeny-wide analysis of social amoeba genomes highlights ancient origins for complex intercellular communication. *Genome Research*, 21(11):1882–1891.

Heitz, E., 1928. Das heterochromatin der Moose. *I. Jahrb Wiss Bot* 69:762-818.

Henikoff, S., 2014. The budding yeast Centromere DNA Element II wraps a stable Cse4 hemisome in either orientation in vivo. *Elife*, 3:e01861.

Hennig, B.P. et al., 2012. Chd1 chromatin remodelers maintain nucleosome organization and repress cryptic transcription. *EMBO Reports*, 13(11):997–1003.

Hewawasam, G. et al., 2010. Psh1 is an E3 ubiquitin ligase that targets the centromeric histone variant Cse4. *Molecular Cell*, 40(3):444–454.

Hildebrand, E.M. & Biggins, S., 2016. Regulation of budding yeast CENP-A levels prevents misincorporation at promoter nucleosomes and transcriptional defects. *PLoS Genetics*, 12(3):e1005930.

Hirschhorn, J.N. et al., 1992. Evidence that SNF2/SWI2 and SNF5 activate transcription in yeast by altering chromatin structure. *Genes & Development*, 6(12A):2288–2298.

Ho, L. & Crabtree, G.R., 2010. Chromatin remodelling during development. *Nature*, 463(7280):474–484.

van Holde, K.E., 1989. Chromatin. Springer-Verlag, New York.

Hong, J. et al., 2014. The catalytic subunit of the SWR1 remodeler is a histone chaperone for the H2A.Z-H2B dimer. *Molecular Cell*, 53(3):498–505.

Hou, C. et al., 2012. Gene density, transcription, and insulators contribute to the partition of the Drosophila genome into physical domains. *Molecular Cell*, 48(3):471-484.

Howman, E.V. et al., 2000. Early disruption of centromeric chromatin organization in centromere protein A (Cenpa) null mice. *Proceedings of the National Academy of Sciences of the United States of America*, 97(3):1148–1153.

Huang, S. & O'Shea, E.K., 2005. A systematic high-throughput screen of a yeast deletion collection for mutants defective in PHO5 regulation. *Genetics*, 169(4):1859-1871.

Hughes, A.L. et al., 2012. A functional evolutionary approach to identify determinants of nucleosome positioning: a unifying model for establishing the genome-wide pattern. *Molecular Cell*, 48(1):5–15.

Hughes, T.R. et al., 2000. Functional discovery via a compendium of expression profiles. *Cell*, 102(1), pp.109–26.

Hurd, E. a et al., 2007. Loss of Chd7 function in gene-trapped reporter mice is embryonic lethal and associated with severe defects in multiple developing tissues. *Mammalian Genome*, 18(2):94–104.

Ioshikhes, I. et al., 1996. Nucleosome DNA sequence pattern revealed by multiple alignment of experimentally mapped sequences. *Journal of Molecular Biology*, 262(2):129–139.

Ishihara, K., Oshimura, M. & Nakao, M., 2006. CTCF-dependent chromatin insulator is linked to epigenetic remodeling. *Molecular Cell*, 23(5):733–742.

Iyer, V.R., 2012. Nucleosome positioning: Bringing order to the eukaryotic genome. *Trends in Cell Biology*, 22(5):250–256.

Jang, C.W. et al., 2015. Histone H3.3 maintains genome integrity during mammalian development. *Genes & Development*, 29(13):1377-1392.

Jenuwein, T. & Allis, C.D., 2001. Translating the histone code. *Science*, 293(5532):1074-1080.

Jessen, W.J. et al., 2006. Active PHO5 chromatin encompasses variable numbers of nucleosomes at individual promoters. *Nature Structural & Molecular Biology*, 13(3):256–263.

Jin, T., Xu, X. & Hereld, D., 2008. Chemotaxis, chemokine receptors and human disease. *Cytokine*, 44(1):1–8.

Johnson, S.M. et al., 2006. Flexibility and constraint in the nucleosome core landscape of *Caenorhabditis elegans* chromatin. *Genome Research*, 16(12):1505–1516.

Jones, K.M. et al., 2014. CHD7 maintains neural stem cell quiescence and prevents premature stem cell depletion in the adult hippocampus. *Stem Cells*, 33(1):196-210.

Joseph, J.M. et al., 2008. The actinome of *Dictyostelium discoideum* in comparison to actins and actin-related proteins from other organisms. *PLoS ONE*, 3(7):e2654.

Kadoch, C. et al., 2013. Proteomic and bioinformatic analysis of mammalian SWI/SNF complexes identifies extensive roles in human malignancy. *Nature Genetics*, 45(6):592–601.

Kaplan, N. et al., 2009. The DNA-encoded nucleosome organization of a eukaryotic genome. *Nature*, 458(7236):362–366.

Kassabov, S.R. et al., 2003. SWI/SNF unwraps, slides, and rewraps the nucleosome. *Molecular Cell*, 11(2):391–403.

Kay, R.R. et al., 2008. Changing directions in the study of chemotaxis. *Nature Reviews. Molecular Cell Biology*, 9(6):455–463.

Keim-Reder, M., 2006. PhD Thesis.

Kenneth B. Raper, 1940. Pseudoplasmodium formation and organization in *Dictyotelium discoideum*. *Journal of the Elisha Mitchell Scientific Society*, 56(2):42.

Kent, N.A. et al., 2001. In vivo chromatin remodeling by yeast ISWI homologs Isw1p and Isw2p. *Genes & Development*, 15(5):619–626.

Kent, N.A. et al., 2011. Chromatin particle spectrum analysis: a method for comparative chromatin structure analysis using paired-end mode next-generation DNA sequencing. *Nucleic Acids Research*, 39(5):e26.

Khattak, S. et al., 2002. Genetic characterization of *Drosophila* Mi-2 ATPase. *Gene*, 293(1–2):107–114.

Khorosjutina, O. et al., 2010. A chromatin-remodeling protein is a component of fission yeast mediator. *Journal of Biological Chemistry*, 285(39):29729–29737.

Kim, J.H., Choi, D. & Kende, H., 2003. The AtGRF family of putative transcription factors is involved in leaf and cotyledon growth in *Arabidopsis*. *Plant Journal*, 36(1):94–104.

Kim, J.Y., Kwak, P.B. & Weitz, C.J., 2014. Specificity in circadian clock feedback from targeted reconstitution of the NuRD corepressor. *Molecular Cell*, 56(6):738–748.

Klochendler-Yeivin, A. et al., 2000. The murine SNF5/INI1 chromatin remodeling factor is essential for embryonic development and tumor suppression. *EMBO Reports*, 1(6):500–506.

Knecht, D.A. & Loomis, W.F., 1987. Antisense RNA inactivation of myosin heavy chain gene expression in *Dictyostelium discoideum*. *Science*, 236(4805):1081–1086.

Kobor, M.S. et al., 2004. A protein complex containing the conserved Swi2/Snf2-related ATPase Swr1p deposits histone variant H2A.Z into euchromatin. *PLoS Biology*, 2(5):E131.

Konev, A.Y. et al., 2007. CHD1 motor protein is required for deposition of histone variant H3.3 into chromatin in vivo. *Science*, 317(5841):1087–1090.

Konijn, T.M. et al., 1969. Identification of adenosine-3',5'-monophosphate as the bacterial attractant for myxamoebae of *Dictyostelium discoideum*. *Journal*

of Bacteriology, 99(2):510–512.

Korber et al., 2004. Evidence for histone eviction in trans upon induction of the yeast PHO5 promoter. *Molecular Cell Biology*, 24(24):10965-10974.

Korber, P. & Barbaric, S., 2014. The yeast PHO5 promoter: from single locus to systems biology of a paradigm for gene regulation through chromatin. *Nucleic Acids Research*, 42(17):10888-10902.

Kornberg, R.D., 1974. Chromatin structure: a repeating unit of histones and DNA. *Science*, 184(4139):868-871

Kraushaar, D. et al., 2013. Genome-wide incorporation dynamics reveal distinct categories of turnover for the histone variant H3.3. *Genome Biology*, 14(10):R121.

Krogan, N.J. et al., 2003. A Snf2 family ATPase complex required for recruitment of the histone H2A variant Htz1. *Molecular Cell*, 12(6):1565–1576.

Krueger, F. et al., 2012. DNA methylome analysis using short bisulfite sequencing data. *Nature Methods*, 9(2):145-151.

Kruger, W. et al., 1995. Amino acid substitutions in the structured domains of histones H3 and H4 partially relieve the requirement of the yeast SWI/SNF complex for transcription. *Genes & Development*, 9(22):2770–2779.

Kubik, S. et al., 2015. Nucleosome stability distinguishes two different promoter types at all protein-coding genes in yeast. *Molecular Cell*, 60(3):422–434.

Kulkarni, S. et al., 2008. Disruption of chromodomain helicase DNA binding protein 2 (CHD2) causes scoliosis. *American Journal of Medical Genetics, Part A*, 146(9):1117–1127.

Kustatscher, G., 2005. Splicing regulates NAD metabolite binding to histone macroH2A. *Nature Structural and Molecular Biology*, 12(7):624-625.

Lai, A.Y. & Wade, P.A. 2011. Cancer biology and NuRD: a multifaceted chromatin remodelling complex. *Nature Reviews. Cancer*, 11(8):588–596.

Lalani, S.R. et al., 2006. Spectrum of CHD7 Mutations in 110 Individuals with CHARGE syndrome and genotype-phenotype correlation. *American Journal of Human Genetics*, 78(2):303–314.

Landt, S.G. et al., 2012. ChIP-seq guidelines and practices of the ENCODE and modENCODE consortia. *Genome Research*, 22(9):1813-1831.

Langmead, B. et al., 2009. Ultrafast and memory-efficient alignment of short

DNA sequences to the human genome. *Genome Biology*, 10(2):R25.

Lathrop, M.J. et al., 2010. Deletion of the Chd6 exon 12 affects motor coordination. *Mammalian Genome*, 21(3–4):130–142.

Laurent, B.C., Treich, I. & Carlson, M., 1993. The yeast SNF2/SWI2 protein has DNA-stimulated ATPase activity required for transcriptional activation. *Genes and Development*, 7(4):583–591.

Laurent, B.C., Yang, X. & Carlson, M., 1992. An essential *Saccharomyces cerevisiae* gene homologous to SNF2 encodes a helicase-related protein in a new family. *Molecular and Cellular Biology*, 12(4):1893–1902.

Lee, R.S. et al., 2012. A remarkably simple genome underlies highly malignant pediatric rhabdoid cancers. *The Journal of Clinical Investigation*, 122(8):2983–2988.

Lee, W. et al., 2007. A high-resolution atlas of nucleosome occupancy in yeast. *Nature Genetics*, 39(10):1235-1244.

Lettice, L.A. et al., 2011. A long-range Shh enhancer regulates expression in the developing limb and fin and is associated with preaxial polydactyly. *Human Molecular Genetics*, 12(14):1725-1735.

Lettice, L.A. et al., 2011. Enhancer-adoption as a mechanism of human developmental disease. *Human Mutation*, 32(12):1492–1499.

Li, J. et al., 2014. An antisense promoter in mouse L1 retrotransposon open reading frame-1 initiates expression of diverse fusion transcripts and limits retrotransposition. *Nucleic Acids Research*, 42(7):4546-4562.

Li, W. & Mills, A., 2014. Architects of the genome: CHD dysfunction in cancer, developmental disorders and neurological syndromes. *Epigenomics*, 6(4):381–395.

Liebermann-Aiden, E. et al., 2009. Comprehensive mapping of long-range interactions reveals folding principles of the human genome. *Science*, 326(5950):289-293.

Lin, J.J. et al., 2011. Mediator coordinates PIC assembly with recruitment of CHD1. *Genes & Development*, 25(20):2198–2209.

Loomis, W.F., 2014. Cell signaling during development of *Dictyostelium*. *Developmental Biology*, 391(1):1–16.

Luger K., et al. 1997. Crystal structure of the nucleosome core particle at 2.8A resolution. *Nature*, 389(6648):251-260.

Luger, K., Dechassa, M.L. & Tremethick, D.J., 2012. New insights into nucleosome and chromatin structure: an ordered state or a disordered affair? *Nature Reviews. Molecular Cell Biology*, 13(7):436-447.

Luger, K. & Richmond, T.J., 1998. The histone tails of the nucleosome. *Current Opinion in Genetics and Development,* 8(2):140146.

Luk, E. et al., 2010. Stepwise histone replacement by SWR1 requires dual activation with histone H2A.Z and canonical nucleosome. *Cell*, 143(5):725–736.

Lund, C. et al., 2014. CHD2 mutations in Lennox-Gastaut syndrome. *Epilepsy and Behavior*, 33:18–21.

Lusser, A. & Kadonaga, J.T., 2003. Chromatin remodeling by ATP-dependent molecular machines. *BioEssays*, 25(12):1192–200.

Lusser, A., Urwin, D.L. & Kadonaga, J.T., 2005. Distinct activities of CHD1 and ACF in ATP-dependent chromatin assembly. *Nature Structural & Molecular Biology*, 12(2):160–166.

Maeshima, K., et al., 2016. Liquid-like behaviour of chromatin. *Current Opinions in Genetics & Development*, 37:36-45.

Marfella, C.G. et al., 2006. Mutation of the SNF2 family member Chd2 affects mouse development and survival. *Journal of Cellular Physiology*, 209(1):162–171.

Marfella, C.G. & Imbalzano, A.N., 2007. The Chd family of chromatin remodelers. *Mutation Research*, 618(1):30–40.

Marom, R. et al., 2006. Expression and regulation of CReMM , a chromodomain helicase-DNA-Binding (CHD), in marrow stroma derived osteoprogenitors. *Journal of Cellular Physiology*, 207(3):628–635.

Mavrich, T.N. et al., 2008. Nucleosome organization in the *Drosophila* genome. *Nature*, 453(7193):358–362.

McDaniel, I.E. et al., 2008. Investigations of CHD1 function in transcription and development of *Drosophila melanogaster*. *Genetics*, 178(1):583–587.

McDowall, A.W., Smith, J.M. & Dubochet, J. Cryo-electron microscopy of vitrified chromosomes *in situ*. *The EMBO Journal*, 5(6):1395-1402.

McKnight, J.N. et al., 2011. Extranucleosomal DNA binding directs nucleosome sliding by Chd1. *Molecular and Cellular Biology*, 31(23):4746–59.

Mellor, J. & Morillon, A., 2004. ISWI complexes in *Saccharomyces cerevisiae*.

Biochimica et Biophysica Acta, 1677(1–3):100–112.

Mendiburo, M.J. et al., 2011. Drosophila CENH3 is sufficient for centromere formation. *Science*, 334(6056):686-690.

Meneghini, M.D., Wu, M. & Madhani, H.D., 2003. Conserved histone variant H2A.Z protects euchromatin from the ectopic spread of silent heterochromatin. *Cell*, 112(5):725-736.

Miccio, A. et al. 2010. NuRD mediates activating and repressive functions of GATA-1 and FOG-1 during blood development. *The EMBO Journal*, 29(2):442–456.

Mieczkowski, J. et al. 2016. MNase titration reveals differences between nucleosome occupancy and chromatin accessibility. *Nature Communications*, 7:11485.

Miranda, E.R. et al. 2013. ABC Transporters in Dictyostelium discoideum Development. *PloS ONE*, 8(8):e70040

Mizuguchi, G. et al. 2004. ATP-driven exchange of histone H2AZ variant catalyzed by SWR1 chromatin remodeling complex. *Science*, 303(5656):343–348.

Modena, P. et al. 2005. SMARCB1/INI1 Tumor Suppressor Gene Is Frequently Inactivated in Epithelioid Sarcomas Inactivated in Epithelioid Sarcomas. *Cancer Research*, 65:4012–4019.

Morettini, S. et al., 2011. The chromodomains of CHD1 are critical for enzymatic activity but less important for chromatin localization. *Nucleic Acids Research*, 39(8):3103–3115.

Morillon, A. et al., 2003. Isw1 chromatin remodeling ATPase coordinates transcription elongation and termination by RNA polymerase II. *Cell*, 115(4):425–345.

Morris, S.A. et al., 2014. Overlapping Chromatin Remodeling Systems Collaborate Genome-wide at Dynamic Chromatin Transitions. *Nature Structural & Molecular Biology*, 21(1):73–81.

Morrison, A.J. & Shen, X., 2009. Chromatin remodelling beyond transcription: the INO80 and SWR1 complexes. *Nature Reviews. Molecular Cell Biology*, 10(6):373–384.

Mueller-Planitz, F., Klinker, H., Ludwigsen, J., et al., 2013. The ATPase domain of ISWI is an autonomous nucleosome remodeling machine. *Nature Structural & Molecular Biology*, 20(1):82–89.

Mueller-Planitz, F., Klinker, H. & Becker, P.B., 2013. Nucleosome sliding mechanisms: new twists in a looped history. *Nature Structural & Molecular Biology*, 20(9):1026–1032.

Muramoto, T. & Chubb, J.R., 2008. Live imaging of the *Dictyostelium* cell cycle reveals widespread S phase during development, a G2 bias in spore differentiation and a premitotic checkpoint. *Development*, 135(9):1647–1657.

Murawska, M. & Brehm, A., 2011. CHD chromatin remodelers and the transcription cycle. *Transcription*, 2(6):244–253.

Musladin, S. et al., 2014. The RSC chromatin remodeling complex has a crucial role in the complete remodeler set for yeast PHO5 promoter opening. *Nucleic Acids Research*, 42:4270-4282.

Myers, S.A., Leeper, L.R. & Chung, C.Y., 2006. WASP-interacting protein is important for actin filament elongation and prompt pseudopod formation in response to a dynamic chemoattractant gradient. *Molecular Biology of the Cell*, 17(10):4564–4575.

Nagano, T. et al., 2013. Single-cell Hi-C reveals cell-to-cell variability in chromosome structure. *Nature*, 502(7469):59-64.

Nagl, N.G. et al., 2007. Distinct mammalian SWI/SNF chromatin remodeling complexes with opposing roles in cell-cycle control. *The EMBO Journal*, 26(3):752–763.

Narlikar, G.J., Sundaramoorthy, R. & Owen-Hughes, T., 2013. Mechanisms and functions of ATP-dependent chromatin-remodeling enzymes. *Cell*, 154(3):490–503.

Nasmyth, K., 2001. Disseminating the Genome: Joining, Resolving, and Separating Sister Chromatids During Mitosis and Meiosis. *Annual Review of Genetics*, 35:673–745.

Neef, D.W. & Kladde, M.P., 2003. Polyphosphate loss promotes SNF/SWI- and Gcn5-dependent mitotic induction of Pho5. *Molecular and Cellular Biology*, 23(11):3788-3797.

Neigeborn, L. & Carlson, M., 1984. Genes affecting the regulation of SUC2 gene expression by glucose repression in *Saccharomyces cerevisiae*. *Genetics*, 108:845–858.

Nishino, Y. et al., 2012. Human mitotic chromosomes consist predominantly of irregularly folded nucleosome fibres without a 30-nm chromatin structure. *The EMBO Journal*, 31(7):1644-1653.

Nishiyama, M. et al., 2004. Early embryonic death in mice lacking the beta-catenin-binding protein Duplin. *Molecular and Cellular Biology*, 24(19):8386–8394.

Nora, E.P. et al., 2012. Spatial partitioning of the regulatory landscape of the X-inactivation centre. *Nature*, 485:381–385.

O'Sullivan, A. et al., 2004. STAT4 Is Required for Interleukin-12-induced Chromatin Remodeling of the CD25 Locus. *Journal of Biological Chemistry*, 279(8):7339–7345.

Ogawa, S. et al., 2000. The mitochondrial DNA of *Dictyostelium discoideum*: complete sequence, gene content and genome organization. *Molecular & General Genetics*, 263(3):514–519.

Olins, A.L. & Olins, D.E., 1974. Spheroid chromatin units (v bodies). *Science*, 183(4122):330-332.

Papamichos-Chronakis, M. et al., 2010. Global regulation of H2A.Z localization by the INO80 chromatin remodeling enzyme is essential for genome integrity. *Cell*, 144(2):200–213.

Papamichos-Chronakis, M., Krebs, J.E. & Peterson, C.L., 2006. Interplay between Ino80 and Swr1 chromatin remodeling enzymes regulates cell cycle checkpoint adaptation in response to DNA damage. *Genes & Development*, 20(17):2437–2449.

Parikh, A. et al., 2010. Conserved developmental transcriptomes in evolutionarily divergent species. *Genome Biology*, 11(3):R35.

Park, D., Shivram, H. & Iyer, V.R., 2014. Chd1 co-localizes with early transcription elongation factors independently of H3K36 methylation and releases stalled RNA polymerase II at introns. *Epigenetics & Chromatin*, 7(1):32.

Parnell, T.J., Huff, J.T. & Cairns, B.R., 2008. RSC regulates nucleosome positioning at Pol II genes and density at Pol III genes. *The EMBO Journal*, 27(1):100–110.

Patterton, H.G. et al., 1998. The biochemical and phenotypic characterization of Hho1p, the putative linker histone H1 of Saccharomyces cerevisiae. *The Journal of Biological Chemistry*, 273(13):7268-7276.

Pegoraro, G. et al., 2009. Ageing-related chromatin defects through loss of the NURD complex. *Nature Cell Biology*, 11(10):1261–1267.

Pennings, S., Meersseman, G. & Bradbury, E.M., 1994. Linker histones H1 and

H5 prevent the mobility of positioned nucleosomes. *Proceedings of the National Academy of Sciences of the United States of America*, 91(22):10275-10279.

Peterson, C.L. & Herskowitz, I., 1992. Characterization of the yeast SWI1, SWI2, and SWI3 genes, which encode a global activator of transcription. *Cell*, 68(3):573–583.

Phelan, M.L. et al., 1999. Reconstitution of a core chromatin remodeling complex from SWI/SNF subunits. *Molecular Cell*, 3(2):247–253.

Phillips-Cremins, J.E. et al., 2013. Architectural protein subclasses shape 3D organization of genomes during lineage commitment. *Cell*, 153(6):1281–1295.

Pickersgill, H. et al., 2006. Characterisation of the *Drosophila melanogaster* genome at the nuclear lamina. *Nature Genetics*, 38(9):1005-1014.

Platt, J.L., 2013. *A study of the Chd family of ATP-dependen chromatin remodellers in Dictyostelium discoideum*. Cardiff University.

Platt, J.L. et al., 2013. Different CHD chromatin remodelers are required for expression of distinct gene sets and specific stages during development of *Dictyostelium discoideum*. *Development* , 140(24):4926–4936.

Pointner, J. et al., 2012. CHD1 remodelers regulate nucleosome spacing in vitro and align nucleosomal arrays over gene coding regions in S. pombe. *The EMBO journal*, 31(23):4388–4403.

Qiu, H. et al., 2015. Genome-wide cooperation by HAT Gcn5 , remodeler SWI/SNF, and chaperone Ydj1 in promoter nucleosome eviction and transcriptional activation. *Genome Research*, 26(2):211–225.

R Development Core Team, 2016. R: A language and environment for statistical computing. *R Foundation for Statistical Computing, Vienna, Austria.* Available at: https://www.r-project.org.

Racki, L.R. et al., 2009. The chromatin remodeller ACF acts as a dimeric motor to space nucleosomes. *Nature*, 462(7276):1016–1021.

Radman-Livaja, M. et al., 2012. A Key Role for Chd1 in Histone H3 Dynamics at the 3′ Ends of Long Genes in Yeast. *PLoS Genetics*, 8(7):e1002811.

Rafati, H. et al., 2011. Repressive LTR nucleosome positioning by the BAF complex is required for HIV latency. *PLoS Biology*, 9(11):1–31.

Ramachandran, S., Zentner, G.E. & Henikoff, S., 2015. Asymmetric nucleosomes flank promoters in the budding yeast genome. Genome

Research, 25(3):381-390

Rando, O.J. & Winston, F., 2012. Chromatin and transcription in yeast. *Genetics*, 190(2):351-387.

Rangasamy, D., Greaves, I. & Tremethick, D.J., 2004. RNA interference demonstrates a novel role for H2A.Z in chromosome segregation. *Nature Structural & Molecular Biology*, 11(7):650–655.

Ranjan, A. et al., 2013. Nucleosome-free region dominates histone acetylation in targeting SWR1 to promoters for H2A.Z replacement. *Cell*, 154(6):1232–1245.

Ranjitkar, P. et al., 2010. An E3 Ubiquitin Ligase Prevents Ectopic Localization of the Centromeric Histone H3 Variant via the Centromere Targeting Domain. *Molecular Cell*, 40(3):455–464.

Raper, K.B., 1935. *Dictyostelium discoideum*, a new species of slime mold from decaying forest leaves. *Journal of Agricultural Research*, 50(2):135–147.

Raper, K.B., 1950. Stalk Formation in *Dictyostelium*. *Science*, 112(2912):450.

Reinke, H. & Hörz, W., 2003. Histones are first hyperacetylated and then lose contact with the activated PHO5 promoter, *Molecular Cell,* 11:1599-1607.

Reyes, J.C. et al., 1998. Altered control of cellular proliferation in the absence of mammalian brahma (SNF2α). *The EMBO Journal*, 17(23):6979–6991.

Reynolds, N. et al., 2012. NuRD-mediated deacetylation of H3K27 facilitates recruitment of Polycomb Repressive Complex 2 to direct gene repression. *The EMBO Journal*, 31(3):593–605.

Rhee, H.S. 2014. Subnucleosomal structures and nucleosome asymmetry across a genome. *Cell*, 159(6):1377-1388.

Rhee, H.S. & Pugh, B.F., 2012. ChIP-exo method for identifying genomic location of DNA-binding proteins with near-single-nucleotide resolution. *Current Protocols in Molecular Cell Biology*, Chapter 21:Unit 21.24.

Rippe, K. et al., 2007. DNA sequence- and conformation-directed positioning of nucleosomes by chromatin-remodeling complexes. *Proceedings of the National Academy of Sciences of the United States of America*, 104(40):15635–15640.

Rogers, B.J., 2010. *ATP-dependent chromatin re-modeling factors regulate expression of genes involved in Dictyostelium discoideum development and chemotaxis*. Cardiff University.

de Rop, V., Padeganeh, A. & Maddox, P.S., 2012. CENP-A: The key player behind centromere identity, propagation, and kinetochore assembly. *Chromosoma*, 121(6):527–538.

Rosengarten, R.D. et al., 2015. Leaps and lulls in the developmental transcriptome of *Dictyostelium discoideum*. *BMC Genomics*, 16(1):294.

Rowe, H.M. & Trono, D. Dynamic control of endogenous retroviruses during development. Virology, 411(2):273-287.

Ruhl, D.D. et al., 2006. Purification of a human SRCAP complex that remodels chromatin by incorporating the histone variant H2A.Z into nucleosomes. *Biochemistry*, 45(17):5671–5677.

Rusk, N., 2011. Torrents of sequence. Nature Methods, 8(1):44.

Ryan, D.P. & Owen-Hughes, T., 2011. Snf2-family proteins: chromatin remodellers for any occasion. *Current Opinion in Chemical Biology*, 15(5):649–56.

Sanborn, A.L. et al., 2015. Chromatin extrusion explains key features of loop and domain formation in wild-type and engineered genomes. *Proceedings of the National Academy of Sciences*, 112(47):e6456-65.

Santisteban, M.S., Kalashnikova, T. & Smith, M.M., 2000. Histone H2A.Z regulats transcription and is partially redundant with nucleosome remodeling complexes. *Cell*, 103(3):411–422.

Sasaki, K. et al., 2008. An immediate-early gene, srsA: its involvement in the starvation response that initiates differentiation of Dictyostelium cells. *Differentiation*, 76(10):1093-1103.

Schneider, C. a, Rasband, W.S. & Eliceiri, K.W., 2012. NIH Image to ImageJ: 25 years of image analysis. *Nature Methods*, 9(7):671–675.

Schones, D.E. et al., 2008. Dynamic regulation of nucleosome positioning in the human genome. *Cell*, 132(5):887–898.

Schwabish, M.A. & Struhl, K., 2007. The Swi/Snf complex is important for histone eviction during transcriptional activation and RNA polymerase II elongation in vivo. *Molecular and Cellular Biology*, 27(20):6987–6995.

Segal, E. et al., 2006. A genomic code for nucleosome positioning. *Nature*, 442(7104):772–778.

de la Serna, I.L., Ohkawa, Y. & Imbalzano, A.N., 2006. Chromatin remodelling in mammalian differentiation: lessons from ATP-dependent remodellers. *Nature Reviews. Genetics*, 7(6):461–73.

Sexton, T. et al., 2012. Sensitive detection of chromatin coassociations using enhanced chromosome conformation capture on chip. Nature Protocols, 7(7):1335-1350.

Shahbazian, M.D. & Grunstein, M., 2007. Functions of site-specific histone acetylation and deacetylation. *Annual Review of Biochemistry*, 76:75-100.

Shain, A.H. & Pollack, J.R., 2013. The Spectrum of SWI/SNF Mutations, Ubiquitous in Human Cancers. *PLoS ONE*, 8(1):e55119.

Sharma, A. et al., 2011. Crystal structure of the chromodomain helicase DNA-binding protein 1 (Chd1) DNA-binding domain in complex with DNA. *The Journal of Biological Chemistry*, 286(49):42099–42104.

Shema-Yaacoby, E. et al., 2013. Systematic identification of proteins binding to chromatin-embedded ubiquitylated H2B reveals recruitment of SWI/SNF to regulate transcription. *Cell Reports*, 4(3):601–608.

Shen, X. et al., 2000. A chromatin remodelling complex involved in transcription and DNA processing. *Nature*, 406(6795):541–544.

Shen, X. et al., 2003. Involvement of actin-related proteins in ATP-dependent chromatin remodeling. *Molecular Cell*, 12(1):147–155.

Shim, Y.S. et al., 2012. Hrp3 controls nucleosome positioning to suppress non-coding transcription in eu- and heterochromatin. *The EMBO Journal*, 31(23):4375–4387.

Shimbo, T. et al., 2013. MBD3 Localizes at Promoters, Gene Bodies and Enhancers of Active Genes. *PLoS Genetics*, 9(12):e1004028

Shivaswamy, S. & Iyer, V.R., 2008. Stress-dependent dynamics of global chromatin remodeling in yeast: dual role for SWI/SNF in the heat shock stress response. *Molecular and cellular Biology*, 28(7):2221–2234.

Shur, I. & Benayahu, D., 2005. Characterization and functional analysis of CReMM, a novel chromodomain helicase DNA-binding protein. *Journal of Molecular Biology*, 352(3):646–655.

Siggens, L. et al., 2015. Transcription-coupled recruitment of human CHD1 and CHD2 influences chromatin accessibility and histone H3 and H3.3 occupancy at active chromatin regions. *Epigenetics & Chromatin*, 8(1):4.

Simic, R. et al., 2003. Chromatin remodeling protein Chd1 interacts with transcription elongation factors and localizes to transcribed genes. *The EMBO Journal*, 22(8):1846–1856.

Sims, J.K. & Wade, P. A, 2011. SnapShot: Chromatin remodeling: CHD. *Cell*,

144(4):.626–626.

Sims, R.J. et al., 2005. Human but not yeast CHD1 binds directly and selectively to histone H3 methylated at lysine 4 via its tandem chromodomains. *The Journal of Biological Chemistry*, 280(51):41789–41792.

Siriaco, G. et al., 2009. *Drosophila* ISWI regulates the association of histone H1 with interphase chromosomes *in vivo*. *Genetics*, 182(3):661–669.

Smallwood, A. & Ren, B., 2013. Genome organization and long-range regulation of gene expression by enhancers. *Current Opinion in Cell Biology*, 25(3):387–394.

Smolle, M. et al., 2012. Chromatin remodelers Isw1 and Chd1 maintain chromatin structure during transcription by preventing histone exchange. *Nature Structural & Molecular Biology*, 19(9):884–892.

Smolle, M. & Workman, J.L., 2013. Transcription-associated histone modifications and cryptic transcription. *Biochimica et Biophysica Acta*, 1829(1):84–97.

Song, F. et al., 2014. Cryo-EM study of the chromatin fiber reveals a double helix twisted by tetranucleosomal units. *Science*, 344(6182):376:380.

Srinivasan, S. et al., 2005. The *Drosophila* trithorax group protein Kismet facilitates an early step in transcriptional elongation by RNA Polymerase II. *Development*, 132(7):1623–1635.

Steger, D.J. et al., 2003. Regulation of chromatin remodeling by inositol polyphosphates. *Science*, 299:114-116.

Stern, M., Jensen, R. & Herskowitz, I., 1984. Five SWI genes are required for expression of the HO gene in yeast. *Journal of Molecular Biology*, 178(4):853–868.

Stevense, M., Chubb, J.R. & Muramoto, T., 2011. Nuclear organization and transcriptional dynamics in *Dictyostelium*. *Development, Growth & Differentiation*, 53(4):576–586.

Stokes, D.G., Tartof, K.D. & Perry, R.P., 1996. CHD1 is concentrated in interbands and puffed regions of *Drosophila* polytene chromosomes. *Proceedings of the National Academy of Sciences of the United States of America*, 93(14):7137–7142.

Stopka, T. & Skoultchi, A.I., 2003. The ISWI ATPase Snf2h is required for early mouse development. *Proceedings of the National Academy of Sciences of*

the United States of America, 100(24):14097–14102.

Strahl, B.D. & Allis, C.D., 2000. The language of covalent histone modifications. *Nature*, 403(6765):41-45.

Strobeck, M.W. et al., 2002. Compensation of BRG-1 function by Brm. Insight into the role of the core SWI/SNF subunits in retinoblastoma tumor suppressor signaling. *Journal of Biological Chemistry*, 277(7):4782–4789.

Struhl, K. & Segal, E., 2013. Determinants of nucleosome positioning. *Nature Structural & Molecular Biology*, 20(3):267–273.

Sucgang, R. et al., 2011. Comparative genomics of the social amoebae *Dictyostelium discoideum* and *Dictyostelium purpureum*. *Genome Biology*, 12(2):R20.

Sucgang, R., 2003. Sequence and structure of the extrachromosomal palindrome encoding the ribosomal RNA genes in *Dictyostelium*. *Nucleic Acids Research*, 31(9):2361–2368.

Suls, A. et al., 2013. De novo loss-of-function mutations in CHD2 cause a fever-sensitive myoclonic epileptic encephalopathy sharing features with dravet syndrome. *American Journal of Human Genetics*, 93(5):967–975.

Sussman, R. & Sussman, M., 1967. Cultivation of Dictyostelium discoideum in axenic medium. *Biochemical and Biophysical Research Communications*, 29(1):52-55.

Svotelis, A., Gévry, N., Gaudreau, L., 2009. Regulation of gene expression and cellular proliferation by histone H2A.Z. *Biochemistry and Cell Biology*, 87(1):179-188.

Takemoto, K. et al., 1990. cAMP regulation of the expression of prespore-sepcific genes, SP96 and Dp87, in disaggregated slug cells of Dictyostelium discoideum. *Cell Differentiation and Development*, 31(2):89-96.

Tan, M. et al., 2011. Identification of 67 histone marks and histone lysine crotonylation as a new type of histone modification. *Cell*, 146(6):1016-1028.

Tang, L., Nogales, E. & Ciferri, C., 2010. Structure and function of SWI/SNF chromatin remodeling complexes and mechanistic implications for transcription. *Progress in Biophysics and Molecular Biology*, 102(2–3):122–128.

Thoma, F., Koller, T. & Klug, A., 1979. Involvement of histone H1 in the organization of the nucleosome and of the salt-dependent superstructures

of chromatin. *Journal of Cell Biology*, 83(2 Pt 1):403-427.

Thompson, B.A. et al., 2008. CHD8 is an ATP-dependent chromatin remodeling factor that regulates beta-catenin target genes. *Molecular and Cellular Biology*, 28(12):3894–3904.

Thompson, P.M. et al., 2003. CHD5, a new member of the chromodomain gene family, is preferentially expressed in the nervous system. *Oncogene*, 22(7),:1002–1011.

Tirosh, I., Sigal, N. & Barkai, N., 2010. Widespread remodeling of mid-coding sequence nucleosomes by Isw1. *Genome Biology*, 11(5):R49.

Trapnell, C. et al., 2010. Transcript assembly and quantification by RNA-Seq reveals unannotated transcripts and isoform switching during cell differentiation. *Nature Biotechnology*, 28(5):511–515.

Tsukiyama, T. et al., 1999. Characterization of the Imitation Switch subfamily of ATP-dependent chromatin-remodeling factors in *Saccharomyces cerevisiae*. *Genes & Development*, 13:686–697.

Tsukiyama, T., Becker, P.B. & Wu, C., 1994. ATP-dependent nucleosome disruption at a heat-shock promoter mediated by binding of GAGA transcription factor. *Nature*, 367(6463):525–532.

Tsukiyama, T. & Wu, C., 1995. Purification and properties of an ATP-dependent nucleosome remodeling factor. *Cell*, 83(6):1011–1020.

Uyeda, T.Q.P., Kitayama, C. & Yumura, S., 2000. Myosin II-independent cytokinesis in *Dictyostelium*: its mechanism and implications. *Cell Structure and Function*, 25(1):1–10.

Valouev, A. et al., 2008. A high-resolution, nucleosome position map of C. elegans reveals a lack of universal sequence-dictated positioning. *Genome Research*, 18(7):1051–1063.

Valouev, A. et al., 2011. Determinants of nucleosome organization in primary human cells. *Nature*, 474(7352):516–20.

Varga-weisz, P.D. et al., 1997. Chromatin-remodelling factor CHRAC contains the ATPases ISWI and topoisomerase II. *Nature*, 388:598–602.

Versteege, I. et al., 1998. Truncating mutations of hSNF5/INI1 in aggressive paediatric cancer. *Nature*, 394(6689):203–206.

Vetterkind, S. et al., 2002. The rat homologue of Wiskott-Aldrich syndrome protein (WASP)-interacting protein (WIP) associates with actin filaments, recruits N-WASP from the nucleus, and mediates mobilization of actin from

stress fibers in favor of filopodia formation. *Journal of Biological Chemistry*, 277(1):87–95.

Wade, P.A. et al., 1998. A multiple subunit Mi-2 histone deacetylase from Xenopus laevis cofractionates with an associated Snf2 superfamily ATPase. *Current Biology*, 8(14):843–846.

Wang, H.B. & Zhang, Y., 2001. Mi2, an auto-antigen for dermatomyositis, is an ATP-dependent nucleosome remodeling factor. *Nucleic Acids Research*, 29(12):2517–2521.

Wang, W., Xue, Y., et al., 1996. Diversity and specialization of mammalian SWI/SNF complexes. *Genes & Development*, 10(17):2117–2130.

Wang, W., Côté, J., et al., 1996. Purification and biochemical heterogeneity of the mammalian SWI-SNF complex. *The EMBO journal*, 15(19), pp.5370–82.

Watanabe, S. et al., 2013. A histone acetylation switch regulates H2A.Z deposition by the SWR-C remodeling enzyme. *Science*, 340(6129):195–199.

Watts, D.J. & Ashworth, J.M., 1970. Growth of myxameobae of the cellular slime mould *Dictyostelium discoideum* in axenic culture. *The Biochemical Journal*, 119(2):171–174.

Whitehouse, I. et al., 2007. Chromatin remodelling at promoters suppresses antisense transcription. *Nature*, 450(7172), pp.1031–5.

Widom, J. & Klug, A., 1985. Structure of the 300A chromatin filament: X-ray diffraction from oriented samples. *Cell*, 42(1):207-213.

Wilson, B.G. & Roberts, C.W.M., 2011. SWI/SNF nucleosome remodellers and cancer. *Nature Reviews. Cancer*, 11(7):481–492.

Winston, F. & Carlson, M., 1992. Yeast SNF/SWI transcriptional activators and the SPT/SIN chromatin connection. *Trends in Genetics*, 8(11):387–391.

Woodage, T. et al., 1997. Characterization of the CHD family of proteins. *Proceedings of the National Academy of Sciences of the United States of America*, 94(October):11472–11477.

Woodcock, C.L., Frado, L.L. & Rattner, J.B., 1984. The higher-order structure of chromatin: evidence for a helical ribbon arrangement. Journal of Cell Biology, 99(1 Pt 1):42-52.

Workman, J.L. & Buchman, A.R., 1993. Multiple functions of nucleosomes and regulatory factors in transcription. *Trends in Biochemical Sciences*,

18(3):90–95.

Wu, C., 1980. The 5’ ends of *Drosophila* heat shock genes in chromatin are hypersensitive to DNaseI. *Nature*, 286(5776):854-860.

Wu, J.I. et al., 2007. Regulation of Dendritic Development by Neuron-Specific Chromatin Remodeling Complexes. *Neuron*, 56(1):94–108.

Wu, J.I., Lessard, J. & Crabtree, G.R., 2009. Understanding the words of chromatin regulation. *Cell*, 136(2):200–206.

Xi, R. & Xie, T., 2005. Stem cell self-renewal controlled by chromatin remodeling factors. *Science*, 310(5753):1487–1489.

Xi, Y. et al., 2011. Nucleosome fragility reveals novel functional states of chromatin. *Genome Research*, 21:718–724.

Xue, Y. et al., 1996. NURD , a novel complex with both ATP-dependent chromatin-remodeling and histone deacetylase activities. *Molecular Cell*, 2(6):851–861.

Yamada, K. et al., 2011. Structure and mechanism of the chromatin remodelling factor ISW1a. *Nature*, 472(7344):448–453.

Yang, N & Kazazian, HH Jr., 2006. L1 retrotransposition is suppressed by endogenously encoded small interfering RNAs in human cultured cells. *Nature Structural and Molecular Biology*, 9:763-771.

Yates, J. a. et al., 2010. Regulation of HOXA2 gene expression by the ATP-dependent chromatin remodeling enzyme CHD8. *FEBS Letters*, 584(4):689–693.

Yen, K. et al., 2012. Genome-wide nucleosome specificity and directionality of chromatin remodelers. *Cell*, 149(7):1461–1473.

Yen, K., Vinayachandran, V. & Pugh, B.F., 2013. SWR-C and INO80 chromatin remodelers recognize nucleosome-free regions near +1 nucleosomes. *Cell*, 154(6):1246–1256.

Yuan, G.C. et al., 2005. Genome-scale identification of nucleosome positions in *S. cerevisiae*. *Science*, 309(5734):626–630.

Yuan, G.C. & Liu, J.S., 2008. Genomic sequence is highly predictive of local nucleosome depletion. *PLoS Computational Biology*, 4(1):164–174.

Zang, J. et al., 1997. On the Role of Myosin-II in Cytokinesis : Division of *Dictyostelium* Cells under Adhesive and Nonadhesive Conditions. *Molecular Biology of the Cell*, 8:2617–2629.

Zawadzki, K.A., Morozov, A.V. & Broach, J.R. 2009. Chromatin-dependent transcription factor accessibility rather than nucleosome remodeling predominates during global transcriptional restructuring in Saccharomyces cerevisiae. *Molecular Cell Biology*, 20(15):3503-3513.

von Zelewsky, T. et al., 2000. The *C. elegans* Mi-2 chromatin-remodelling proteins function in vulval cell fate determination. *Development*, 127(24):5277–5284.

Zentner, G.E. et al., 2010. Molecular and phenotypic aspects of CHD7 mutation in CHARGE syndrome. *American Journal of Medical Genetics, Part A*, 152(3):674–686.

Zentner, G.E., Tsukiyama, T. & Henikoff, S., 2013. ISWI and CHD chromatin remodelers bind promoters but act in gene bodies. *PLoS Genetics*, 9(2):e1003317.

Zhang, H. & Reese, J.C., 2007. Exposing the core promoter is sufficient to activate transcription and alter coactivator requirement at RNR3. *Proceedings of the National Academy of Sciences of the United States of America,* 104(21):8833-8888.

Zhang, H., Roberts, D.N. & Cairns, B.R., 2005. Genome-wide dynamics of Htz1, a histone H2A variant that poises repressed/basal promoters for activation through histone loss. *Cell*, 123(2):219–231.

Zhang, Y. et al., 2008. Model-based analysis of ChIP-Seq (MACS). *Genome Biology*, 9(9):R137.

Zhang, Y. et al., 1998. The dermatomyositis-specific autoantigen Mi2 is a component of a complex containing histone deacetylase and nucleosome remodeling activities. *Cell*, 95(2):279–289.

Zheng, Y. et al., 2013. Generation and characterisation of yeast two-hybrib cDNA libraries derived from two distinct mouse pluripotent cell types. *Molecular Biotechnology*, 54(2):228-237.

Zigmoid, S.H., 1988. Orientation chamber in chemotaxis. *Methods in Enzymology*, 162:65-72.

Zink, L.M. & Hake, S.B., 2016. Histone variants: nuclear function and disease. *Current Opinion in Genetics & Development*, 37:82-89.

Zofall, M., Persinger, J. & Bartholomew, B., 2004. Functional role of extranucleosomal DNA and the entry site of the nucleosome in chromatin remodeling by ISW2. *Molecular and Cellular Biology*, 24(22):10047–10057.